DEPOSITIONAL PROCESSES AND GEOLOGICAL SIGNIFICANCE OF BIOGENIC MAGNETITE AND Fe-SULFIDE BY IRON BACTERIA AT ANTHONY'S NOSE, WESTCHESTER COUNTY, NEW YORK.

"A PROPOSED METHOD OF REMEDIATION OF BIOGENIC IRON FROM WATER SYSTEMS USING APPLIED MAGNETIC FIELDS"

by

ARONA DIOUF

A dissertation submitted to the Graduate Faculty in Earth and Environmental Sciences in partial fulfillment of the requirements for the degree of Doctor of Philosophy, The City University of New York

2004

INFORMATION TO USERS

The quality of this reproduction is dependent upon the quality of the copy submitted. Broken or indistinct print, colored or poor quality illustrations and photographs, print bleed-through, substandard margins, and improper alignment can adversely affect reproduction.

In the unlikely event that the author did not send a complete manuscript and there are missing pages, these will be noted. Also, if unauthorized copyright material had to be removed, a note will indicate the deletion.

ProQuest Information and Learning Company
300 North Zeeb Road
P.O. Box 1346
Ann Arbor, MI 48106-1346

This manuscript has been read and accepted for the Graduate Faculty in Earth and Environmental Sciences in satisfaction of the dissertation requirement for the degree of Doctor of Philosophy.

12/2/2003 — Gerald M. Friedman

Date — Gerald M. Friedman, Chair of Examining Committee

12/16/03 — Jeffrey Osleeb

Date — Jeffrey Osleeb, Executive Officer

Professor C. E. Nehru, Brooklyn College

Professor Michael K. Weisberg, Kingsborough College

Professor Henry Ehrlich, Rensselaer Polytechnic Institute

Supervisory Committee

THE CITY UNIVERSITY OF NEW YORK

Abstract

DEPOSITIONAL PROCESSES AND GEOLOGICAL SIGNIFICANCE OF BIOGENIC MAGNETITE AND Fe-SULFIDE BY IRON BACTERIA AT ANTHONY'S NOSE, WESTCHESTER COUNTY, NEW YORK.

"A PROPOSED METHOD OF REMEDIATION OF BIOGENIC IRON FROM WATER SYSTEMS USING APPLIED MAGNETIC FIELDS"

by

ARONA DIOUF

Adviser: Distinguished Professor Gerald M. Friedman

In the Earth's biosphere, more than 80 different kinds of inorganic minerals are known to be produced by bacteria or human beings (Lowenstam, 1981). The study of biomineralization is a multi-disciplinary project that involves biotechnologists, geologists, microbiologists, and physicists. Biogenic minerals are important clues for paleoenvironment and rock paleomagnetism. They can be deposited in sediments and import a natural remanent magnetization preserving a record of the ancient geomagnetic field (Hawthorne and McKenzie, 1993) .

Magnetotactic bacteria (MTB) orient and migrate along the geomagnetic field towards favorable habitats, a behavior known as magnetotaxis (Blakemore et al., 1980). They are a morphologically diverse and cosmopolitan group of aquatic

microorganisms inhabiting freshwater and marine environments ranging from aerobic to anoxic (Blakemore, 1975).

This research provided new insight into the stratigraphic and mineralogical setting of Anthony's Nose located at Westchester County New York. It gives full consideration to novel interpretations of the evolution of the biogenic iron. The ultimate goal is to present arguments on the developments of biomineralization and to use geochemical and stratigraphic methodology that lead to the discovery of a "biogenic signature" at the research site.

MTB produced perfect little bar magnets (magnetosomes), which differ strikingly from those of inrganic origin. All magnetite (Fe_3O_4) crystals are octahedral; that is, they have the shape of two 4-sided pyramids put together at their bases. Magnetites from magnetotactic bacteria are elongated by the addition of six faces which enforce their magnetic pull that helps them locate sources of food and energy in the milieu. The study of their processes of deposition can provide significant informations about a region paleoenvironmental setting.

The final aspect of this research addressed the environmental effects of the magnetosomes when they contaminated our water systems or oil pipes. The author constructed a design used for space flight experiments by NASA scientists to establish functional weightlessness and pseudogravity that can reorient the microorganisms trajectory (Doyle et al., 1999). The main idea is to isolate the microorganisms and to precipitate their biologically produced magnetite before sedimentation with the induction of a greater magnetic field in their environment.

AKNOWLEDGEMENTS

Indebtedness is expressed to Distinguished Professor G. M. Friedman for opening up an opportunity and getting the author interested in the biogenic minerals debates. Sincere appreciation is extended to Professors C. E. Nehru and M. K. Weisberg, who accepted to help me in producing this dissertation. Thanks are due to Professors J. Osleeb, R. B. Frankel and Henry Ehrlich who responded to my inquiries for information and for their valuable suggestions. Professors Ehrlich and Friedman also edited this manuscript.

Dedication

To my Father El Hadji Coumba NDoffene Diouf

and Serigne Cheikh Fall Khady Gueye.

PREFACE

Bacteria are present in many geologic environments where they represent a significant proportion of the overall surface area exposed to fluids containing dissolved solutes. The most celebrated examples of organisms containing biogenic magnetite are magnetotactic bacteria. These bacteria contain magnetite crystals arranged in chains and held within a magnetosome. Transmission electron microscopy (TEM) has revealed that magnetite grains in magnetotactic bacteria (and in a wide variety of other organisms) are within the stable single-domain (SD) size and shape range (Butler and Banerjee, 1975). Accordingly, individual single domain magnetite crystals in bacterial magnetosomes have maximum intensity and stability of magnetization. Furthermore, magnetite crystals are aligned within the magnetosme so that magnetocrystalline easy directions are parallel to the chain with the result that magnetic moments of individual crystals collectively produce a very effective and stable magnet. This magnet serves as a geomagnetic sensor that guides magnetotactic bacteria down magnetic flux lines, helping to remain within the preferred habit of oxygen –poor zones within muddy layers of accumulation.

When magnetotactic bacteria die, their magnetosomes can be deposited and preserved in sediments, resulting in a (post) depositional remanent magnetization (Clement and Kent, 1983). The single-domain SD size of magnetosomes makes them excellent recorders of the paleoenvironmental field and their unique hexagonal crystal forms provide a means for identifying magnetosomes via electron microscopy of biogenic mineral extracted from sediments (Tauxe et al., 1983).

The research site was located in the vicinity of Anthony's Nose, Westchester County, New York (Figure 2), a prominent highland east of the Hudson River in New York State (Hall, 1968). Anthony's nose region has a rich and natural geologic history. In researching the location, many references were found to Anthony's Nose in old mineralogical literature dating back to 1825 (Robinson, 1825) . The location of the site has caused confusion. It lies on the border between Putnam and Westchester counties. This has complicated research into the site because references must be checked under both county listings.

The first mineral and rock reports about Anthony's Nose, contain no information about biogenic magnetite or iron sulfide deposited by Fe-bacteria ("biogenic signature") (Zodac, 1933). Most of mineral and rock descriptions date from the railroad excavation for the Central Hudson Line during 1840 (Beck, 1842). Since that time, there are no reports in the literature of newly excavated specimens, though several books mentioned the occurrence of new minerals, often attributing to them incorrect location, and none of them ever mentioned the formation of biogenic minerals.

Using a geological frame work, the first phase objectives of this research is to determine the local and stratigraphic setting of the region. This was done through field work, observations, scientific inquiries, laboratory analysis, library studies and applications of stratigraphic and geochemical investigations. The second phase focused on the finding of "biogenic signatures" using both geochemical and sedimentological investigations at Anthony's Nose, Westchester County New York. These findings are based on the morphological comparison of biogenic magnetite to

those from igneous origin, using transmission electron microscopy and scanning electron microscopy (Matsuda et al., 1983). These results were used to determine the various forms and processes of biogenic minerals deposition.

A third important aspect of this research dealt on its environmental component. Inspired by a NASA project on bacterial microgravity (Doyle and Todd, 1999), the author used an innovative method he called "Magnetic Remediation of Biogenic Iron Minerals which employs an Applied Magnetic Field". The purpose was to isolate the biogenic iron minerals produced by micoorganisms present in water/sediment systems, by imposing on them an induced (calculated) magnetic field. The main goal was to reorient the bacterial trajectory in the medium, then to precipitate their biogenic products before sedimentation in either aerobic or anaerobic systems.

Table of Contents

List of Tables

List of Figures

INTRODUCTION

Since Blakemore discovered the magnetotactic bacteria in 1975, there have been a lot of developments in the understanding of the iron biomineralization processes. Conferences and seminars were held around the world (Lowenstam and Weiner, 1989). The first iron biominerals conference was held at the University of Hampshire in Durham, in July 31 of 1999. Eminent biochemists, microbiologists, molecular biologists, geochemists, and geologists were invited. Since then, the interesting knowledge on biogenic iron minerals has grown.

Magnetotactic bacteria are able to produce biologically tiny iron-containing magnetic particles (Blakemore, 1975). Each of these particles is a magnet with a north pole and a south pole, arranged in a line to make one long magnet. The formation of magnetite and iron-sulfide is known to occur either of biologically induced mineralization (BIM) or biologically controlled mineralization (BCM) (Bazylinski, 1992). In the former, the biominerals are formed extracellularly, as a result of dissimilatory reduction of Fe(III). In the later case, they are produced intracellularly by magnetotactic bacteria and some higher organisms and are well-ordered crystals that exhibit narrow size distributions and morphologies. The biominerals in the magnetotactic bacteria are within the single-domain size range (35 to 120 nm in length) and are usually arranged in a chain motif, providing the cell with a permanent dipole moment. This arrangement causes a cell to align along Earth's inclined geomagnetic field lines, functioning as an efficient means of locating and maintaining an optimal position in vertical chemical gradients.

The first phase of the research in this thesis focuses on the search for biogenic magnetite and Fe-sulfide from fresh fracture samples, collected at Anthony's Nose, Westchester County New York. Transmission eclectron microscopy (TEM) and scanning electron microscopic (SEM) TEM examinations have shown that biogenic magnetite crystals have morphologies that are distinct from magnetite of igneous or authigenic origin (figure 1), (Bazylinski and Garrat-Reed, 1993). Examination of magnetite crystals therefore allows identification of biogenic magnetite in sedimentary rocks or/and in bedrocks pockets. These magnetites will be referred as magnetofossils, and should be the smallest mineral fossils yet found on the sedimentary record at Anthony's Nose. Their abundance implies that they play an important, if not major, role in revealing the paleoenvironment of Anthony's Nose, Westchester New York.

The second phase of this research determined the various forms of the depositional processes of the biogenic minerals found at Anthony's Nose Westchester County New York (figure 2) in a stratigraphic and sedimentological frame work to fit these findings in the regional geological setting (mineralogy). Results from analyzed samples show that biogenic minerals are found in a form of veins of fine-grained iron oxide within collected sediments or rocks. TEM and SEM studies indicate that they originated from secondary mineralization.

The third phase of this research was an environmental study of the biogenic minerals leading to the proposal of a method of magnetic remediation when these minerals contaminate our water systems. Magnetotactic bacteria are thought to respond to magnetic fields to guide tactic movement (Blakemore, 1975). Owing to its internal magnetite particles, cells can also be moved and guided by externally applied magnetic

fields, which can be combined in various ways with a gravity vector. This research emphasized that in a culture of microorganisms collected at Anthony's Nose, the magnetotactic bacteria could be isolated or suspended and removed from the medium to prevent sedimentation of their bioproducts. The author designed a set up that provided a modified magnetic field, using a current-carrying wire coil which induced a magnetic force greater than the Earth geomagnetic field's intensity. This resulted in a field mapping and a greater magnetic field intensity that reorients the bacteria to a vertical trapping region.

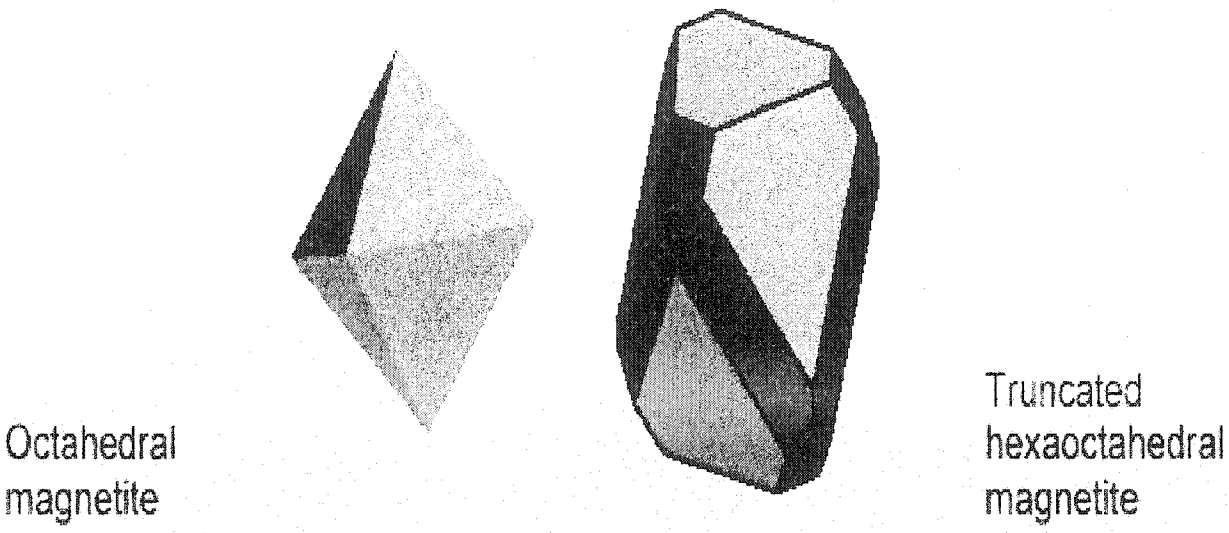

Figure 1: *Schematic representation showing a comparison of an octahedral inorganic magnetite and a "truncated hexaoctahedral" magnetite produced inside the cells of a Magnetotactic Bacterium. This diagram helps to explain the biogenic magnetite's unique morphology. On the left, the two 4-sided pyramids shape is shown that is common to all magnetite. On the right, the additional 6 faces, shown in red and are typical for biogenic magnetite. (Kirschvink and al., 1992).*

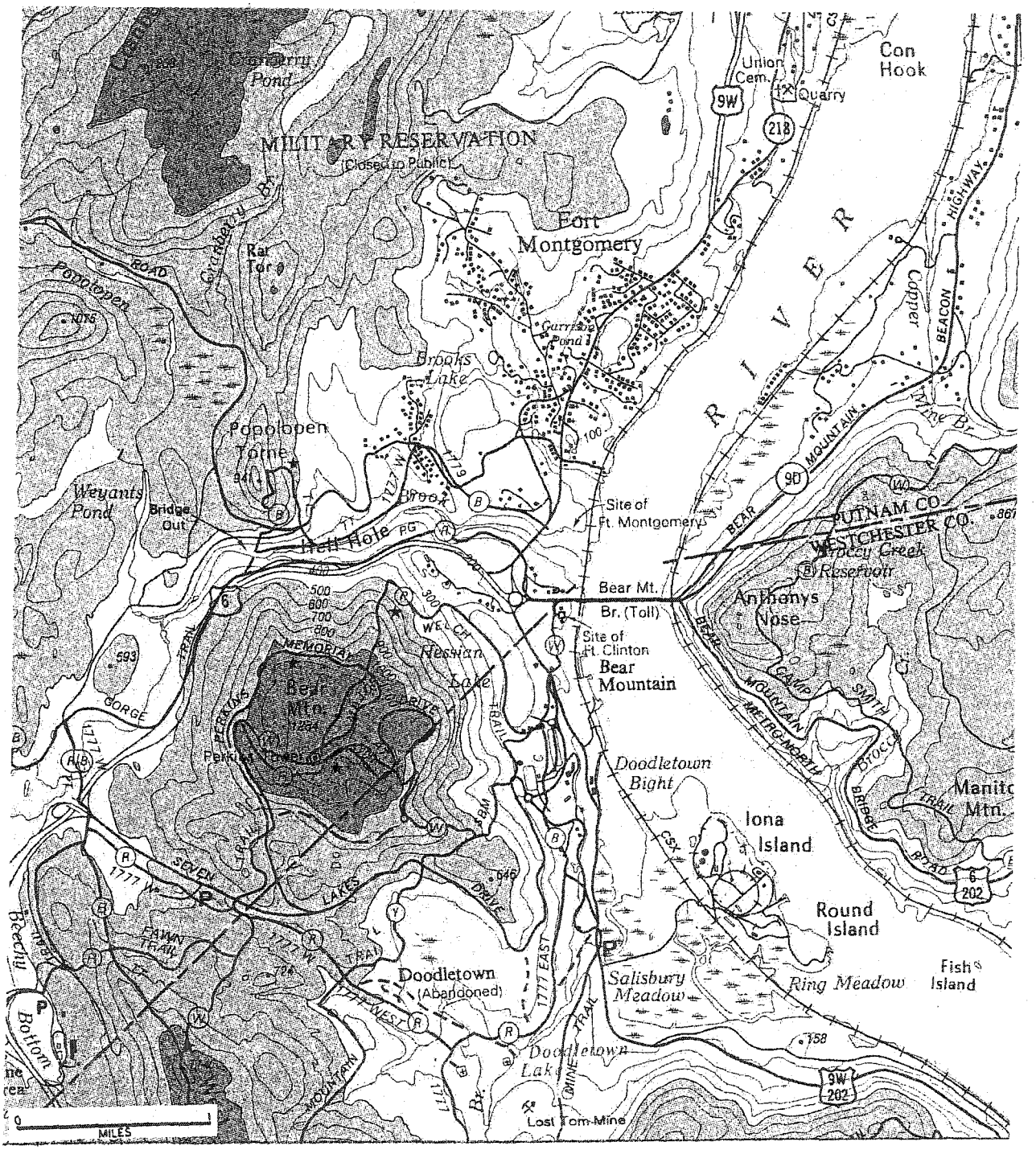

Figure 2: Anthony's Nose Westchester County New York and the Bear Mountain New Jersey; New York - New Jersey Trail Conference, 2001, New York Walk Book, 7th edition, p. 442.

RESEARCH OBJECTIVES

The research is based on field work conducted from July 17 to September 24, 2002, observations in the field, scientific inquiry, laboratory analysis, library studies and applications of stratigraphic methods and geochemical studies.

The objectives were:

- Geology: To determine the regional and local geology as well as the stratigraphic setting of Anthony's Nose, Westchester County through field work and sampling conducted at different sites, supported by a detailed library investigation on the region's mineralogy;
- Geochemistry: To use geochemical laboratory technics to study selected samples of rocks, soils, water and sediments collected at the research site Anthony's Nose, Westchester County; and, to interpret results obtained from transmission electron microscopy (TEM), scanning electron microscopy (SEM), and X-Ray Diffraction of biogenic magnetite and iron sulfide found and to make a classification based on their crystal size and morphology;
- Stratigraphy/Sedimentology: To determine the various mechanisms of deposition of biogenic minerals found in sediment and/or rock pockets at Anthony's Nose, Westchester County New York; and, to investigate if these findings are compatible with the existence of biogenic magnetite or/and iron sulfide produced by magnetotactic bacteria (MTB) and/or by other iron bacteria contained in a fluid (marine or fresh water) that penetrated along fractures and pore spaces of rocks, which then became the sites of secondary mineralization by biogenic activity (Blakemore, 1975);

- Paleoenvironment: To determine if the biogenic minerals we found have geochemical characteristics which are significant as biomarkers for paleoenvironmental studies of Anthony's Nose, Westchester County New York;
- Environmental Science: To describe an innovative method called "biogenic minerals magnetic remediation" that employs the bacteria's magnetic susceptibility and magnetic moment and an application of an external magnetic field that reorients their trajectory so they can be removed before sedimentation.

Twenty field trips were conducted during which one hundred and ten samples were collected. Fifty samples are presently being processed at two different laboratories: the Hackensack Environmental Center in New Jersey and the JC Board of Education J. Ferris HS Science Research Laboratory, New Jersey. Fourty five sample results have been obtained and are interpreted. The environmental phase experiments were conducted at the JC-Ferris HS Science Laboratory directed and supervised by the author.

CHAPTER 1: GEOLOGICAL SETTING OF ANTHONY'S NOSE

Local Geology

The rolling topography of Anthony's Nose, Westchester County New York is a southwestern extension of the crystalline highlands of western New England (Loveman, 1911) (Figure 1). Complex structures, extensive erosion, and glacial features make the landscape difficult to classify as plains, plateau or mountains. It is best characterized as a very mature landscape of ancient mountain roots. Elevations range from sea level along Long Island Sound and the Hudson River, to maximum elevations nearly 900 feet above sea level in the northern parts of the county. Anthony's Nose Westchester lies within the Manhattan and Reading Prongs of the New England Highlands (Tracy et al., 1987).

The land area of Anthony's Nose, Westchester County is about 150 square miles (Figure 1.4). Putnam County, to the north, lies within the Hudson Highlands, an upthrust fault block of ancient PreCambrian high grade metamorphic rocks (Pough, 1936). Westchester lies on the east by the Hudson River. Across the Hudson in Rockland County is the Triassic Newark fault basin, which contains sediment and igneous rocks (including the Palisades intrusion) from the Mesozoic era. To the south are the Bronx and Manhattan, another part of the same geologic and physiographic province as Westchester. Long Island Sound borders the region on the southeast and separates it from Long Island. At the east, the hills of Westchester blend into the metamorphic terrain of western Connecticut.

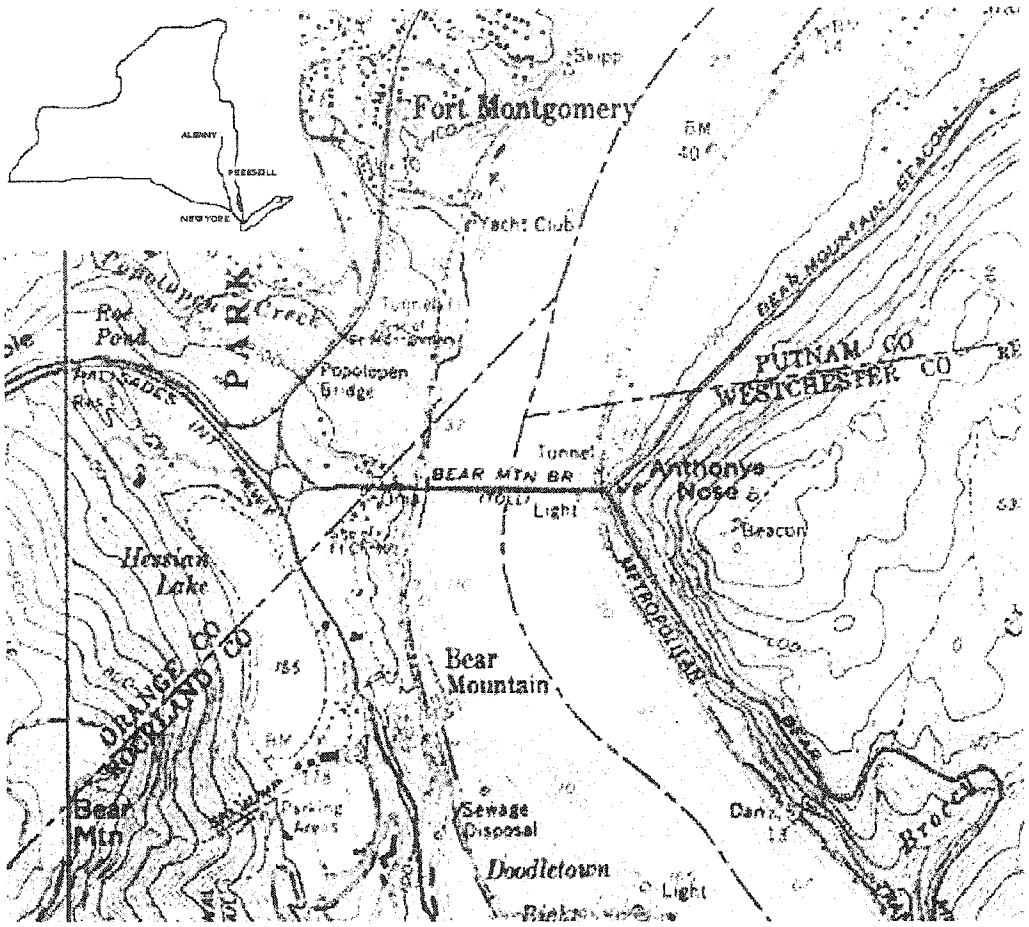

Figure 1.1: USGS topographic map of the Anthony's Nose Westchester/Putnam Counties upstate New York and the Hudson River (USGS Map, 1994).

Most of the local rock units have been dated with radiometric techniques as late PreCambrian and early Palaeozoic ages (Long, 1969). The rare fossils, found in local rock units and correlations with adjacent regions of lower metamorphism, are consistent with this age determination (Berkey, 1911).

Regional Geology

The prominent summits in the Hudson highlands, including Anthony's Nose and nearby Dunderberg are likely cores of eroded anticlines and the surrounding sedimentary and metamorphic rocks are the troughs of synclines (Figure 1.5). Anthony's Nose is composed of Canada Hill granite, a medium to coarse grained granite (Kemp, 1894). Often this granite has a streaked, foliated appearance due to crudely oriented biotite crystals. Other minerals include microcline and orthoclase feldspars, gray quartz, red-violet garnets and rutile needles. Upon weathering the Canada Hill granite takes on a dull gray appearance with quartz and garnet becoming prominent due to their resistance (Berkey, 1911). Canada Hill granite has been dated by Potassium-Argon dating to between 800-900 million years old by the Lamont-Doherty Earth Observatory of Columbia University (Schuberth, 1968).

Within the Canada Hill granite are lenticular pods of Grenville gneiss that predate its formation. It has been noted that the Canada Hill granite was particularly effective at assimilating the older rocks it invaded (Beck, 1842). Current theories about the origin of the Canada Hill granite propose that it formed through the granitization of an older rock of similar mineralogy, possibly an arkose sandstone, without ever going through

a fluid phase. This process is thought to be the result of the introduction of hot fluids and gases from a deeper magmatic body nearby (Schuberth, 1968).

Because Canada Hill granite are among the oldest granites in the region, much of the Grenville and Pre-Cambrian faulting has been obscured through rehealing, injection, or recrystallization (Dana, 1892). One fault in particular that runs from south-southwest to north-northeast extending from the north end of Iona Island, through two of the mineral locations in this paper is perfectly rehealed and completely crystalline, exhibiting equal strength to that of surrounding rock (Berkey, 1921).

The surficial geology of Anthony's Nose

The various landforms, around Anthony's Nose, are mainly the result of weathering and erosion, which attack different types of rock at different rates (Prucha et al., 1968). Lowlands form on easily erodible rocks, highlands on resistant ones, with all gradations in between.

A skin of soil and other loose material generally covers the bedrock, resulting from weathering of the surface rock. The loose materials may remain in place or be eroded, transported, and deposited by water, wind, or glacial ice. In 90 percent of Anthony' Nose region, bedrock is buried by surficial deposits that are more or less one meter thick. A continental glacier and ice sheets, that were perhaps 2 km thick, left most of these deposits (Waite, 1940). Continental glaciation played a modifying role in the development of Anthony's Nose's landscape in the recent geological past. On its advance to the south, the glacier removed and transported existing soils and eroded the surface of the bedrock. As the ice melted, this debris (mud, sand, gravel, and

boulders) was left at new sites in a great variety of depositional landforms. Melting caused the glacier to retreat across the region from south to north between 20,000 and 10,000 years ago (Wissig, 1979).

In the low plains north and west of Anthony's Nose, the bedrock is covered extensively by glacial till and by layers of sand and mud deposited in melt water lakes (Cadwell et al, 1989). Flat layers of sedimentary rock underlie this area. Remarkable field of streamlined hills of glacial till called drumlins appears to the west. Their beautiful alignment shows the direction of ice movement in this area.

Till is the most abundant glacial deposit in the area. It is an unsorted mixture of mud, sand, gravel, cobbles, and boulders that the glacier spread over the countryside. Till can be up to 2 meters thick or 50 meters thick at some others points. It is generally thickest in valleys and thinnest over highlands(Wissig, 1979).

Moraines are elongate ridges or strings of hills that formed at the edge of the glacier and are composed of sand, gravel, or till. The Ronkonkoma and Harbor Hill moraines dominate the Long Island landscape. The Valley Heads moraine dams the south ends of the Finger Lakes (Newman et al, 1969).

Glacial lakebeds are broad on layers of mud (deep water) and sand (shore zone) that were deposited in that formed in front of the glacier as the ice melted.

Outwash is sand and gravel deposited by melt water streams that flowed from the front of the glacier. These kinds of deposits have a wide range of thickness. In places, they are piled one on top of the other (Wissig, 1979).

CHAPTER 2: STRATIGRAPHY

Introduction

General Stratigraphic History of the Region including Anthony's Nose , Westchester County, New York

The local rock layers designate the PreCambrian Fordham Gneiss as the local basement rock (Hall, 1968). Radiometric dating has established the age of the Fordham at about 1300 million years (Mose, 1982). Hall (1968) has split the Fordham into four mappable units, each distinguishable by its mineral content. In general, the Fordham is a highly resistant and well-banded gneiss with intricate folds. In the late PreCambrian Grenvillian period of mountain building, the Fordham Gneiss was metamorphosed and, later, extensively eroded. The associated Pound Ridge Granite Gneiss and Yonkers Gneiss have been found to be about half that age (Long, 1969). These later gneisses are probably metamorphosed intrusions or volcanic deposits. The Yonkers Gneiss generally shows mineral foliation, but less banding than the Fordham and it contains more pink feldspar.

The (Ordovician) Lowerre Quartzite was deposited as an arkose sandstone which was extensively eroded before the deposition of limestone (Loveman, 1911). That limestone survived as the Inwood Marbles and Dolostones. The Lowerre Formation is a tan or buff colored granofels quartzite and feldspathic schist that outcrops very sparsely. The Inwood Marble is highly variable in character, but it is commonly white, tan or gray with swirls of impurities (including small pyrite crystals). It

weathers to a friable sugary tan or gray sand. It is hard to identify this formation at Anthony's Nose.

The Manhattan Schist is a highly variable formation of schist, gneiss and amphibolite units (Merguerian, 1987). It commonly shows fine mica foliation and it is more resistant to weathering than the Inwood Formation, but not quite as hard as the Fordham Gneiss. Hall has divided the Manhattan Schist into three sub-units. This formation probably originated as a variety of sedimentary and igneous strata. Charles Merguerian (1987) has suggested that the upper two units of the Manhattan, where they are exposed at Anthony's Nose are actually complex east- over-west thrust slices where older rock layers have been pushed over younger layers. The following is Merguerian's table of rock formation (Tables 2.1, 2.2, and 2.3):

Deformed and undeformed rocks Table 2.1

FORMATION	AGE	LOCATION	DESCRIPTION
SEDIMENTARY ROCKS	LATE PROTEROZOIC TO PALEOZOIC	NORTH AMERICA CRATON – SHALLOW SEAS	TECTONICALLY PASSIVE
BASALTIC LAVA FLOWS AND DIABASE FEEDERS	LATE TRIASSIC TO EARLY JURASSIC	ONSHORE AND OFFSHORE BASINS	OPENING OF THE ATLANTIC OCEAN
GRANITIC PLUTONS	JURASSIC AND CRETACEOUS	WHITE MOUNTAINS NEW HAMPSHIRE AND MONTEREGIAN	CRUSTIAL STRECHING RELATED TO THE OCEAN ATLANTIC OPENING
MARINE AND CONTINENTAL SEDIMENTS	CRETACEOUS TO RECENT IN AGE	NEAR SEA LEVEL	PASSIVE CONTINENTAL MARGIN EAST COAST OF NORTH AMERICA
OFFSHORE SUBMARINE SEDIMENTTS	JURASSIC	NORTH EASTERN AMERICAN OFFSHORE	PASSIVE CONTINENTAL MARGIN
VOLCANIC AND GRANITIC ROCKS	2.7 BYRS	SUPERIOR PROVINCE	LOW GRADE METAMORPHISM

Deformed and undeformed rocks Table 2.2

NORTH AMERICAN CRATON	MIDDLE PROTEROZOIC	GRENVILLE PROVINCE CANADA SHIELD ANDIRONDACK MOUNTAINS	HIGH GRADE METAMORPHISM
ACADIAN AND ALLEGHANIAN ORGONIES	PROTEROZOIC	GRENVILLE OROGENY	THREE OROGENIES
MARINE SEDIMENTARY ROCKS	LATE PROTEROZOIC TO ORDOVICIAN	SHELF, SLOPE, RIFT VOLCANIC AND RIFT SEDIMENTS	TACONIAN , ACADIAN, AND ALLEGHANIAN ORGENIES
EARLY PALEOZOIC ULTRAMAFIC ROCKS	EARLY PALEOZOIC	CORTLAND COMPLEX SOUTHEASTERN NEW YOK	SLIVERS OF SERPENTINIZED OCEANIC CRUST
METAMORPHIC AND MARINE SEDIMENTARY ROCKS	CAMBRIAN TO DEVONIAN	TERRANE METAMORPHOSED VOLCANIC ISLAND ARC ROCKS	LOW TO HIGH GRADE METAMORPHISM
METAMORPHOSED MARINE AND VOLCANIC	CAMBRIAN TO DEVONIAN	MERRIMACK SYNCLINORIUM	PRIMARILY DEFORMED BY THE ACADIAN OROGENY

Deformed and undeformed rocks Table 2.3

IGNEOUS AND METAMORPHOSED GRANITIC ROCKS	DEVONIAN TO PENSYLVANIAN	NORTH AMERICAN CRATON	ACADIAN AND ALLEGHANIAN OROGENIES
MARINE AND TERRESTRIAL SEDIMENTARY	MISSIPPIAN AND PENSYLVANIAN	FILLED BASINS SIDEWAYS-SLIP OF ALLEGHANIAN OROGENY	AVALON TERRANE ATTACHED TO NORTH AMERICA
PLATFORM ROCKS	CAMBRIAN AND ORDOVICIAN	VALLEY AND RIDGE FOLD BELT	ANTHRACITE GRADE MISSISSIPIAN AND PENNSYLVANIAN
SEDIMENTARY ROCKS	PALEOZOIC	NORTH AMERICAN PLATFORM	FOLDS GRADUALLY DIMISHING INTO UNFOLDED STRATA

(Source: Merguerian, 1987).

Local Stratigraphy

Anthony's Nose local Stratigraphy shows an iron ore body, lenticular in shape, approximately 100 feet wide and over 300 feet deep, associated with feldspar, pyroxene, hornblende, quartz. All the ore minerals are disseminated through the surrounding rock (Figure 2.1, Zodac, 1933).

The ore is primarily magnetite, slightly pyrrhotite with small percentages of pyrite and chalcopyrite. In addition to iron, the ore has a 30 percent sulfur content, 5 percent copper content, and 3 percent nickel content (Loveman (1911).

The stratigraphic sequence of the iron ore deposition was pyrite first, followed by magnetite, with pyrrhotite and chalcopyrite last. The relative age of magnetite has not been determined. In thin sections can been seen reaction rims around the magnetite of successive fringes of titanite and biotite. The presence of titanite is an indication that the magnetite is titanium-rich and is partly ilmenite. Loveman (1911) has proposed the following sequence for the local stratigraphy:

The quartz diorite country rock was intruded by a monzonite. Followed by dynamic disturbances which produced a gneissoid character to the intrusion and the country rock.

A second intrusion of a pyroxene diorite appeared at the contact between the mozonite and the country rock. This intrusion was to become the wall rock of the iron ore-body.

This intrusion, mentioned previously, was likely a line of weakness and was subsequently highly fracture by local faulting producing a crush zone that provided voids for the future iron ore deposition.

Hydrothermal water deposited pyrite in the crush zone and in part replaced the silicates of the diorite.

Further shattering provided additional voids. Additional hydrothermal solutions deposited the magnetite then the pyrrhotite. The chalcopyrite appears to be simultaneous to the pyrrhotite deposition.

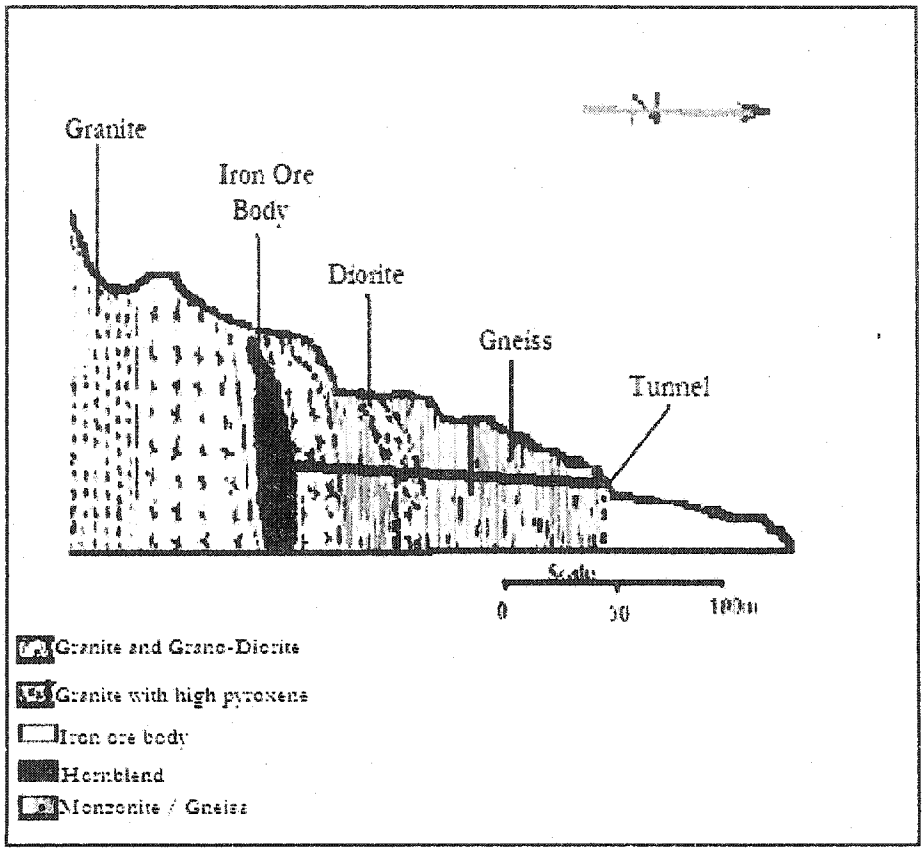

Figure 2.1: Section showing Anthony's Nose, Westchester County New York local stratigraphic sequence and the tunnel that was constructed for the iron ore exploitation at the Phillips Mine (from Zodac, 1933).

CHAPTER 3: MATERIALS AND METHODS

Introduction

The various minerals found in the Anthony's Nose environments come from the rocks and sediments surrounding them. The minerals are altered as they are transported by water or wind (or human beings), through exposure to oxygen, organic molecules, bacteria, different pH environments and many other weathering agents. By studying the mineral composition of this region, and comparing the results to similar analyses from modern discoveries in biomineralization, our primary objective is to be able to determine the presence of biogenic magnetite and iron sulfide produced by magnetotactic bacteria or other iron bacteria at Anthony's Nose in Westchester County.

METHODS

Field Trips

Field trips were conducted from July 17 through September 24, 2002. We used the entire summer for field investigation. We wanted to study our site accurately, benefiting from the summer weather condition. The sites where samples were collected were located on 1:63,360-scale topographic maps ((Figure 3.1), described recorded, and often photographs were taken. Wet samples were dried, packed into small 10x10x10cm cubes and weighed.

During the field work, eight separate locations of interest became apparent in the Anthony's Nose Westchester region. Each location judged opportune, represented a

site for investigation. The stops are named Stop A, Stop B, ...to Stop H.. The following describes their sites and these locations (Figure 3.1).

Stop locations and descriptions

Stop A: Along the Hudson Railroad, Cortlandt in Westchester County, New York

This location is easily accessible and it contains an unusual variety of rock types; igneous, metamorphic and sedimentary (Figure Map 3.1). We visited this location twice, at low tide (checking the weather report section in a local newspaper for the time of low tide). It is about 1 mile west of the Croton-Harmon railroad station. From Route 9 at the railroad station, we followed the viaduct and the road west to the main parking lot. Sampling may be found along the shore either north or south of the parking lot. Some of the best samples can be obtained along the river 100 meters south of the large grassy picnic area. The following were collected:

Calcite coated with drusy quartz found along the Hudson Railroad,

Samples of carbonate of lime;

Calcareous spar [calcite] in the form of flat, six-sided tables, of various sizes, from half an inch to two inches in diameter, found in the coarse granite on the banks of the Hudson River. There are two basic types from collected samples: calcite with drusy quartz overgrowth, and plain calcite crystals. Both show calcite crystals up to two inches across as thin tabular six-sided crystals (Zodac, 1933). Those with the overgrowth of quartz in places show a reddish-brown color probably due to iron

staining by weathering or biomineralization. During our visits to the site no visible signs of the calcite were left inside the tunnels or nearby cuts. However nearby in the surrounding bedrock small veins up to six inches wide were observed. It is assumed that the calcite specimens were extracted from pockets within a large calcite vein in the Canada Hill granite. This assumption is supported by the nearby rock dumped to build the railroad bed that likely came from the tunnel excavations. Calcite specimens found in the railroad bed are confined to a short length of the tracks south of the second railroad tunnel. The localized occurrence indicates that these calcites were not imported material, rather the result of blasting the adjacent tunnel.

Samples collected at this location are named: AN-101, AN-102, AN-103, AN-104, AN-105, AN-106, and AN-107. These samples are described in the next chapter (Figure 3.1).

Stop B: The Tilly Foster Quarries

This site is located at the south side of US Route 6 about half way between Brewster and Carmel in Putnam County. It is on a point in the Middle Branch Reservoir just east of the intersection of Route 6 and County Road 57.

The Tilly Foster mine was a source of magnetite iron ore in the early part of this century (Newman, 1969). The rocks were extracted from a very deep pit along the east side of the entry road. This location is famous for a great variety of common and unusual minerals. A variety of minerals can be found in the piles of spoils, mostly to the south of the mine pit. The Tilly Foster was named after a local farmer Tillingham Foster who was an early settler of the area (Zodac, 1933).

Samples of gneiss (AN-110 and AN-111), amphibolites (AN-112, AN-113 and AN-114), magnetite (AN-108 and AN-109), clinochlorite (rust stained) (AN-115, AN-116, and AN-117), and milky quartz were collected here (AN-120). In the Anthony's Nose rock and mineral literatures, a total of about 80 different minerals have been identified from the Tilly Foster Mine (Robinson, 1825).

Stop C: Copper Mine Road

Baylis Quarry is a private property, which displays a pegmatite body mined primarily for high-grade feldspar. We did not acquire permission to get any closer than about two meters. We could not have samples.

According to the mineralogy literature, large biotite crystals were developed and the muscovite-mica mingles with masses of pink rose quartz which can be observed in the quarry walls, about 1/2 mile east of Bedford Village on the road to Greenwich, onto Oliver Road (Agar, 1933). A wide variety of minerals have been identified from this location, but the most common minerals include feldspar (plagioclase and orthoclase).

Stop D: Philips Mine, Philips town, in Putnam County, New York

This is the oldest mining location in the Anthony's Nose region (Klemic et al., 1959). Surprisingly the mine tunnels are still open and accessible to this day. Local residents have often visited the mines and many tell stories about descending the tunnel into a large "glory hole" at the bottom. The hole was filled with water and there was a small boat that they used to paddle around the pool. Presently there is little chance for

underground collecting that would be worth the risk. We focused on the wide variety of rocks and minerals found on the dumps, which contain sedimentary, igneous and metamorphic rocks, and wet muds.

An interesting discovery was the phosphate of lime, asparagus stone, in sulphate of iron (Samples: AN-130, AN-131, AN-132, and AN-133). The phosphate of lime occurs in some varieties and is found in most of the mines of magnetic iron in around Anthony's Nose region, with commonly yellowish white, or reddish grains.

We collected samples of the soils, and samples of wet muds that may have come from the remains of what once could have been a pond (AN-140, AN-141, AN-142, AN-143, AN-144, AN-145).

We observed samples of hornblende, in large tabular masses, with pyrite and phosphate of lime. This assemblage could have originated from the dump, where can be seen many other mixtures: sulphate of iron, in large quantities, mingled with common pyrites, and phosphate of lime, red hematite; sulphate of barytes, calcareous spar, and asbestos. These are the samples collected for analysis: AN-150, AN-151, AN-152, AN-153, AN-154, AN-155, AN-156, and AN-157 (Table 3.4).

Brownish to yellow green colored crystals were found next to the sulphate of lime and presumed to be apatite. They vary from half to one inch in length. We observed some pyrites that had decomposed with formation of the sulphate of iron. According to our literature investigation of the local mineralogy, after copper mining was abandoned, the Philips mine was worked as a source of sulfur for the production of sulfuric acid (Loveman, 1911). The mine ore was carted to a sulfuric acid plant on the Hudson River near the sight of the Highlands train station. The ore was burned to

create sulfur dioxide, the first step in the production of sulfuric acid. The resulting cinders were hematite (ferric oxide), and some attempts were made at using them in iron production (Newland and Hartnagel, 1928). By 1894 the ore from the Philips mine was no longer used in the production of acid because cheaper Sicilian sulfur was available. However, during mining the ore from the Philips mine was highly prized due to the complete absence of arsenic (Kemp, 1894).

Stop E: Route 6 Road Cut, Cortlandt, in Westchester County, New York

This location is a modern site whith the road cut widened by the New York Department of Transportation in 1991, three quarters of a mile southeast of the Bear Mountain Bridge. Collecting at this site is best in the excavated rock that was dumped down the hill across the Route 6 road cut northeast of the parking area.

Various samples of soils, sedimentary and weathered metamorphic rocks were collected: AN-166, AN-167, AN-168-a, AN-168-b, and AN-169.

Stop F: Road Cut At Goldens Bridge

This is a public access. We collected small pods of garnet (Samples: AN-118, AN-119-a). They are common in this exposure of the Manhattan Formation. We walked about 1/4 mile north of the intersection of Route 138, along New York Route 22. At this stop large exposures lie along the east side of Route 22. A car dealership is at the top of the outcrop. Samples of schist, quartz (milky) and small pods of garnet are common here (Samples: AN-119-b).

Stop G: Peekskill Granite Quarries

This is also private land. According to the literature, the quarry at the north side of Route 202 was used to supply some of the facing stone for the Cathedral of St. John the Divine in northern Manhattan (Retsky, 1988). The quarry south of US 202 was used to mine the facing stones for the Croton Dam, about 5 miles to the south. A railroad led from the quarry down-grade to the dam site.

About half way between Peekskill and Yorktown Heights, one quarry is on the west side of a hill opposite Curry Chevrolet, about 1/4 mile north of Route 202. The other quarry is located about a mile to the west, along the north side of a hill 1/4 mile south of 202 and about 1/4 mile east of Croton Avenue. Attractive samples of gray and rusty granite can be found at these quarries (Samples AN-121, AN-122, and AN-123).

Migmatite on I 684 near Mt. Kisco: this road cut exposes an attractive pink granite pegmatite, gneiss and amphibolites (Luquer, 1896). Along I 684 southbound just before the exit at NY 172, or along New York Route 172 at the southbound exit from Interstate 684. From route 172 only, we walk about 1/4 mile north to the road cut. Good samples of granite pregmatite, gneiss, and amphibolite were collected but not labeled.

Along I 287: Public access. This exposure, under the Ridge Street Bridge, is a rock type called serpentinite. It was formed from a mafic intrusion near the suture of two tectonic plates. Serpentinite is a retrograde metamorphic rock formed by the slow cooling of a rock rich in minerals of iron and magnesium (Fleischer, 1987). The readily visible minerals include feldspar, quartz, biotite, and hornblende amphibole.

There was noted at the top of the outcrop banding and glacial polish and striations. We collected beautiful samples without labeling them for laboratory processing.

Stop H (Courtesy stop): Old Emery-Crete quarry. Crampon, Cortlandt.

Professor Friedman made a perspective and resourful study of this site in 1956 to determine the origin of emery deposition at this location (Friedman, 1956). Emery is a mixture of corundum (Al2O3) and magnetite (Fe3O4). (Ruby and sapphire are pure forms of corundum.) The emery formed when sections (screens) of the surrounding Manhattan schist fell into the still molten Cortlandt intrusion. This rock was used as an aggregate in concrete to make it wear resistant. The material was sold for the construction of industrial floors that have constant, abrasive traffic. Purer foreign emeries were used for emery paper and high quality abrasives, but even in these applications, ceramic abrasives have replaced emery. Samples: AN-171, AN-172, and AN-173.

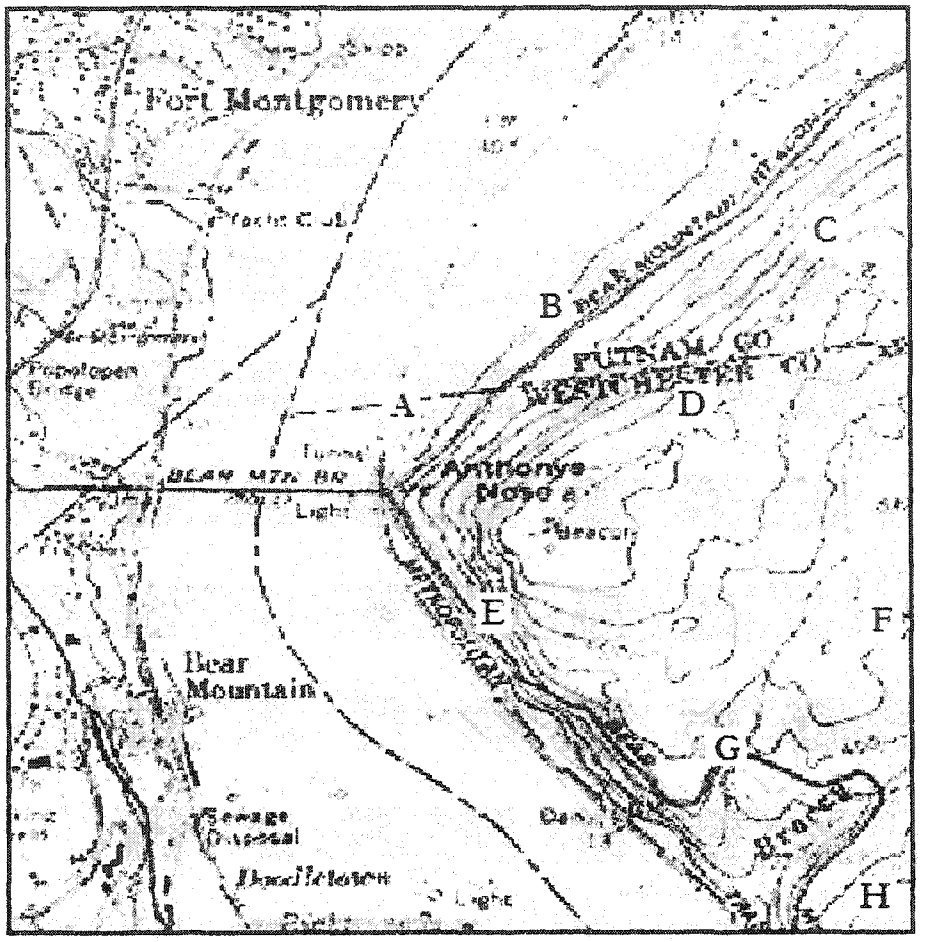

Figure 3.1: Map of Anthony's Nose, showing the field trip stops: Along the Hudson River (A), The Tilly Foster Quarries (B), Copper mine Road (C), Phillips Mine (D), Route 6/202 Road-Cut in Cortlandt (E), Road-Cut at Goldens Bridge (F), Old Emery-Crete Quarry (G), Peekskill Granit Quarries (H).

Sample collections

Sampling was done during field trips conducted from July 17 through September 24, 2002. A total of 110 samples was collected from the Anthony's Nose Westchester region. Fifty samples were sent to be processed for laboratory analyses. Wet samples were air-dried and ground to pass a 100-mesh (149 μm) sieve. Twelve of the samples were chosen for duplicate analyses.

Most minerals were encrusted with iron-oxide coating making collecting and field identification difficult. Larger rocks must be broken open to expose fresh surfaces and cavities for collectable mineral specimens. Pyrrhotite ore is easily recognized in a dump by the iron oxide (limonite/goethite) coating. The product of the pyrrhotite decay drips to the bottom forming a coating and conglomerating with nearby rocks and debris.

The collecting sites are over 150 years old and have been long forgotten (Zodac, 1933). Yet surprisingly, minerals and rocks may still be easily collected at these sites.

Samples are presented and described in following tables 3.1, 3.2, 3.3, 3.4 and 3.5:

TABLES OF SAMPLE LOCATIONS AND DESCRIPTIONS

Table 3.1

SAMPLE NAMES	LOCATION	STOPS	STATUS P=Processed U=Unprocessed S=In progress	DESCRIPTION
AN-101	Hudson Railroad	Stop A	U	Calcite coated with drusy quartz found along the Hudson Railroad
AN-102-a	Hudson Railroad	"	P	Carbonate of lime white, but some yellowish or reddish
AN-103	Hudson Railroad	"	P	Calcareous spar [calcite] in the form of flat, six-sided tables, of carious sizes, from half an inch to two inches in diameter, found in the coarse granite, on the banks of the Hudson River.
AN-104-JC	Hudson Railroad	"	P	Dark rock with metallic luster
AN-105	Hudson Railroad	"	P	Unknown

Table 3.2

AN-106	Hudson Railroad	"	U	Calcite specimens, extracted from pockets within a large calcite vein in the Canada Hill granite.
AN-107	Hudson Railroad	"	S	Soils
AN-108	Tilly Foster	Stop B	S	Magnetite, from the mine
AN-109	Tilly Foster	"	U	Magnetite, from the dump
AN-110	Tilly Foster	"	U	Gneiss, from the dump
AN-111	Tilly Foster	"	U	Unknown
AN-112	Tilly Foster	Stop B	U	Amphibolite (?)
AN-113	Tilly Foster	"	S	Talc
AN-114	Tilly Foster	"	U	Amphibolite (?)
AN-115	Tilly Foster	"	S	Clinochlorite
AN-116	Tilly Foster	"	U	Clinochlorite

Continue table 3.2

AN-117	Tilly Foster	"	U	Gypsum
AN-118	Tilly Foster	"	S	Unknown
AN-120	Tilly Foster	"	U	Milky Quartz
AN-118-a	Golden Bridge	Stop D	U	Small pods of garnet, common in the Manhattan formation.
AN-119-a	Golden Bridge	"	U	Schist

Table 3.3

AN-119-b	Golden Bridge	"	U	Milky Quartz with small pods of garnet
AN-121	Peekskill	Stop E	U	Attractive samples of gray and rusty granite from the quarry
AN-122	Peekskill	"	U	Pink granite pegmatite, gneiss and amphibolites in the excavated materials.
AN-123	Peekskill	"	U	Good samples of granite pegmatite, gneiss, and amphibolite in the excavated rocks.

Continue table 3.3

AN-123	Peekskill	"	U	Good samples of granite pegmatite, gneiss, and amphibolite in the excavated rocks.
AN-130	Phillips Town	Stop F	S	Phosphate of lime, asparagus stone
AN-131	Phillips Town	"	S	Sulphate of iron reddish
AN-132	Phillips Town	"	U	Phosphate of lime that reveals some varieties found in most of the mines of magnetic iron in or around Anthony's Nose region, often in yellowish white, or reddish grains.
AN-133	Phillips Town	"	S	Sample of mud
AN-136	Phillips Town	"	S	Unknown
AN-137	Phillips Town	"	P	Unknown
AN-138	"	"	S	Unknown
AN-139	Phillips Mine	"	U	Unknown with a metallic luster and dense.

Continue table 3.3

AN-140	Phillips Town	"	S	Samples of the soils, and samples of wet mud that could come from pond sediments.
AN-141	Phillips Town	"	U	Soil sample
AN-142-JC	Phillips Town	"	U	Soil sample
AN-142-a	Phillips Town	"	P	Unknown

Table 3.4

AN-142-b	Phillips Town	"	P	Unknown
AN-143	Phillips Town	"	U	Soil
AN-143-X	Phillips Town	"	P	Unknown
AN-144	Phillips Town	"	S	Chalcopyrite
AN-147			U	Magnetite
AN-148			P	Black
AN-148a	Phillips Town	"	S	Pyrite
AN-148-b			S	Unknown

Continue table 3.4

AN-148-X	Phillips Town	"	P	Unknown
AN-151-a	Phillips town	"	U	Samples of hornblende, in large tabular masses.
AN-151-b	Phillips Town	"	U	Sample of mud
AN-152	Phillips Town	"	U	Pyrite and phosphate of lime, s assemblage that could be originated from the dump, seen with many other mixtures.
AN-154	Phillips Town	"	U	Unknown
AN-153-X	Phillips Town	"	U	Sulphate of iron, in large quantities, mingled with common pyrites
AN-153	Phillips Town	"	S	Phosphate of lime, red hematite, a few meters South from the Mine; it occurs mammilary and botryoidally,
AN-155	Phillips Town	"	P	Unknown

Table 3.5

AN-156	Phillips Town	"	P	Calcareous spars
AN-156-a	Phillips Town	"	P	Unknown
AN-157	Phillips Town	"	P	Sulphate of barytes, in the vicinity.
AN-157-b	Phillips Town	"	P	Soil Sample
AN-166	Route 6 Road Cut	Stop G	U	Soil
AN-167	Route 6 Road Cut	"	U	Sedimentary rock with unknown composition.
AN-168-a	Route 6 Road Cut	"	S	Soil with reddish color.
AN-168-b	Route 6 Road Cut	"	U	Weathered metamorphic rock unknown mineral composition.
AN-169	Route 6 Road Cut	"	U	Weathered rocks.
AN-171	Old Emery	Stop H	P	Unknown
AN-172	Old Emery	"	U	Unknown
AN-173	Old Emery	"	U	Unknown

MATERIALS

We used several techniques to find the presence of biogenic minerals and to deduce their processes of deposition at Anthony's Nose sediments and rock pockets:

Visual Examination: We examined samples without any pretreatment with a small hand-held lens. Placing the samples on a microscope slide allows higher magnification examination and scanning-electron microscope (SEM), which creates a highly magnified picture for visual inspection. This investigation was done at m New Jersey BOED Laboratory of J. Ferris High School. About forty samples were processed this way. After analysis those samples were re-labeled AN-101-JC.

X-Ray Diffraction (XRD): Samples were sent to the Hackensack New Jersey Environmental Center Laboratory for X-Ray Diffraction (XRD) to measure the angle and intensity of diffracted X-rays as they pass through different minerals in a sample. By examining the angles of various x-ray intensity peaks, we can identify particular minerals. This technique is relatively fast, requires minimal sample preparation, and does not destroy the material (so XRD samples can be used for other analyses).

Inductively Coupled Plasma Spectroscopy (ICP): Samples for ICP analyses are dissolved in acids, and then vaporized to form plasma. This process releases photons that are detected by a spectromassmeter. The spectral patterns of different minerals are known, so we identified sample minerals by matching the spectral pattern of their photons to known patterns.

Tables of Analyzed Samples

Samples, were obtained from field trips to various stops at Anthony's Nose and surrounding regions. Selected samples were sent to the New Jersey Hackensack Environmental Center Laboratory and/or to the Ferris HS JC BOED Lab for processing (Tables 3.6, 3.7 and 3.8). The geochemical studies were the main focus of our research. These extraction and sample-preparation procedures were the same as those described by Chang and Kirschvink (1984). X-ray analysis was made by the Debye-Scherrer method.

P=Processed U=Not processed S=in progress

SAMPLES	LOCATION	LABORATORY	STATUS
AN-102-a	Hudson Railroad	Ferris J. JCHS Lab	P
AN-103	Hudson Railroad	Hackensack ECH	P
AN-155-HSK	Tilly Foster	Hackensack ECH	P
AN-156-a	Phillips Town	Hackensack	P
AN-157-b	Tilly Foster	Hackensack ECH	P
AN-105	Hudson Railroad	Hackensack ECH	P
AN-111	Tilly Foster	Hackensack	U
AN-104-JC	Hudson Railroad	Hackensack ECH	P
AN-118	Phillip Mine	Hackensack ECH	U
AN-118-a	Phillips Mine	Hackensack	U
AN-136	Phillips Town	Hackensack	U
AN-137	Phillips Town	Hackensack	P

Table 3-6: Tables showing the locations of analyzed samples, their description and their processing status (P=Processed U=Not processed S=in progress).

AN-139	Phillips Town	Hackensack	U
AN-140	Phillips Town	Hackensack	P
AN-142-JC	Phillips Town	Hackensack	U
AN-142-a	Phillips Town	Hackensack	P
AN-142-b	Phillips Town	Hackensack	P
AN-143	Phillips Town	Hackensack	U
AN-143-X	Phillips Town	Hackensack	P
AN-147	Phillips Town	Hackensack ECH	U
AN-148-b	Phillips Town	Ferris J. JCHS Lab	S
AN-144	Hackensack	Hackensack ECH	U
AN-148-a	Phillips Town	Hackensack ECH	U
AN-148-X	Old Emery	Hackensack	P
AN-144	Ferris Mine	Ferris J. JCHS Lab	S
AN-117	Tilly Foster	Ferris J. JCHS Lab	U
AN-151-b	Phillips Town	Hackensack	U

Table 3-7: Tables showing the locations of analyzed samples, their description and their processing status (P=Processed U=Not processed S=in progress).

AN-153	Phillips Town	Hackensack	U
AN-154	Phillips Town	Hackensack	U
AN-155	Phillips Town	Hackensack	P
AN-157-b	Phillips Town	Hackensack	U
AN-Soil-001	Hudson railroad	Ferris J. JCHS Lab	S
AN-Soil-002	Route 6 Cut	Ferris J. JCHS Lab	P
AN-Soil-003	Golden Bridge	Hackensack ECH	U
AN-Soil-004	Ferris Mine	Hackensack ECH	U
AN-Water-005	Golden Bridge	Hackensack ECH	S
AN-Excav-011	Ferris Mine	Hackensack ECH	P
AN-Veget-021	Peekskill	Ferris J. JCHS Lab	S
AN-Unkwn-031	Dump	Hackensack ECH	S

Table 3.8: Tables showing the locations of analyzed samples, their description and their processing status (P=Processed U=Not processed S=in progress).

CHAPTER 4: RESULTS AND INTERPRETATION

Introduction

Part of this research was based on the finding of biogenic magnetite and iron sulfide produced by iron bacteria. These findings were based on morphologic comparison to samples of igneous origin, using TEM and SEM investigations. Three distinctive particle morphologies of biogenic magnetite have been reported to date (Figure 4.1), including subrounded cubes and rectangles (Balkwill et al 1980), hexagonal prisms with flat ends (Towe and Moench, 1981; Matsuda et al., 1983), and a rare teardrop shape in some bacteria from New Zealand (Blakemore et al., 1980).

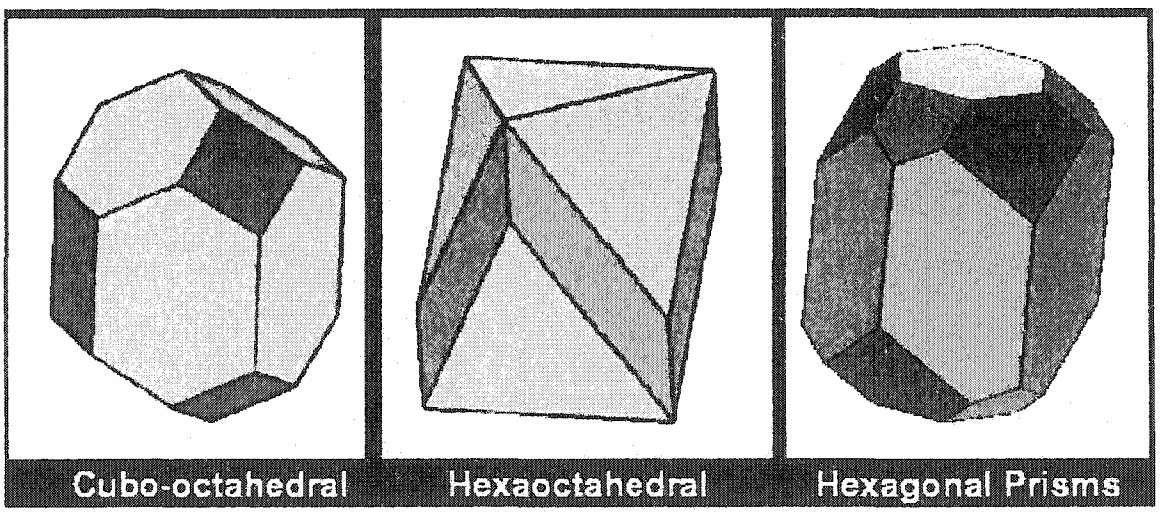

Figure 4.1: The three different morphologies of biogenic magnetite. All of these forms are clearly distinct from the octahedral, spherical, and framboidal magnetite particles that commonly form through igneous processes in nature (Balkwill et al, 1980; Towe and Moench, 1981; Matsuda et al., 1983; Blakemore et al., 1980).

EQUIPMENT

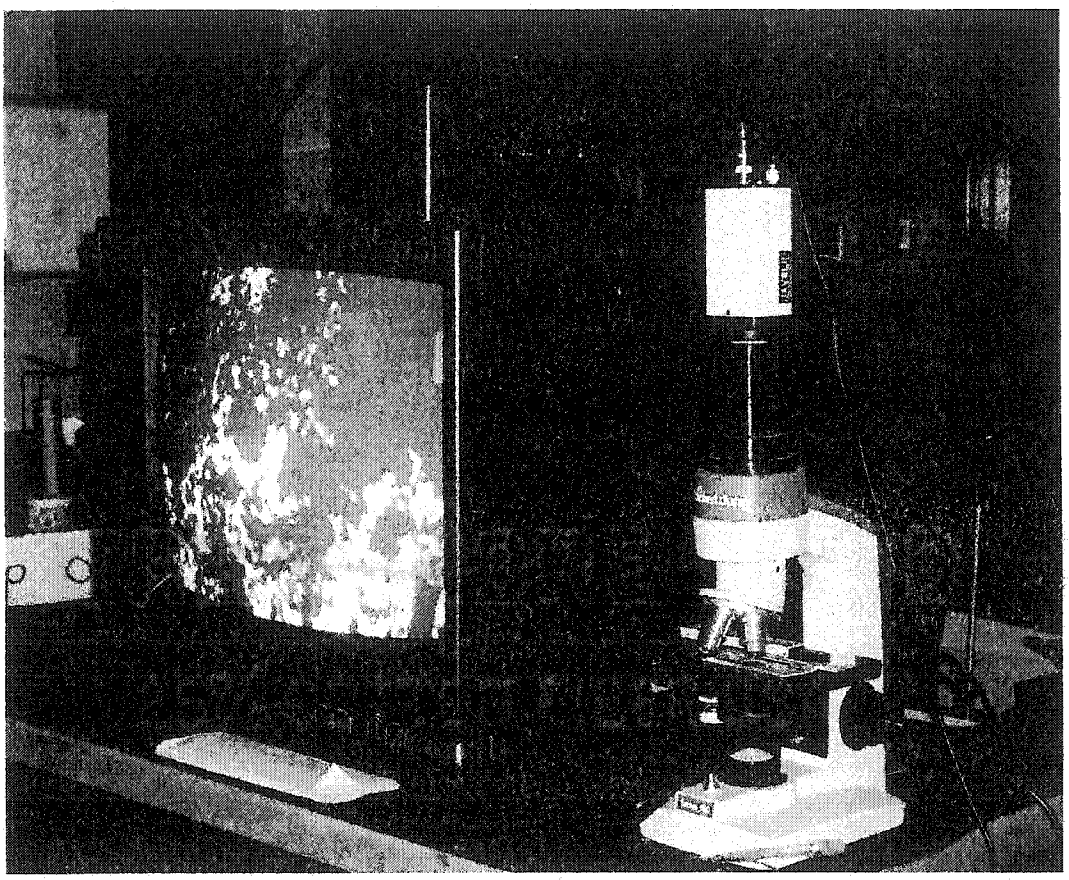

Figure 4.2: Microscopic Enhancement Materials at the BOED NJ Ferris HS Science Lab New Jersey, October 2002.

Results of analyzed samples

Sample AN-102-a

This sample was processed at the Ferris HS-BOED in Jersey City, New Jersey. Low magnification of fresh fracture surfaces of sample AN-102-a reveals particles with morphologic characterization (figure 4.2). Under the high magnification, AN-102-a sample shows the presence of several distinct crystal types, some of which closely resemble those formed by the magnetotactic bacteria (Figure 4.3).

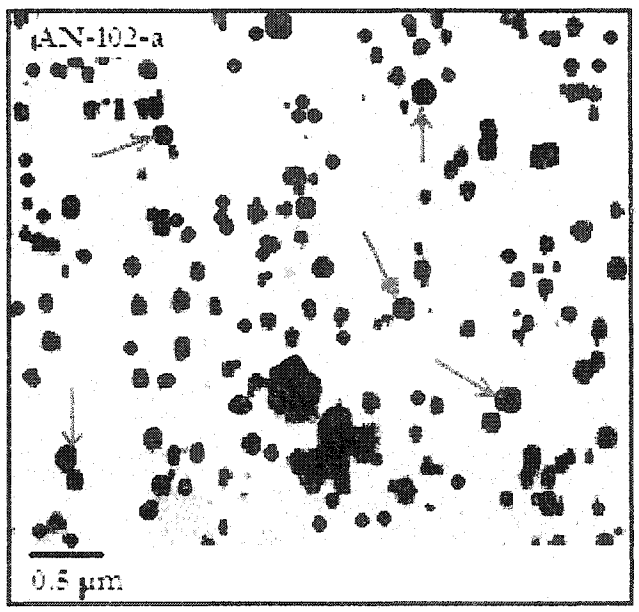

Figure 4.3: Low-magnification electron micographs of magnetites (showed in red arrows) from sample AN-102-a, processed at the Ferris HS-JCBOED Lab. Scale bar = 0.5µm.

We assume that magnetite crystals formed by the magnetotactic bacteria were a potential source of this ultrafine-graine biochemically d fraction in the sample AN-102-a. These objects may constitute the smallest mineral fossils yet recovered from Anthony's Nose sedimentary record.

We used Scanning Electron Microscopy (SEM) rather than Transmission Electron Microscopy (TEM) to characterize these particles. With SEM it is easy to identify grains larger than 0.5μm (i.e., the pseudo-single-domain to multidomain range for magnetite).

Sample AN-155-HSK

Thin sections from sample AN-155-JC were processed at the Hackensack NJ Environmental Center X-Ray Lab. High-resolution transmission electron microscopy (HRTEM) and energy dispersive spectroscopy (EDS) showed an iron sulfide (FeS) phase associated with an iron- rich region. This Fe-sulfide is pyrrhotite. Pyrrhotite particles are composed of S and Fe only. We did not observe any oxygen in the pyrrhotite spectra. Particles have atomic Fe/S ratios ranging from 0.92 to 0.97. The size and shape of the FeS particles vary. Single euhedral crystals of pyrrhotite range up to 100 nm across; polycrystalline particles have more rounded shapes ranging from 20 to 60 nm across. High-resolution TEM of these particles showed that their basal spacing is 0.57 nm, which corresponds to the {111} reflection of the pyrrhotite in a 4C monoclinic system. This pyrrhotite is associated with fine grains of magnetite. The magnetite is distributed uniformly in the region, whereas the pyrrhotite seems to be distributed randomly in distinct domains 5 to 10 μm long (Figure 4.4).

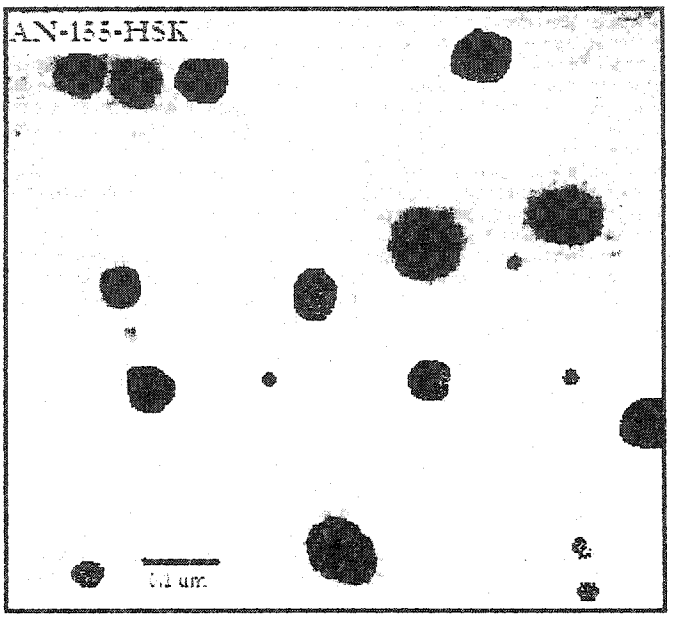

Figure 4.4: Electron micrograph of magnetite for sample AN-155-HSK, showing typical single-domain particles (black). Scale bar = 0.1 μm.

Sample AN-105

This sample was collected along the Hudson Railroad. TEM images of a thin section showed the morphology of the iron sulfide phases associated with magnetite. The iron sulfide phase (greigite? Fe_3S_4) was located in a magnetite-poor region separate and distinct from the magnetite-rich regions. TEM also showed a cross section of a single unknown crystal (we assumed that it was carbonate by its partial dissolution). This crystal was represented by large black regions (Figure 4.5). A vein of fine-grained quartz (light gray) was observed within greigite and secondary magnetite (fine, dark crystals) has been precipitated in this fine-grained matrix. There was a direct relation between the presence of quartz and the concentration of the fine-grained magnetite and iron sulfide phases. Some regions showed fewer iron rich particles, while others contain abundant iron rich particles. A representative elongated iron sulfide particle, located in the drusy region of the quartz is most likely composed of greigite. The morphology and chemical composition of these particles from the sample AN-105 were similar to biogenic greigite. Magnetite crystals biochemically precipitated by the magnetotactic bacteria were a potential source of this ultrafine-grained fraction in these sediments.

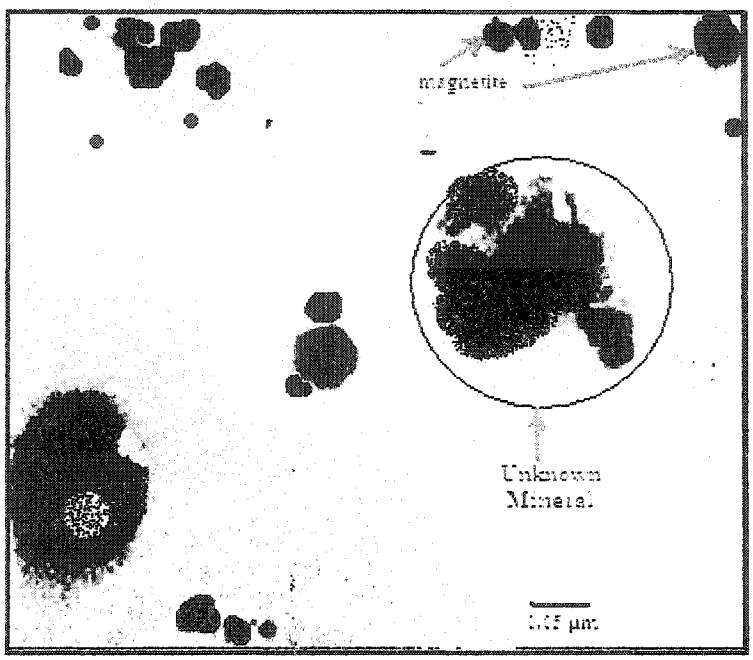

Figure 4.5: Electron micrograph of magnetite extracts from sample AN-105. Scale bar = 0.5 μm. High magnification image of one paramagnetic (SPM) grain (indicated by red arrowhead) and a partially dissolved mineral, assumed to be calcite (scale bar = 0.05μ m).

Sample AN-104

TEM images of a thin section obtained from sample AN-104-JC showed two distinct regions of mineral associations:

- An area, whose image at low magnification showed fine-grained magnetite and iron sulfide phases and their association with the surrounding orthopyroxene. High magnification revealed a magnetite-rich area with the distribution of individual magnetite crystals (high contrast) within the fine-grained orthopyroxene (low contrast). A high magnification of a pyrrhotite-rich region showed the distribution of individual pyrrhotite particles together with magnetite within the fine-grained orthopyroxene (low contrast). Magnetite grains in sample AN-104-JC did not contain detectable amounts of minor elements. In addition, these magnetite grains were single-domain crystals having no structural defects;

- A distinct region, located toward the center of the section showed carbonate (confirmed by an acid test reaction), spheroid, but completely separated from the magnetite-rich region with an accumulation of magnetite and an Fe-rich sulfide. This region displayed two types of textures:

  - One was more massive and electron-dense under the TEM
  - The other region was much less electron-dense and is fine-grained and porous.

The porous material occured mainly in crosscutting bands and rarely in isolated patches. We could not interpret the origin of this porous texture. But we speculated that it could be a primary mineralization of an unknown mineral that dissolved sometime after its formation (probably a chemical composition like that of CaCO3). However, the nanometer-size magnetite and Fe-sulfide phases were everywhere associated with the fine-grained and porous Mg-Fe-rich region. In the regions containing high concentrations of magnetite, the dissolution of the unknown mineral was evident. In contrast to the magnetite-rich region, the section area contained few magnetite particles. The Fe-sulfide phases in this magnetite-poor region had a chemical composition similar to that of the pyrrhotite. However, unlike pyrrhotite grains that have a large variety of morphologies, most of these iron-sulfide particles had elongated shapes. We were unable to obtain a diffraction pattern of these iron-sulfide particles because they were unstable in the electron beam. Because of the morphological similarity, we suggested that these Fe-sulfide minerals were probably greigite.

Greigite is isostructural with magnetite and is also ferrimagnetically ordered at room temperature. The greigite particles are characterized by narrow particle size distributions and species-specific crystal forms. Electron microscopy of the greigite particles in several organisms has revealed at least two idealized particle morphologies: (1) cubo-octahedral and (2) elongated cubic with the axis of elongation along the <100> direction (Heywood et al., 1991; Bazylinski et al., 1994).

The intrinsic magnetic properties of greigite are poorly known, but the biogenic particles provide some useful information. First, greigite magnetosomes, which should theoretically fall within the SD range for magnetotaxis, have dimensions between 67-100 nm. These particle dimensions observed for greigite magnetosomes are consistent with some simple calculations for the SD size limit in FeS (Ricci et al, 1993). Second, the greigite magnetosomes are oriented with their <100> axes aligned along the chain axis (Heywood et al., 1990; 1991), instead of <111> directions as observed in their magnetite cousins, implying that the <100> direction is the magnetic easy axis in greigite.

The magnetocrystalline anisotropy constant (K) has never been measured for greigite, the chain arrangement of the biogenic particles indicates that the sign of K must be positive at room temperature. Micromagnetic calculations for greigite should therefore be consistent with a positive anisotropy constant.

Particular species of MTB are usually characterized by a unique magnetosome morphology and mineral composition, the magnetotactic bacteria found in sulfidic habitats are interesting exceptions. The MTB contains single or double chains of iron particles, each exhibiting several different crystal morphologies but all within a narrow size range of 50-90 nm (Bazylinski and Frankel, 1992; Bazylinski et al., 1994; Heywood et al., 1990). The pyrite particles seem to be the dominant phase but the arrangement of the greigite/pyrite particles within the chains or the function of the pyrite particles is unknown (Heywood et al., 1991). In addition, copper has been identified in association with some of the greigite-pyrite particles in bacteria and is

the first evidence that a transition metal other than iron could be biomineralized by MTB (Bazylinski et al., 1993b).

Lastly, the MTB described by Bazylinski et al.(1993a) produce both magnetite and greigite magnetosomes. Both ferrimagnetic mineral phases are co-organized in the same magnetosome chain, but each phase has a distinct crystal morphology and crystallographic orientation. The magnetite magnetosomes are arrowhead-shaped, whereas the greigite ones are rectangular. Furthermore, the magnetite and greigite crystals are aligned with their respective <111> and <100> easy axes along the chain direction.

MEASUREMENTS

Measurements using the Butler/Banerjy SD Stability Diagram

Extant bacteria have been found living in both marine and freshwater environments, principally in the poorly oxygenated zone near the mud-water interface (Blakemore, 1975, 1982). They exist in both the Northern and Southern Hemispheres and at the geomagnetic equator (Kirschvink, 1980; Blakemore et al., 1980; Frankel et al., 1981), and have been found in open marine environments (Blakemore and Frankel, 1981). The dimensions of all bacterial magnetite crystals measured with the TEM and published to date plot within the boundaries of single domain stability field as determined by Butler and Banerjee, 1975 (figure 4.6).

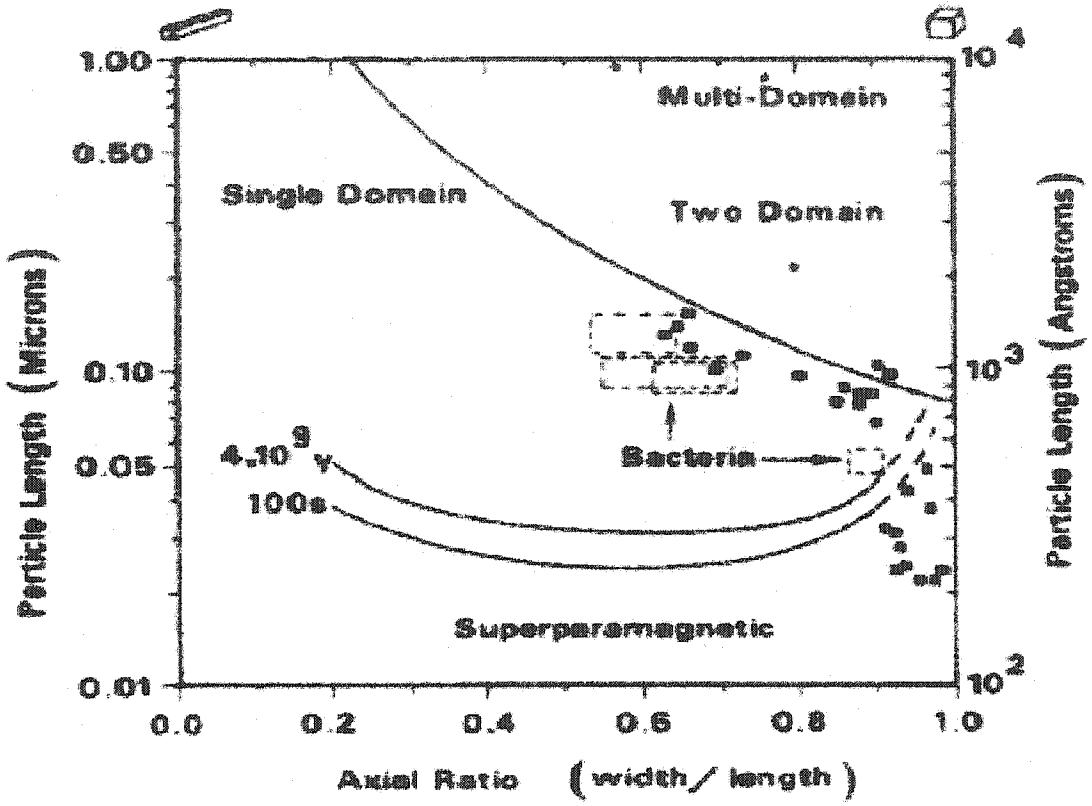

Figure 4.6: Plotted into single-domain stability field diagram for magnetite (Butler and Banerjee, 1975), size and shape distribution of grains shown in this figure range from superparamagnetic to multidomain. Each solid square represents average of 50 grains. Each asterisk represents one individual grain.

As can be seen in figure 4.6, many minerals that are precipitated biochemically under matrix-mediated control have crystal shapes that are distinctly different from their inorganic counterparts (Lowenstam, 1981). It should therefore be possible to recognize some of the biogenic magnetites, particularly those from the magnetotactic bacteria, on the basis of particle size and morphology alone.

The Butler and Banerjee axial/ratio diagram, TEM reveals three general classes of fine-grained magnetite particles that we designate as A, B, and C as follows:

- Type A grains are 0.02 to 0.05μm in length, and their aspect ratios vary from 0.9 to 1.0μm (e.g., superparamagnetic);
- Type B grains are 0.06 to 0.15μm in length, and their aspect ratios vary from 0.6 to 0.9μm (single-domain);
- Type C grains are pseudosingle-domain and multidomain particles longer than about 0.2μm.

The sizes and shapes of particles measured from the final extract of the samples AN-102-A, an-155-hsk, AN-105, AN-104, and many others from our collection, fall mainly in type B, which overlaps with those of typical single-domain grains from magnetotactic bacteria. They also share some of the same cuboidal and hexagonal forms as those of bacterial magnetite. It is also clear from these results that single-domain magnetite crystals that resemble those of biogenic origin are present in these samples, although there is as yet no direct evidence that the magnetotactic bacteria produced these forms. These interpretations were based only on similarity studies.

On the basis of observed population densities and growth rates, Kirschvink and Lowenstam (1979) and Towe and Moench (1981) conclude that the potential bacterial contribution in the deep sea was large enough to produce a significant fraction of the observed natural remanent magnetization. With the possible exception of green algae and chitons (class Polyplacophora), none of the other organisms that are known to produce magnetite crystals (tuna, salmon, cetaceans, etc.) are found in large enough

numbers to contribute a significant amount to the sediments (Walker and al., 1984). Yellowfin tuna, for example, make only about 20 ng of magnetite in a small tissue within the dermethmoid bone, but the crystal morphology strongly resembles the morphologies of the bacteria (Walker et al., 1984,). Chiton teeth have not yet been found in the fossil record, nor are the fate of the individual crystal clumps released by tooth wear known (Kirschvink and Lowenstam, 1979). Reports of magnetotactic algae remain undocumented to date, and no other magnetotactic microorganisms have been reported from marine plankton.

Our research has found abundant particles of single-domain magnetite in all sediments with medium to high $CaC0_3$ content. If the sample AN-105 is a marine sediment, the presence of single-domain magnetite crystals of apparent biogenic origin will contribute to a stable natural remanent magnetization, found in most research on biogenic magnetite in marine sediments (Kirschvink and Lowenstam, 1979). We did not study the magnetic remanence of our samples during our research. This is one of our postdoctoral projects.

If these particles are indeed of biogenic origin, they would be by far the smallest fossils yet recovered at Anthony's Nose Westchester. We could justifiably call them either picofossils or magnetofossils (Chang et al., 1985). They may provide very important information about Anthony's Nose paleoenvironment at the time of their formation. A wide variety of other microorganisms are also known to precipitate similar sized minerals (Lowenstam, 1981), but they have not yet been found in the fossil record.

INTERPRETATION

Processes of formation of biogenic magnetite and iron sulfide at Anthony's Nose, Westchester County New York

The occurrence of the fine-grained magnetite and iron sulfide phases in analyzed samples from Anthony's Nose sites could be explained by either inorganic or biogenic processes. Single-domain magnetite can precipitate inorganically under ambient temperature and neutral pH conditions by partial oxidation of ferrous solutions. This synthetic magnetite ranges in size from about 1 to more than 100 nm and is chemically very pure. Simultaneous inorganic precipitation of magnetite and pyrrhotite requires strongly reducing conditions at high pH (Verosub, 1977).

However, the unknown mineral, that showed areas of dissolution in various sample, could be a carbonate (Figure 4.5). These dissolutions phases are found in various calcite samples and carbonate of lime collected along the Hudson Railroad. Carbonate is normally stable at high pH, and the observed dissolution of the calcite mineral would normally require low pH conditions at the research site (paleoenvironment). We did not test the paleo-acidity under which these samples were formed. But we can possibly extrapolate on the paleo-acidity, based on the conditions of formation required by these samples (Tauxe et al., 1983). It is possible that the iron sulfides, magnetite, and the calcite samples (carbonates) all formed under high pH conditions, and the acidity changed at some point to low pH causing the partial dissolution of the calcite mineral (McCabe and al., 1983). But the iron sulfide and magnetite do not appear to have undergone any corrosion or dissolution except those found in the dumps (figure 4.7), which would have likely occurred under acidic conditions.

Moreover, as previously mentioned, the dissolution of the calcite is always intimately associated with the presence of iron sulfide and magnetite. Consequently, neither simultaneous precipitation of iron sulfides and magnetite along with dissolution of calcite nor sequential dissolution of calcite at a later time without concurrent dissolution of iron sulfides and magnetite seems plausible in a simple inorganic model.

If we consider the co-existence of calcite, iron sulfide and magnetite in our samples, we may infer a contrast in these processes of deposition. The co-existence of magnetite and iron sulfide phases within partially dissolved calcite could explain the biogenic origin whose formation is known to operate under extreme disequilibrium conditions. Intracellular co-precipitation of iron sulfides and magnetite within individual bacteria has been reported (Vali and al., 1990). In addition, extracellular biomediated precipitation of iron sulfides and magnetite can take place under anaerobic conditions (Blakemore, 1975, Blakemore, 1982).

Magnetite particles found in these samples are chemically, structurally, and morphologically similar to magnetite particles known as magnetofossils, which are fossil remains of bacterial magnetosomes found in a variety of sediments and soils and classified as single-domain (20 to 100 nm) or superparamagnetic (<20 nm) magnetite (Chapter 5) (Matsuda and al., 1983). Single-domain magnetite has been reported in ancient limestones and interpreted as biogenic (Karlin and Levi, 1983). Some of the magnetite crystals in these samples resemble extracellular precipitated superparamagnetic magnetite particles produced by the growth of anaerobic

bacterium strain GS-15 (*bacterium Geobacter metallireducens,* Butler and Banerjee, 1975).

A tentative explanation is that the nanosize magnetite and Fe-sulfides, found at Anthony's Nose, are the products of microbiological activity. It could be argued that these features in analyzed samples formed either by biogenic processes or by inorganic weathering. It is unlikely that reduced phases, such as iron sulfides, would form in Anthony's Nose during inorganic weathering because reported sulfur-bearing phases from Westchester soils are sulfates or hydrated sulfates. In general, secondary minerals in Anthony's Nose are oxidized or hydrated (Broughton and al., 1966).

Alternatively, if the magnetite and iron sulfide are products of biologic activity, a low-temperature formation would be indicated (paleotemperature). Their morphologies are similar to bacterially induced magnetite (Matsuda and al., 1983).

Single domain magnetite crystals of both biogenic and inorganic affinities appear to be present in varying amounts, but the biogenic fraction dominates the thin section of the selected and analysed samples from Anthony's Nose. They are biogenic particles, and may be of use for measuring paleo-oxygen levels, and so the paleotemperature (Stolz, 1992). The abundance of fine-grained magnetite implies that it played an important, if not major, role in informing about the paleoenvironment of Anthony's Nose, Westchester County New York. These results provide no clue as to the origin of biogenic or inorganic ions.

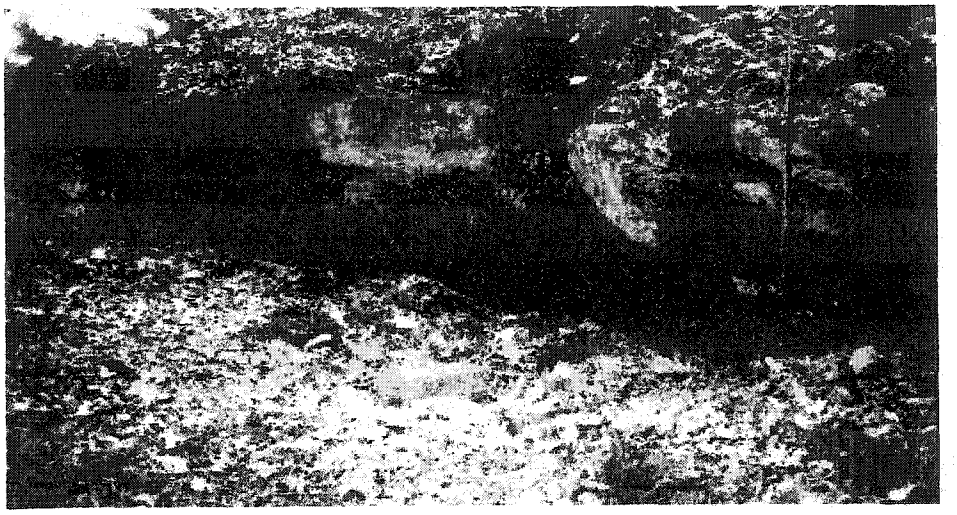

Figure 4-7: Weathered and heavily decayed dumps from the Philips Mine at Anthony's Nose Westchester County New York.

Processes of deposition

The biogenic magnetite and iron sulfide found in Anthony's Nose sediments and rocks are located in a poor magnetite-phase region (figure 4.5). Generally two distinctive regions were found in the analyzed samples. One was always associated with a magnetite aggregate rich region. Another one showed a poor region and was always separated by the magnetite-rich regions.

As shown by the TEM results, measurements revealed usual mingling of biogenic magnetite and iron sulfide with partially dissolved minerals. One sample revealed a carbonate content. Others were not tested. In some samples, the unknown mineral was represented by large black regions.

Biogenic magnetite formed veins of fine-grained iron within the sediments or rocks. They are assumed to be produced by secondary mineralization. The biogenic minerals may also have simply been precipitated in a fine-grained matrix after the microorganisms.

There was a direct relation between the presence of quartz and the concentration of the fine-grained biogenic magnetite and iron sulfide phases. Accumulations of biogenic iron varied considerably from region to another. Higher accumulations were found in some areas and low ones in other areas. This reveals the mode of deposition of the biogenic minerals and most importanly the conditions of the environmental setting in which these bacteria have performed their biological activities that led to biogenic iron formation. In a first estimation, we assume that at the time of formtion of bigogenic minerals found at Anthony's, the fresh or marine water level fluctuated.

Another consideration was the grain size. The abundance of biogenic iron determine an iron rich environment. Anthony's Nose geology cosntitutes a perfect site for such bacteria' biological needs, being an iron-mined region. Biogenic magnetite synthesis requires large amounts of iron, magnetotactic bacteria can be anticipated to use very efficient uptake systems for the assimilation of iron. Although several studies have focused on iron uptake, the exact mechanisms and components involved are not well understood.

The initial finding of Paoletti and Blakemore (1986) that cells of Magnetospirillum magnetotacticum produced a hydroxamate type siderophore under high iron condition, has not been replicated in other studies and no unequivocal evidence for the involvement of siderophores in the formation of magnetite has been found so far. Nakamura et al. (1993) hypothesized that ferric iron was taken up by *Magnetospirillum magnetotacticum* AMB-1 by a periplasmic binding protein-dependent iron transport system. In *Magnetospirillum gryphiswaldense*, the major portion of iron is taken up as Fe(III) in an energy-dependent process with a V_{max} and K_m of 0.86 nmol min^{-1} (mg dry weight)$^{-1}$ and 3 μM, respectively (Schüler and Baeuerlein, 1996). The high rates of ferric iron uptake may reflect the extraordinary requirement for iron in these bacteria. Both the amount of magnetite formed and the rates of iron uptake were close to maximum at extracellular iron concentrations of 15-20 μM Fe, indicating that this bacterium is able to accumulate copious amounts of iron from relatively low concentrations. These results are showing in most of Anthony's Nose processed samples.

Other research has revealed that size and morphologies of mature magnetite crystals are affected by environmental conditions The number of magnetosome particles per cell can vary considerably and strongly depends on the growth conditions. Besides the availability of micromolar amounts of iron, microaerobic conditions are required for magnetite formation (Blakemore et al., 1985; Schüler et al., 1995; Schüler and Baeuerlein, 1998).

Cells of *Magnetospirillum gryphiswaldense*, which are non-magnetic during aerobic growth, start to produce Fe_3O_4 when shifted to microaerobic growth conditions corresponding to an oxygen concentration of about 2-7 μM O_2. Growth media with sulfide and redox gradients have proven useful in the proliferation of MTB (Schüler et al., 1999).

All of parameters that affect growth of MTB influence the deposition of biogenic minerals in sediments and bedrocks pockets. In our research, it is apparent that the percent of biogenic mineral found in analyzed samples depends on an environment with high iron content.

Like the gypsum and calcite, biogenic magnetite and iron sulfide can appear as micro crystal coatings in cavities and on other rocks. It is likely that some of these minerals formed before or since mining began, as they are visible in analyzed samples collected in the tunnels and on heavily decayed minerals in the dump (figure 4.5). Some samples were extracted from pockets within a large calcite vein in the Canada Hill granite.Biogenic magnetite mingled with calcareous spars [calcite] in the form of flat, six-sided tables, of various sizes, from half an inch to two inches in diameter are also found in the coarse granite, on the banks of the Hudson River. Those with an

overgrowth of quartz often showed a reddish-brown color, due to the weathered biogenic iron products.

Paleoenvironment

The morphologies of biogenic magnetite and iron sulfide found in analyzed samples from Anthony's Nose, have a structure similar that produced by bacterially induced magnetite processes (BIM) (Matsuda et al., 1983). Alternatively, if the biogenic magnetite and iron sulfide are products of biologic activity, a low-temperature formation would be indicated.

Another paleoparameter that can be derived from our research of Anthony's Nose paleoenvironment is the paleopH. We found various known and unknown minerals with dissolution phases. Our tests revealed carbonate phases for some samples. Dissolution phase regions are found in various TEM of calcite samples and carbonate of lime collected along the Hudson Railroad. We know that the carbonates are stable at high pH. This meams that any dissolution of these carbonate phases normally require low pH conditions. We can conclude, from this investigation that paleoacidity fluctuated from a high H+ concentration (very acidic environment) to low H+ concentration (very low acidic environmental conditions) at the research site (plaeoenvironment).

It is possible that the biogenic iron sulfides, magnetite, and the calcite samples (carbonates) all formed under high pH conditions, and that the acidity changed at some point to low pH causing the partial dissolution of the calcite mineral (McCabe et al., 1983). But the iron sulfide and magnetite do not appear to have undergone any

corrosion or dissolution (except those found in the dumps). Moreover, as previously mentioned, the dissolution of the calcite is always intimately associated with the presence of iron sulfides and magnetite. Consequently, neither simultaneous precipitation of iron sulfides and magnetite along with dissolution of calcite nor sequential dissolution of calcite at a later time without concurrent dissolution of iron sulfides and magnetite seems plausible in a simple inorganic model.

Other paleonvironmental studies

A study of isotopic ratio of O^{16}/O^{18} can give information on the paleotemperature conditions that determines the paleoclimate at Anthony's Nose. This needs to be addressed in an independent reseach proposal. The ratio of O^{16} to O^{18} measured in fresh water sediments is temperature dependent, meaning that it varies as the environmental temperature varies. O^{16} has less mass than O^{18}, so is more mobile in the environment. In cool climates (glacial times; winters), more mobile O^{16} in lakes or oceans will preferably be taken up in evaporation and deposited in glaciers (snow), leaving the lake or ocean reservoir relatively enriched in O^{18}. Microorganisms in lake or ocean at this time will also be enriched in O^{18}, and will have a "heavier" or more negative isotopic signal. In warm climates (interglacial times; summers), glaciers (snow) melt, releasing the O^{16} in the ice back to the ocean. Aerobic bacteria living in the lake or ocean at this time will be relatively depleted in O^{18}, with a "lighter" or more negative isotopic signal.

The shape, size and and structure ``calibrated" against whole chain cells were used to study compaction, cementation in sediments carbonates (Diaz et al., 1991; McNeill and Kirschvink, 1993). Another approach may prove useful for detecting biogenic chain fractions in sediments.

Some processed samples from Anthony's Nose show ``large" magnetosomes (up to 200 nm) with particle dimensions that are larger than the theoretical single domain (SD) size range for magnetite. These observations have several fascinating implications. Either the magnetosomes are indeed two domain; or (1) the magnetosomes are really SD and the theoretical groundstate SD-TD transition size needs to be slightly revised; or (2) the magnetosomes are uniformly magnetized in an SD state but it is a higher energy metastable SD state within the equilibrium TD range. The second possibility is the most intriguing and, if true, these bacteria can provide validation of micromagnetic models as well as provide a source of metastable SD magnetite particles for study. Interestingly, the magnetosome dimensions are consistent with recent theoretical grain size limits for metastable SD magnetite particles (Dunlop, 1990). There is a direct relationship between bacterial accumulations and biogenic iron during magnetic induction. While the intracellular iron content in pre-magnetic cells is relatively low and in the same range as reported for other non-magnetotactic bacteria, magnetotactic bacteria can accumulate more then 2% iron on a dry weight basis (Blakemore et al., 1979; Schüler and Baeuerlein, 1998).

Identified collected samples are shown in figure 4.8 as well as other processed ones. (Processing results in APPENDIX B).

Identified Samples

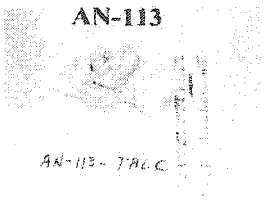

Talc

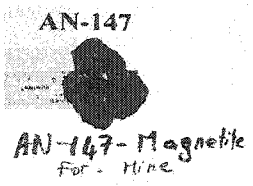

Magnetite

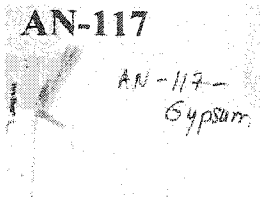

Gypsum

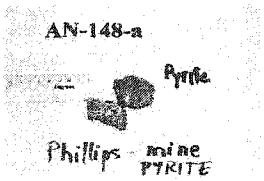

Pyrite

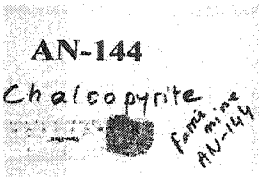

Chalcopyrite

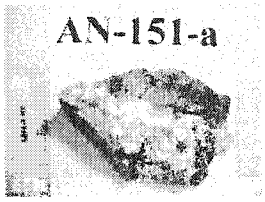

Unknown

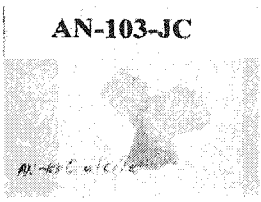

Calcite

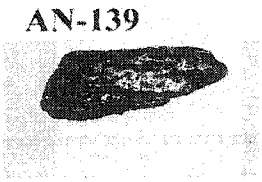

Unknown

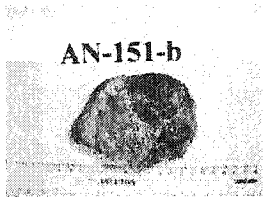

Weathered

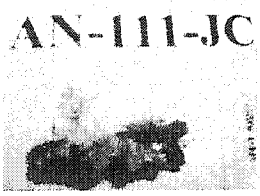

Quartz

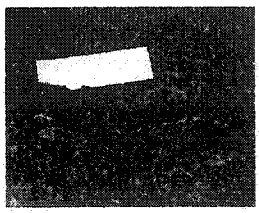

Fe-Soil (dump)

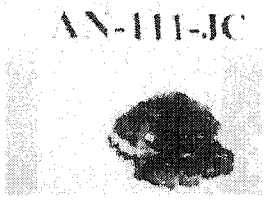

Calcite/Quartz

Figure 4.8: These samples have been identified and explained at APPENDIX B and are presently in the authors' collection.

CHAPTER 5: CHARACTERISTICS OF BIOGENIC MAGNETITE AND INORGANIC MAGNETITE

Introduction

Several studies reported biogenic mineral deposition in lake, marine, and continental eolian sedimentary deposits (Snowball, 1994; Hess, 1994; Evans and Heller, 1994; Hawthorne and McKenzie, 1993) TEM and geochemical methods have confirmed the formation and the destruction of biogenic magnetite in soils (Maher and Thomson, 1992).

Samples of soils and sediments found at different locations at Anthony's Nose during our field trip, revealed both biogenic and inorganic morphologies of the magnetite and iron sulfide found at Anthony's Nose Westchester County New York. This chapter outlines the differentiation between these two forms of magnetite, which is one of the objectives of our research.

Magnetotactic bacteria produce well-ordered membrane-bounded intracellular crystals of magnetite (Fe3O4) and/or greigite (Fe3S4) called ''magnetosomes''. They are generally arranged in chains parallel to the long axis of the cell. The torque induced by the Earth's magnetic field on these chains overwhelms thermal agitation, allowing the bacteria to align passively along the Earth's geomagnetic field lines like a compass needle (Blakemore, 1975; Frankel et al, 1979). Coupled with flagellar motility, aerotaxis, and magnetotaxis, this allows these bacteria to locate and maintain an optimal position in vertical chemical gradients in aquatic environments (Vali, H. & Kirschvink, J. L. 1991). Magnetotactic bacteria exert strict genetic control over the

composition, size, morphology, and crystallographic orientation of their biogenic magnetite to maximize their cellular magnetic moment (Thomas et al, 2000; Clemett et al, 1998). Physical and chemical controls of the biomineralization processes are achieved by precipitating magnetite and greigite within small intracellular membrane vesicles.

Characteristics of Biogenic Magnetite

These characteristics are the result of biochemical and genetic control by the organism and are consistent with natural (Darwinian) selection to maximize the magnetic dipole moment of the individual magnetite crystals as well as that of the entire cell (Thomas-Keprta et al., 2000). These characteristics can be used to define a biosignature. A biosignature is useful only if natural inorganic processes do not produce it; that is, one that does not happen through random, stochastic interactions or is not a product of directed human intervention, which is better described as a synthetic inorganic process. No published reports of inorganic "MV-1-like" truncated hexa-octahedral magnetites are known (Figure 5.1). The chemical and physical principles that underlie these six criteria are universal.

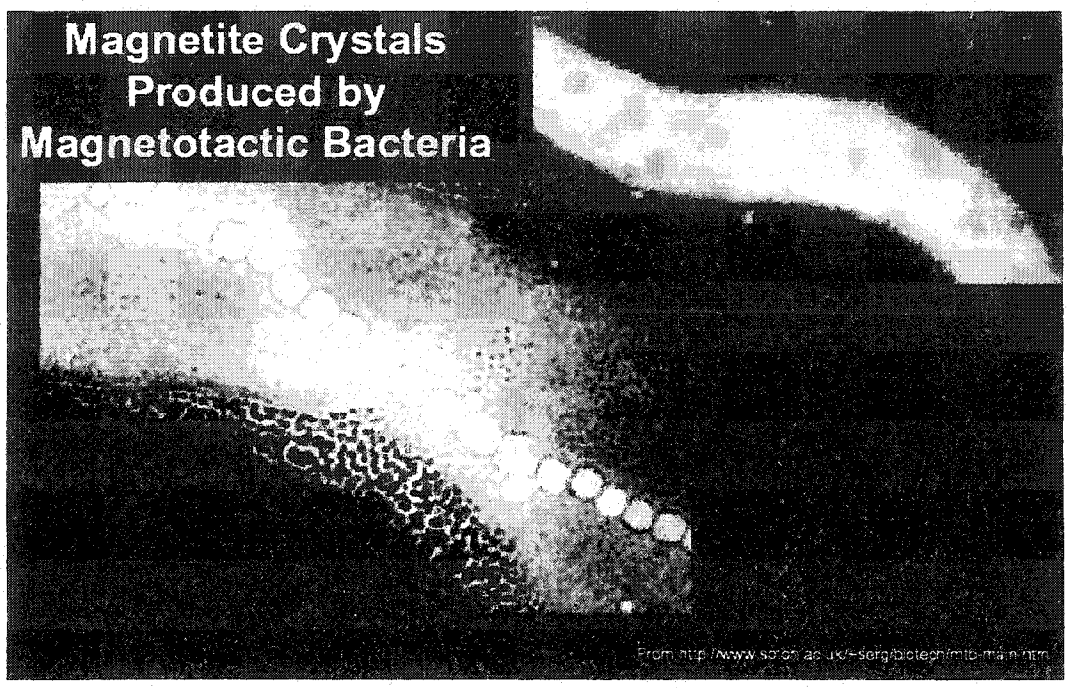

Figure 5.1: Magnetite crystals produced by a magnetotactic bacterium strain MV-1 (2-7), and the presence of single-domain, chemically pure, truncated hexa-octahedral magnetite crystals (Thomas et al., 2000).

The intracellular magnetite crystals produced by magnetotactic bacterium strain MV-1 display six distinctive properties: (*i*) narrow size-range (i.e., single-domain for uniform magnetization) and shape (restricted width-to-length (WyL) ratios); (*ii*) chemical purity; (*iii*) few crystallographic defects; (*iv*) an unusual truncated hexa-octahedral morphology; (*v*) elongation along the [111] axis; and (*vi*) alignment in chains within cells.

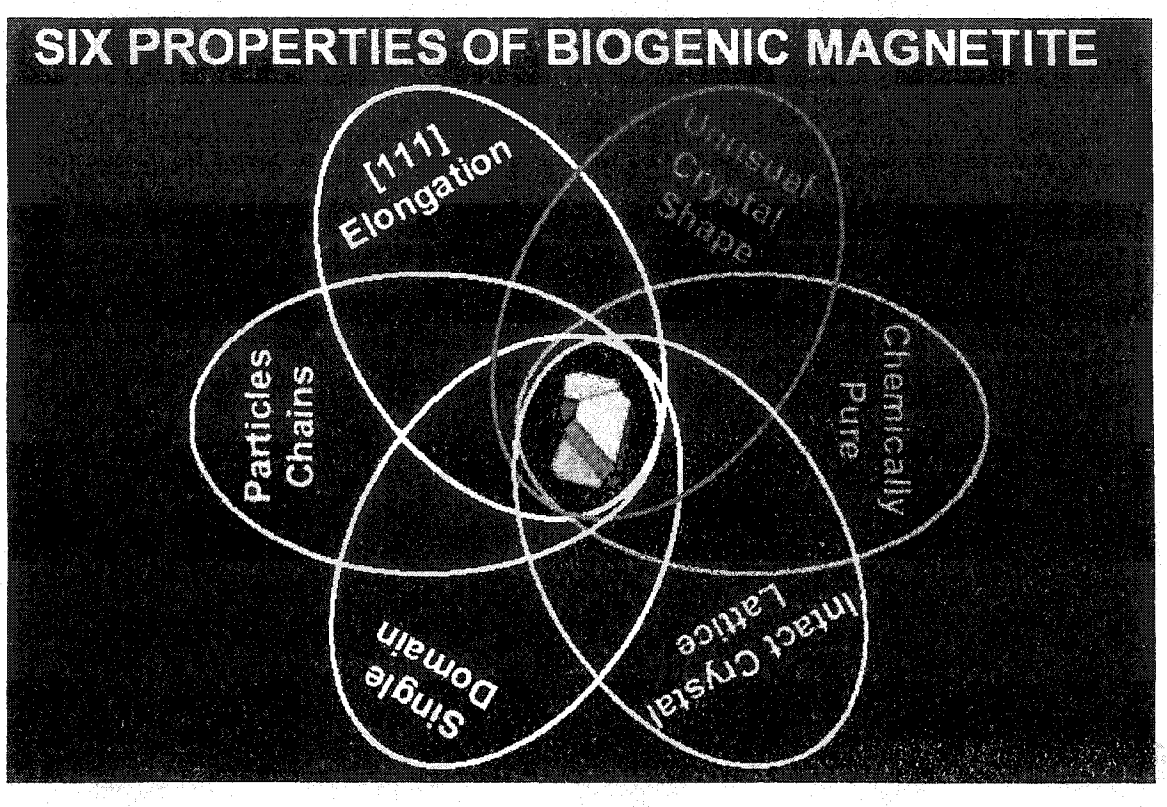

Figure 5.2: These properties all act to optimize the interaction of the magnetites with a magnetic field. Since the strength of magnetic field interactions are much smaller than thermal energies kT, on thermodynamic grounds alone, chemical and biological processes cannot be influenced by magnetic fields to any measurable degree. Hence the six characteristics, outlined above, have *evolved* through the process of natural selection. No published reports of inorganic truncated hexa-octahedral magnetites are known (Bazylinski et al., 1997).

Approximately one-fourth of the magnetites are truncated hexa-octahedral, and share five of the six characteristics that define the crystals biosignature (Figure 5.2).

The truncated hexa-octahedral magnetites cluster in the super- paramagnetic to single-domain region of the Butler–Banerjee plot for magnetites appear to nucleate within a cell membrane (Kirschvink, 1982; Guerinot, 1994; Braun et al., 1998), and grow from the superparamagnetic into the single-domain size range (i.e., they behave as perfect bar magnets) with well defined shape anisotropies and a narrow, asymmetric width-to-length (WyL) distribution. These characteristics can arise from natural selection, as superparamagnetic and multidomain crystals are of no value for magnetotaxis (Leshin, 2000).

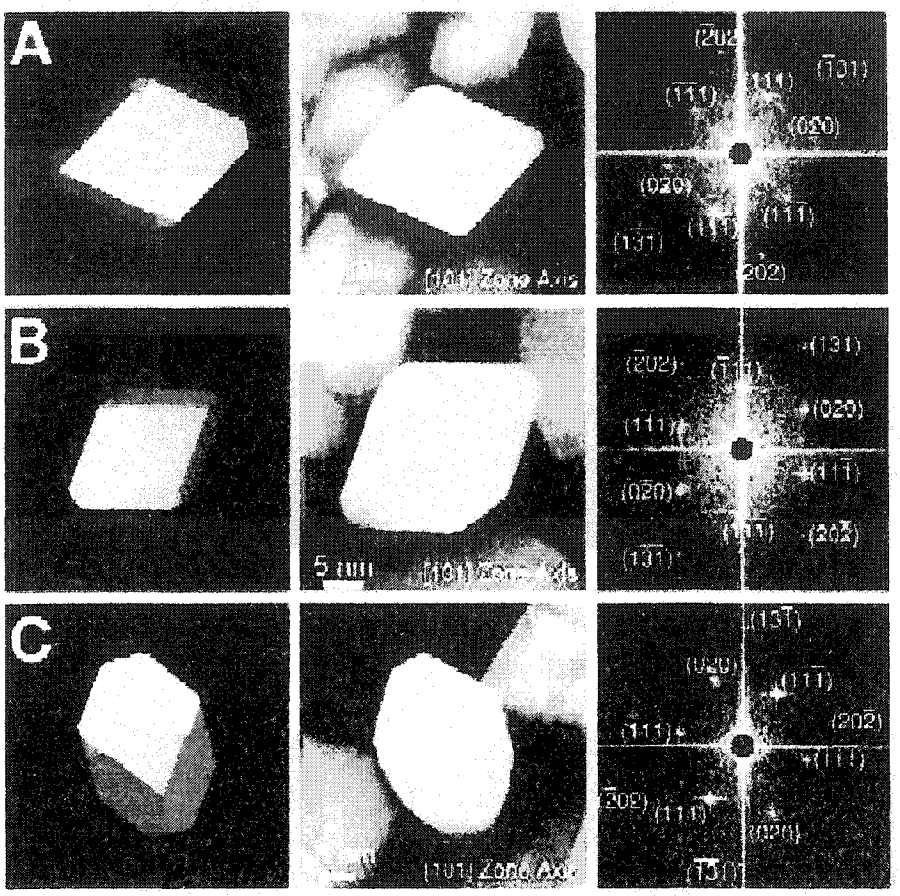

Figure 5.3: Truncated hexa-octahedron representation, transmission electron micrograph, and fast Fourier transform for each of three magnetite crystals (A to C) extracted from magnetotactic bacterial strain MV-1. All of the crystals are viewed down the [101] zone axis and have a diamond-shaped outline. Variations in appearance are due to differences in the sizes of the displayed {110} (red) and {100} (blue) faces. The widths of the {110} faces range from _3 to 10 nm, and the widths of the {100} range from _3 to 8 nm. The {100} faces correspond to the {200} crystallographic lattice planes, and the {110} faces correspond to the {220} crystallographic lattice planes, as shown in the micrographs. (A) Magnetite that is _30 nm long. The $(1\bar{0}1)$,$(10\bar{1})$,$(01\bar{0})$,(010) faces are _3 nm wide. (B) Magnetite that is _35 nm long. This crystal is slightly asymmetric, having an upper $(1\bar{0}1)$ face that is

_5 nm wide and a lower ($10\bar{1}$) face that is _8 nm wide. The ($01\bar{0}$) and (010) faces are _5 nm wide. (C) Magnetite that is _30 nm long with ($1\bar{0}1$) and ($10\bar{1}$) faces that are _10 nm wide and (010) and ($01\bar{0}$) faces that are _6 nm wide (Leshin, L. A. 2000).

Magnetite crystals are chemically pure, containing only Fe and O at detectable levels (.150 ppm). Bacterial Fe-acquisition (siderophore) systems are generally specific for their uptake of Fe (Meyer, 1998), although this depends on the relative availability of Fe relative to other elements that can be complexed by the siderophore. Such chemical specificity is typical of bacterial pathways for Fe acquisition and transport, which involve multiple chelation and redox steps linked with adenosine triphosphate-coupled transport across lipid-bilayer membranes (Gooding and al., 1991). These elements, common as impurities in inorganic magnetite are not detected in biogenic magnetite. Biogenic magnetites have few crystallographic defects that act to attenuate the crystal's ferromagnetic properties and the occasional twin in the {111} plane (Devouard and al., 1998; Chang and al., 1989). The absence of such defects has no effect on the magnetic properties because the unpaired Bohr magnetosomes in the crystal remain aligned perpendicular to the twin plane. The lack of lattice defects acts to optimize the net magnetic moment of the magnetite crystal. Consequently, the ability to grow defect-free crystals is also likely a product of natural selection.

Populations of magnetite are characterized by having a specific crystal habit being elongated prismatic (a term that should be avoided in the future because it is inconsistent with actual morphology) or hexa-octahedral, emphasizing that the crystal

has six {110} hexagonal faces and eight {111} octahedral faces (George W. Hart, personal communication) (Figure 5.3 and 5.4). The term hexa-octahedron does not strictly describe the magnetite crystals on further transmission electron-microscope (TEM) analysis. Rather, we suggest that the crystal habit can now be better described as a *truncated* hexa-octahedron (George W. Hart, personal communication). This modified crystal habit has not previously been recognized for biogenic magnetite (Bazylinsk et al., 1997).

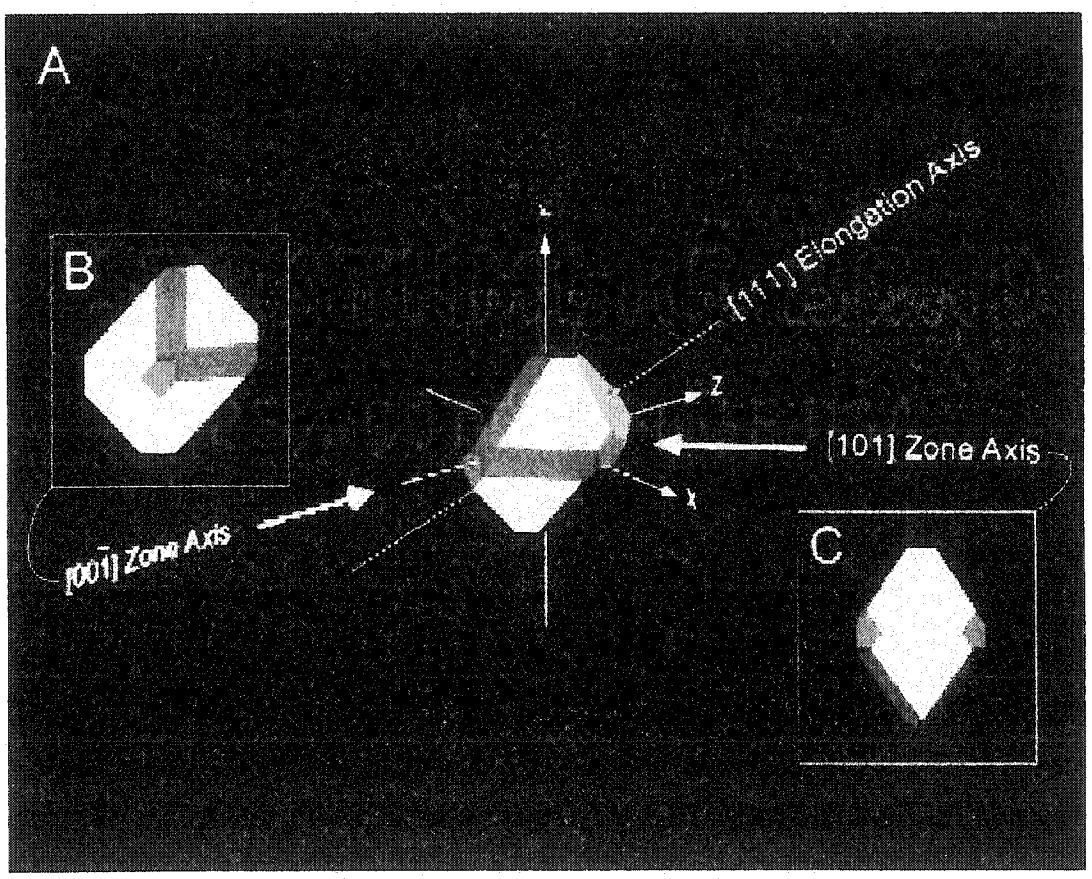

Figure 5.4: (A) Idealized schematic representation of a magnetite crystal displaying a truncated hexa-octahedral geometry with eight {111} octahedral (green) faces, six {110} dodecahedral (red) faces, and six {100} cubic (blue) faces. This is the most

commonly observed geometry of magnetite crystals isolated from magnetotactic bacterial strain MV-1. The principal Cartesian axes (*x*, *y*, and *z*) are indicated in crystallographic nomenclature which corresponds to the [100],[010],[001] zone axes. The crystal is elongated along the [111]7[$1^{-}1^{-}1^{-}$] axis, as shown by the green vector transecting the crystal. Note that because of the symmetry of the truncated hexa-octahedral geometry, all expressed {110} faces, shown in red, are equivalent [i.e., ($11^{-}0$),($1^{-}10$),(101^{-}),($1^{-}01$),(011^{-}),($01^{-}1$)]. (B) Crystal viewed in the [001^{-}] direction. Note that the truncated hexa-octahedral geometry displays six equivalent {100} faces, shown in blue [(100),(010),(001),($1^{-}00$),($01^{-}0$),(001^{-})]. (C) Crystal viewed down the [101] axis. The truncated hexa-octahedron representation has a characteristic diamond-shaped outline. This orientation displays the width of two parallel {100} and two parallel {110} faces. Analyses of multiple individual biogenic magnetite crystals indicate that the degree of truncation (i.e., the size of the {100} faces) of the hexa-octahedral biogenic magnetite is variable between crystals (Fig. 1*b*). This truncated hexaoctahedral habit can be verified by rotating magnetites 6 45° in a TEM. The {110} form is a dodecahedron; however, in the context discussed here only six of the possible twelve {110} faces are expressed. So these six faces are described as ''hexa-octahedral,'' even though this is not strictly correct in a crystallographic context (Bazylinski et al., 1997).

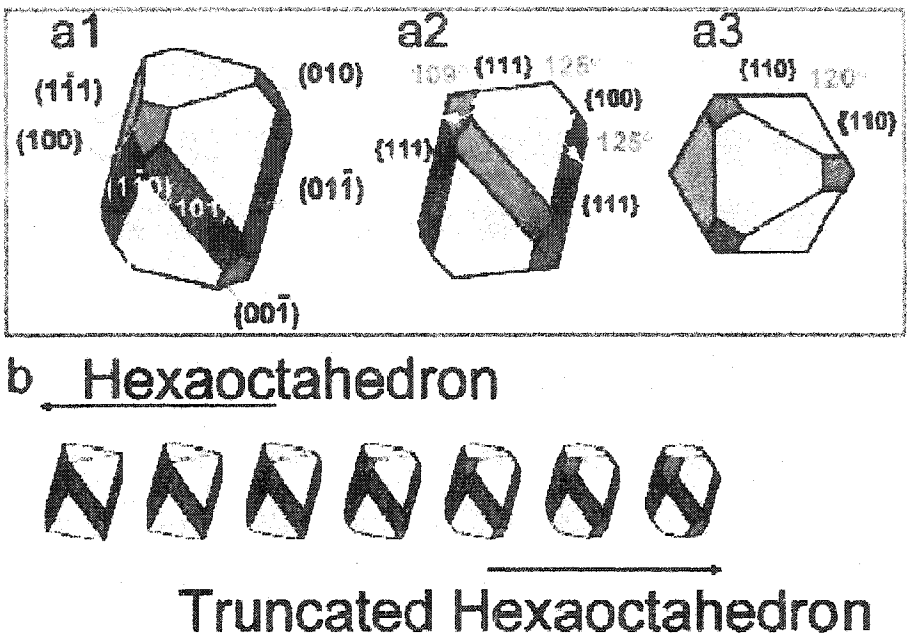

Figure 5.5: Idealized truncated hexa-octahedral crystal habit of magnetite from the magnetotactic bacterium strain MV-1. Previous reports describing the biogenic crystal habit misidentified this type of crystal, defining it as a hexa-octahedron. [Note: In the microbiological community these crystals have been referred to as "parallelepiped"(ref. 10).] Magnetite with hexa-octahedral crystal habit is elongated along one of the [111] axes, with eight {111} octahedral (green) faces and six {110} hexagonal (red) faces (see supplemental data, Fig. 4 *b1–b3*). In contrast, magnetite with truncated hexa-octahedral crystal habit has eight {111} octahedral faces, six {110} hexagonal faces, and six {100} cubic (blue) faces. The two {111} faces perpendicular to the axis of elongation are equivalent to each other but not to the remaining six {111} faces that are not parallel to the elongation axis. Other biogenic magnetite geometries reported in the literature include elongated cubo-octahedrons

(in wild-type bacteria), hexa-octahedrons (in vibroid bacteria), and hexa-octahedrons (in cocci), (*a1*) Orthographic projection of a truncated hexa-octahedron. (*a2*) Truncated hexa-octahedron viewed down the [1–10] zone axis. (*a3*) Truncated hexa-octahedron viewed down the [111] zone axis. (*b*) The transition from hexa-octahedral to truncated hexa-octahedral crystal habit is achieved by adding cubic {100} faces (blue surfaces). The degree of truncation appears variable in the biogenic magnetites, with hexa-octahedral crystal habit being one end member (far left) of the progression shown here (Bazylinski and Moskowitz, 1997).

Evolution special feature

In figure 5.4, the 3-D geometry of a single biogenic magnetite crystal is observed with four rotation angles spanning '60°. The 3-fold symmetry and presence of {100} faces is indicative of the truncated hexa-octahedral habit. Both populations of magnetite crystals are elongated along the zone axis [111] (Figures 5.5 and 5.6). This elongation increases the magnetic stability of the crystal (the microscopic coercivity) by aligning the directions of the minimum magnetocrystalline and shape anisotropy energies and enlarging the single-domain stability field (Chang and Kirschvink, 1989; Blakemore, 1975).

Biogenic magnetite crystals are aligned in chains within living cells. In this configuration the magnetic dipole moment of the cell is maximized because the overall magnetic moment of the cell is the sum of the dipole moments of the individual magnetite crystals. When the organism dies the magnetosome membrane decomposes, and the chain collapses to dissipate the magnetostatic potential energy.

Thus, biogenic magnetites from dead organisms embedded in both contemporary and ancient samples rarely show evidence of their former arrangement in chains (Blakemore, 1975).

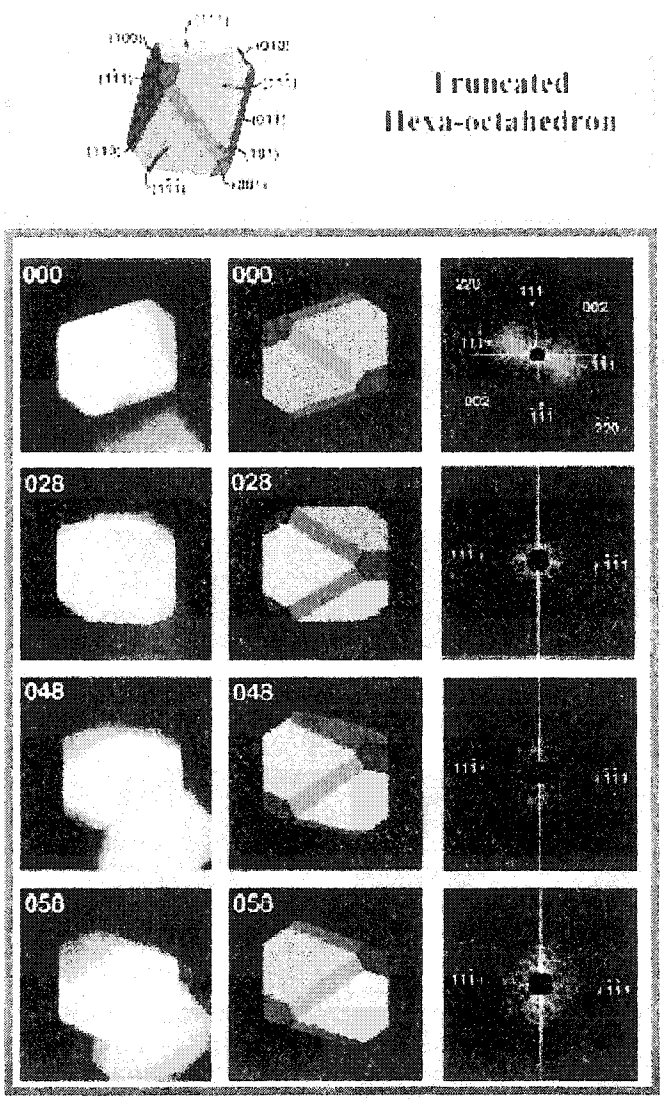

Figure 5.6: Idealized truncated hexa-octahedral crystal habit of magnetite (green box). A truncated hexaoctahedron is elongated along one of the [111] zone axes and displays eight {111} octahedral (green), six {110} dodecahedral (red), and

six {100} cubic (blue) faces. Example of a single truncated hexa-octahedral MV-1 magnetite examined under incremental TEM stage rotation (red box). Magnetite at 000° is viewed down the [1-10] zone axis. At 058° (~60° rotation) the same magnetite is now viewed approximately down the [-101] zone axis (mirror image of crystal at 000°). Rotation axis is perpendicular to the plane of the page and aligned vertically(Chang, S.-B. R. & Kirschvink, 1989; Blakemore, 1975).

The mineral magnetite

Chemical Formula: Fe3O4, Iron Oxide

Class: Oxides and Hydroxides

Group: Spinel

Uses: Major ore of iron and as mineral specimens

Magnetite is a natural magnet, hence the name, giving it a very nice distinguishing characteristic. Electricity produces magnetic fields just as magnetism produces electric fields. Magnetite is a member of the spinel group which has the standard formula A(B)2O4. The A and B represent usually different metal ions that occupy specific sites in the crystal structure. In the case of magnetite, Fe3O4, the A metal is Fe+2 and the B metal is Fe+3; two different metal ions in two specific sites. This arrangement causes a transfer of electrons between the different irons in a structured path or vector. This electric vector generates the magnetic field.

Magnetic Mineral Magnetism

There are three classes of magnetic minerals; Diamagnetic, Paramagnetic and Ferromagnetic. Each type of mineral can be characterized by its behavior in a magnetic field:

-**Paramagnetic** minerals are attracted towards a positive magnetic field gradient. The attraction into a magnetic field is due to permanent magnetic dipole moments within the paramagnetic mineral, which are normally randomized by thermal activity. An external magnetic field supplies the necessary energy to align the magnetic dipoles. The randomization due to thermal activity still persists within a magnetic field, so the number of the materials magnetic dipoles aligned with the external field, and hence the force of attraction, depends on both the temperature and the strength of the applied field. When a paramagnetic mineral is removed from a magnetic field it immediately loses its magnetism.

-**Diamagnetic** minerals are repelled from a positive magnetic field gradient. The repulsion of a diamagnetic mineral from a magnetic field is caused by the generation of a magnetic dipole moment, within the atoms of the mineral, by the disruption of their electron orbits due to the presence of the magnetic field. The repulsion of a diamagnetic mineral from a magnetic field gradient is far smaller than the attraction of a paramagnetic mineral. Like a paramagnetic mineral, a diamagnetic mineral loses its internal magnetic field once it has been removed from an external magnetic field.

-**Ferromagnetic** minerals are attracted into a positive magnetic field gradient. The attraction for ferromagnetic minerals, however, is far larger than it is for paramagnetic minerals. Ferromagnetic minerals have internal magnetic dipole

moments, due to the spin of electrons within the minerals. For ferromagnets, however the individual dipoles within the mineral, when aligned by an external magnetic field, will tend to remain aligned even when the field is subsequently removed due to quantum mechanical effects arising from the ferromagnetic minerals crystal lattice structure. This remanence leads to magnetic hysteresis, where the ferromagnet remembers past applied fields. A hysteresis loop for a ferromagnetic mineral showing the relationship between applied magnetic field and mineral magnetization is shown in in figure 5.7.

It has also been found that magnetotactic bacteria often have super paramagnetic magnetosomes within their bodies. These magnetosomes have not yet reached single domain size (Moskowitz et al., 1993).

Hysteresis

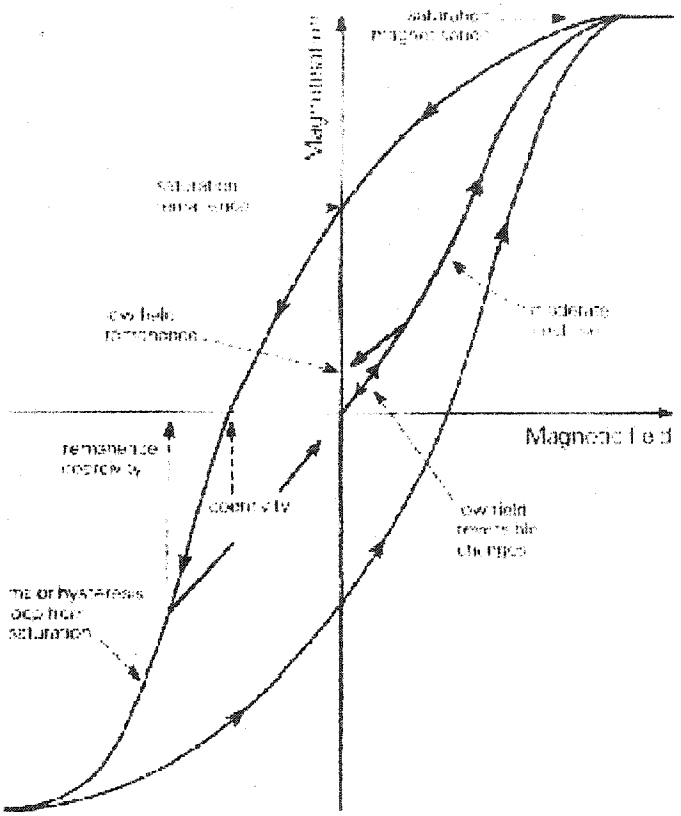

Figure 5.7: Magnetic hysteresis loop with initial magnetization curve (Thompson and Oldfield, 1986)

The magnetic properties of a ferromagnet depend not only on the present conditions affecting it, but also on the past magnetic field to which it has been subjected. In figure 5.7, the magnetic field that a ferromagnetic material is being subjected is plotted on the horizontal axis, against the magnetization induced within the material

on the vertical axis. Also plotted is the low, field magnetic behavior. Up to a certain applied magnetic field the material exhibits no hysteresis effects and when the external field is removed the material returns to an unmagnetised state.

Some important parameters on the hysteresis curve are: Saturation magnetization, which is the largest magnetization that can be imparted to a given ferromagnetic mineral; saturation remanence, which is the remanent magnetization of a material that has been magnetized in a saturating field; Coercive force, which is the magnetic field that has to be applied to reduce the saturation remanence to zero magnetization when measurement is made in the presence of the field (Thompson and Oldfield, 1984).

Ferrimagnetisms and Antiferrimagnetism

The majority of natural magnetic minerals with which palaeomagnetism and environmental magnetism are concerned are the ferrimagnets and imperfect antiferromagnets. Ferrimagnets, and imperfect antiferromagnets, are special classes of ferromagnets that owe their magnetic properties to the alignment of the electrons, in their 3d shell. The relative direction and intensity of the magnetic dipoles of individual atoms at different crystal sites, and the interactions between these sites, determines the different classes of magnetic properties of the ferrimagnetic and antiferromagnetic minerals. The various types of ferrimagnets and antiferromagnets and their crystal lattice interactions are best represented graphically (Figure 5.8).

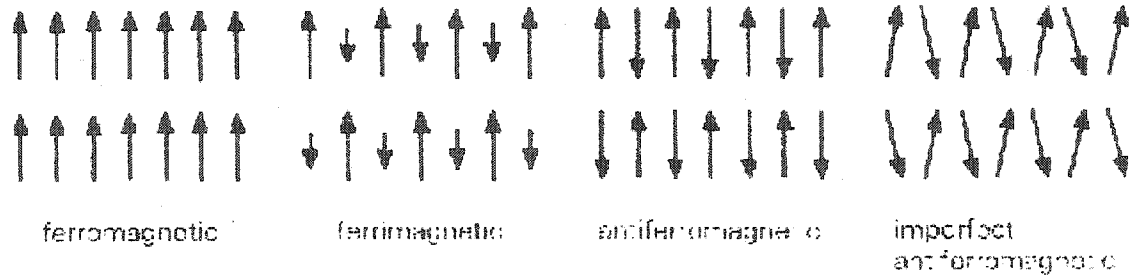

Figure 5.8: Arrangement of magnetic moments in ferrimagnets ferromagnets and anti-ferromagnets (Stacey 1992).

Ferrimagnetic minerals have two types of magnetic crystal lattice sites that naturally align antiparallel. The net magnetic moment within the ferrimagnet is due to either a difference in the ionic make up of different crystal sites, or a crystallographic inhomogeneity between different sites. In antiferromagnetic minerals there are again two different magnetic crystallographic sites, however the magnetic moments of the ions at different sites entirely cancel each other, hence leaving no net magnetic moment. A net magnetic moment can only exist within an antiferromagnet if its individual magnetic ion sites are not entirely antiparallel, this is called imperfect or canted antiferromagnetism. In practice ferrimagnets have strong magnetic properties and moderate coercivities. Imperfect antiferromagnets have weaker magnetic properties but very high coercivities (Figure 5.8). These differences can be used to detect them in natural materials (Thompson and Oldfield, 1984).

Temperature

Ferromagnetism is a temperature dependent phenomenon. In fact ferromagnetism and paramagnetism are at different ends of a thermal energy / magnetic energy scale. At a

low enough temperature, paramagnetic behavior can become ferromagnetic due to the lack of randomizing thermal energy. Likewise at a high enough temperature ferromagnets can become paramagnetic due to thermal energy randomizing the direction of individual ionic dipoles. The temperature at which ferromagnetism breaks down is called the Neel or Curie Temperature and is dependent on mineral composition. Indeed it is often used to identify minerals (Thompson and Oldfield, 1984).

Magnetic Grain Size

Magnetic crystal grain size is a balance between opposing energies as with temperature. For ferromagnetic minerals there are four different balancing points that are dependent on the size of magnetic crystals. For very small ferromagnetic crystals the effect of thermal randomization is stronger than for larger crystals. This leads to a phenomenon called super paramagnetism. As the name suggests these very small minerals exhibit strong paramagnetic properties, and cannot retain remanences.

Super viscous materials are in a grain size between superparamagnetic and single domain, they can hold remanence but will lose it over a short period of time, the exact amount of time depends on the grain size. Both super paramagnetic and super viscous minerals both exhibit a property called frequency-dependent susceptibility. When a frequency dependent sample is subjected to a high-frequency field there is a time lag between the maximum in the field strength and the reaction of the sample, this leads to super paramagnetic particles having a lower susceptibility when measured in high frequency fields (Thompson and Oldfield, 1984).

The next higher size class is the single stable domain crystal. In these grains the thermal energy is overcome by the magnetic energy of larger volume crystals and stable magnetic moment results. When the size is increased again the crystal continues to try and minimize its magnetic energy. In large crystals the division of the magnetic moment into two or more magnetic domains can accomplish this. These domains will substantially reduce the overall magnetic moment of the crystal, and in many cases take it to zero. These large crystals are referred to as multidomain grains (Thompson and Oldfield, 1984).

The relative "hardness" of ferromagnetic minerals can be linked to their magnetic crystal size. A sample consisting of predominantly single domain crystals will be relatively hard and requires high fields to influence its magnetic remanence. On the other hand a sample containing mostly multidomain grains will be magnetically soft and it will be easy to impart a remnant magnetization. There is also an intermediate state in which most of the magnetic crystals have only two or three domains. Intermediate hardness crystals are sometimes called pseudo single domain crystals as they have many properties that are somewhat similar to single domain crystals, but lower magnetic intensities (Thompson, and Oldfield, 1984).

Magnetic Parameters

There are three common magnetic measurements that are referred to in this report, these are:

- Susceptibility
- Isothermal remanent magnetization (IRM)

- Anhysteritic remanent magnetization (ARM)

Susceptibility. The susceptibility of a sample is the ratio of the magnetic field induced within a sample to the magnetic field required to produce the magnetization.

Isothermal remanent magnetization. The IRM of a sample is the magnetization retained by that sample when it has been subjected to a known field at a known temperature (usually room temperature). IRM can be measured at varying fields, typically between 20mT and 3T. By increasing the field that a sample is subjected to in stages and measuring between each stage, it is possible to gain a lot of information about a sample. The saturation IRM or SIRM is the maximum remanence that a sample can acquire by IRM magnetization. SIRM alone can be very indicative of the composition of a material, for instance magnetite will usually reach saturation at approximately 300mT, whereas Hematite is often still unsaturated at applied fields of 2T or 3T. However the overall shape of the IRM curve (the IRM's gained through several successive and increasing magnetizations) contains information about the magnetic properties of a sample. For instance the sample's hardness (a term that describes the relative ease or difficulty with which a sample is magnetized) and an insight into its constituent minerals.

Anhysteritic remanent magnetization. The ARM of a sample, sometimes called perfect magnetization, is similar to the IRM in that it is a measurement of the magnetization of a sample after it has been subjected to a known field. However the ARM field is not applied in the same way as with IRM. Instead of a steady field being applied to the sample, it is magnetized within an alternating magnetic field, with a

steady (d.c.) field applied over the top of ac field, the ac field is increased to a known maximum and then slowly decreased back to zero. The aim of ARM is to drive the magnetization of the sample backward and forward around the origin of its hysteresis loop, while magnetizing it with a small steady field. ARM is generally imparted at a high alternating field measured and then demagnetized using smaller alternating fields, without the application of the steady field. The demagnetization of the sample using known fields builds up an ARM curve, this gives similar information to the IRM curve, however ARM properties are strongly influenced by grain size, and of some minerals ARM the properties are very distinctive.

PHYSICAL CHARACTERISTICS OF MAGNETITE MINERAL:

Color is black.

Luster is metallic to dull.

Transparency: Crystals are opaque

Crystal System is isometric; 4/m bar 3 2/m

Crystal Habits are typically octahedrons but rarely rhombododecahedron or other isometric forms, most commonly massive or granular. Twinning of octahedrons into spinel law twins is seen occasionally.

Cleavage is absent although octahedral parting can be seen on some specimens.

Fracture is conchoidal.

Hardness is 5.5 - 6.5

Specific Gravity is 5.1+ (average for metallic minerals)

Streak is black.

Associated Minerals are talc and chlorite (schists), pyrite and hematite.

Other Characteristics: Magnetism stronger in massive examples than in crystals, striations on crystal faces (not always seen).

Notable occurrences include South Africa, Germany, Russia and many localities in the USA.

Best field indicators are magnetism, crystal habit and streak.

The Oxides Class

The oxide class of minerals is a rather diverse class. It includes minerals that are quite hard (corundum) and some that are quite soft such as psilomelane. It includes metallic minerals such as hematite and gemstones such as corundum, chrysoberyl and spinel. Many oxides are black but others can be very colorful. The large diversity of oxides can be partially attributed to the abundance of oxygen in the Earth's crust. Oxygen comprises over 45% of the Earth's crust by weight. Most of this is locked up in more complex minerals based on chemical complex anions such as CO_3, BO_3, SO_4, NO_3, SiO_4, PO_4 and others (Thompson, and Oldfield, 1984).

Great opportunities exist for single oxygen ions to combine with various elements in many different ways. In a strict sense, minerals that belong to the more complex mineral classes such as the silicates are really oxides. It would be cumbersome for mineralogists to be able to deal with only the four different classes of the elements, such as the halides class, the sulfides class and finally the extremely large oxide class with all of its many subclasses and over 90% of all known minerals. By convention therefore, the oxides are limited to non-complex minerals containing oxygen or

hydroxide. Oxides also contain mostly ionic bonds and this helps to distinguish members from the more complex mineral classes whose bonds are typically more covalent in nature. Quartz, SiO2, would be considered an oxide, and still is in some mineral guides and texts, except for its covalent silicon oxygen bonds and its structural similarity to the other Tectosilicates.

Hydrogen in the positive one (+1) state is really only a single proton and is so small that when it combines with oxygen it disappears into the oxygen and the resulting OH group is almost the same size as a single oxygen ion with a negative two (-2) charge. Hence the OH group can fit into many crystal sites that oxygen would otherwise occupy, but with a charge of only negative one (-1). The crystal would then need to be balanced by additional negative charges or fewer positive charges.

Oxides:

Aeschynite *(Rare Earth Yttrium Titanium Niobium Oxide Hydroxide)*

Anatase *(Titanium Oxide)*

Bindheimite *(Lead Antimony Oxide Hydroxide)*

Bixbyite *(Manganese Iron Oxide)*

Brookite *(Titanium Oxide)*

Chrysoberyl *(Beryllium Aluminum Oxide)*

Columbite *(Iron Manganese Niobium Tantalum Oxide)*

Corundum *(Aluminum Oxide)*

Cuprite *(Copper Oxide)*

Euxenite *(Rare Earth Yttrium Niobium Tantalum Titanium Oxide)*

Fergusonite *(Rare Earth Iron Titanium Oxide)*

Hausmannite *(Manganese Oxide)*

Hematite *(Iron Oxide)*

Ice *(Hydrogen Oxide)*

Ilmenite *(Iron Titanium Oxide)*

Perovskite *(Calcium Titanium Oxide)*

Periclase *(Magnesium Oxide)*

Polycrase *(Rare Earth Yttrium Titanium Niobium Tantalum Oxide)*

Pseudobrookite *(Iron Titanium Oxide)*

The Pyrochlore Group

Betafite *(Rare Earths Calcium Sodium Uranium Titanium Niobium Tantalum Oxide Hydroxide)*

Microlite *(Calcium Sodium Tantalum Oxide Hydroxide Fluoride)*

Pyrochlore *(Sodium Calcium Niobium Oxide Hydroxide Fluoride)*

Ramsdellite (Manganese Oxide)

Romanechite *(Hydrated Barium Manganese Oxide)*

The Rutile Group

Cassiterite *(Tin Oxide)*

Plattnerite *(Lead Oxide)*

Pyrolusite *(Manganese Oxide)*

Rutile *(Titanium Oxide)*

Stishovite *(Silicon Oxide)*

Samarskite-(Y) *(Rare Earth Yttrium Iron Titanium Oxide)*

Senarmontite *(Antimony Oxide)*

The Spinel Group

Chromite *(Iron Chromium Oxide)*

Franklinite (*Zinc Aluminium)*

Gahnite *(Zinc Aluminum Oxide)*

Magnesiochromite *(Magnesium Chromium Oxide)*

Magnetite *(Iron Oxide)*

Spinel *(Magnesium Aluminum Oxide)*

Taaffeite *(Beryllium Magnesium Aluminum Oxide)*

Tantalite (Iron Manganese Tantalum Niobium Oxide)

Tapiolite (Iron Manganese Tantalum Niobium Oxide)

Uraninite *(Uranium Oxide)*

Valentinite *(Antimony Oxide*

Zincite *(Zinc Manganese Oxide)*

Subclass: Hydroxides

Brucite *(Magnesium Hydroxide)*

Gibbsite *(Aluminum Hydroxide)*

Goethite *(Iron Oxide Hydroxide)*

Limonite *(Hydrated Iron Oxide Hydroxide)*

Manganite *(Manganese Oxide Hydroxide)*

Psilomelane *(Barium Manganese Oxide Hydroxide)*

Romeite *(Calcium Sodium Iron Manganese Antimony Titanium Oxide Hydroxide)*

Stetefeldtite *(Silver Antimony Oxide Hydroxide)*

Stibiconite *(Antimony Oxide Hydroxide)*

The Spinel Group

The spinels are a group of oxides that have very similar structures. The spinel group contains over twenty members, but only a few are considered common. Named after their sole gemstone representative, spinel, this is an important group of minerals. It includes one of the most important ores of iron, magnetite; an important ore of chromium, chromite, an important ore of lead, minium; a once important ore of manganese, iron and zinc; franklinite and many other interesting members. The general formula of the Spinel Group is AB_2O_4. The A represents a divalent metal ion such as Magnesium, Iron, Nickel, Manganese and/or Zinc. The B represents trivalent metal ions such as Aluminum, Iron, Chromium and/or Manganese, Titanium may also occupy this site with a +4 charge and lead at +2 can occupy this site. Solid

solutioning is common in this group of minerals, meaning that they may contain certain percentages of different ions in any particular specimen.

The structure of spinel is based on the structure of diamond, which has the same high symmetry, 4/m bar 3 2/m. The position of the A ions is nearly identical to the positions occupied by carbon atoms in the diamond structure. This could explain the relatively high hardness and high density typical of this group. The arrangement of the other ions in the structure conforms to the symmetry of the diamond structure. But, they disrupt the cleavage as there is no cleavage direction in any member of this group. The arrangement of the ions also favors the octahedral crystal habit, which is the predominant crystal form and is in fact the trademark of the spinels. All members of this group that share the spinel structure show the same type of twinning that is named after spinel, called the ***Spinel Law.***

These minerals are some of the more common minerals of the Spinel Group

Chromite *(Iron Chromium Oxide)*

Franklinite *(Zinc Iron Manganese Oxide)*

Gahnite *(Zinc Aluminum Oxide)*

Magnesiochromite *(Magnesium Chromium Oxide)*

Magnetite *(Iron Oxide)*

Minium *(Lead Oxide)*

Spinel *(Magnesium Aluminum Oxide)*

We concluded that truncated hexa-octahedral magnetites on Earth are exclusively the product of biogenic activity - no natural or synthetic inorganic process is known that could explain the observation of truncated hexa-octahedral magnetites in a terrestrial sample.

The probability that an inorganic magnetite will, by chance, meet all these criteria is virtually zero. Biogenic magnetite can certainenly be distinguished from inorganic magnetite. This make it a biogenic sinature..

CHAPTER 6: MAGNETOTACIC BACTERIA THAT DEPOSIT MAGNETITE AND/OR IRON SULFIDE

Introduction

Richard P. Blakemore discovered magnetotactic bacteria in 1975. Blakemore noticed that some of the bacteria that he observed under a microscope always moved to the same side of the slide. If he held a magnet near the slide, the bacteria would move towards the resultant of the bacteria moment and the north end of the magnet. These bacteria are able to do this because they make tiny, iron-containing, magnetic particles. Each of these particles is a magnet with a north pole and a south pole. The bacteria arrange these tiny magnets in a line to make one long magnet. They use this magnet as a compass to align themselves to the earth's geomagnetic field.

Magnetotactic Bacteria

Magnetotactic bacteria (MTB) orient themselves and migrate along the geomagnetic field towards favorable habitats, a behavior known as magnetotaxis (Figure 6.1). Since the first report of magnetotactic bacteria by Blakemore (1975), subsequent studies have shown that MTB are a morphologically diverse and cosmopolitan group of aquatic microorganisms inhabiting freshwater and marine environments ranging from aerobic to anoxic. Three significant findings since the last US Geological Survey report (1998) on biomineralization are (1) an increase in the types of environments where MTB are found besides microaerobic to include anaerobic and aerobic (Bazylinski, 1990; Matsunaga et al., 1991; Sakaguchi et al., 1993); (2) an

increase in the number of identified phases besides magnetite (Fe3O4) to include ferrimagnetic greigite (Fe3S4), possible pyrrhotite (FeS), and non-magnetic pyrite (FeS2) (Mann et al., 1990a; Farina et al., 1990; Bazylinski, 1990); and (3) the discovery of non-magnetotactic magnetite producing bacteria.

In natural habitats, large populations of MTB are usually found near the oxic-anoxic transition zone, which is usually located at the sediment-water interface in freshwater environments or displaced upward into the water column in marine semi-anaerobic environments (Stolz, 1992; Bazylinski and Frankel, 1992).

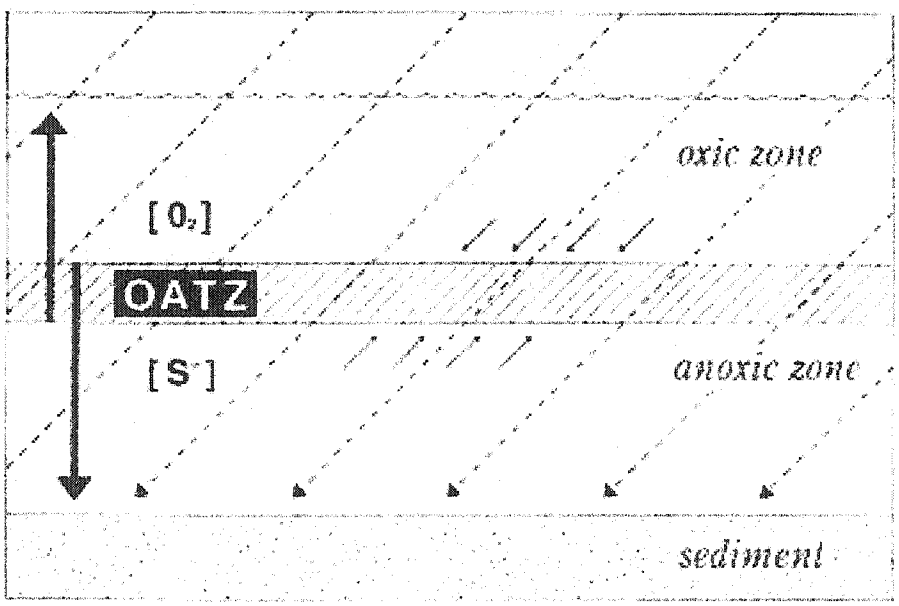

Figure 6.1: Oxic-Anoxic Tranistion Zone (OATZ) at sediment/water interface

In the latter types of environment, magnetites and greigites producing MTB exist in horizontal zones at specific water depths depending on the vertical chemical and redox gradients (Stolz, 1992; Bazylinski, 1991). Petermann and Bleil (1993) identify several different types of living MTB in deep-sea sediments from the South Atlantic, some at water depths of 2000 m. Magnetic bacteria containing intercellular magnetite particles have also been identified in the uppermost horizon of a waterlogged soil in Germany (Fassbinder et al., 1990). Although population densities of the magnetic bacteria were too low at the time of sampling to contribute significantly to the magnetism of the soil, the authors suggest that population densities can change dramatically depending on microenvironmental conditions. However, the question of a biogenic magnetic component in soil must await further confirmation and study.

Magnetotactic bacteria from reducing environments with high concentrations of HS contain Fe-sulphide particles instead of Fe-oxides (Mann et al., 1990; Farina et al., 1990; Bazylinski and Frankel, 1992). The sulphide minerals were identified by indexing single crystal electron diffraction patterns (Mann et al., 1990). Several types of bacteria have been studied including a rod shaped bacterium containing only greigite particles (Bazylinski, 1990), a multicellular magnetotactic prokaryote (MMP) containing a mixture of greigite and pyrite particles (Mann et al., 1990), and another bacterium containing both magnetite and greigite particles (Bazylinski et al., 1993). In another study, ferrimagnetic pyrrhotite (FeS) was proposed as the iron-sulfide mineral in a similar (or perhaps the same) MMP from Brazil (Farina et al., 1990). No single crystal diffraction patterns have yet been obtained that

unequivocally identify the phase as pyrrhotite, so the report of FeS in MTB remains problematical. Finally, Sakaguchi et al. (1993) report a magnetotactic sulphate-reducing bacterium that produces intercellular magnetite and extracellular magnetic iron-sulfide particles. This discovery extends the range of magnetite producing microorganisms to sedimentary levels where sulphate reduction occurs.

Modes of Biomineralization and Biomimetics

Two fundamentally different modes of biomineralization are summarized by Lowenstam and Weiner (1989) (Figure 6.2). One is called biologically induced mineralization (BIM), in which an organism modifies its local microenvironment creating conditions suitable for the chemical precipitation of extracellular mineral phases. The second mode is called boundary organized biomineralization (BOB), in which inorganic particles are grown within or on some organic matrix produced by the organism (Mann et al., 1989).

Bacteria that produce mineral phases by BIM do not strictly control the crystallization process, resulting in particles without a unique morphology and a broad particle size distribution. Non-magnetotactic dissimilatory iron-reducing and sulfate-reducing bacteria produce magnetite, siderite, vivianite, and iron-sulfides by BIM processes (Lovley, 1990; Bazylinski and Frankel , 1992). For example, the iron-reducing *bacterium Geobacter metallireducens* (formerly GS-15) is a non-magnetotactic anaerobe that couples the oxidation of organic matter to the reduction of ferric iron, inducing the extracellular precipitation of fine grained magnetite as a byproduct. In laboratory culture, GS-15 can produce 5000 times more magnetite by weight than an

equivalent biomass of magnetotactic bacteria. However, magnetic measurements show that most of the particles GS-15 produced are within the magnetically unstable, superparamagnetic (SPM) size range for magnetite (<20 nm) at room temperature.

In contrast to BIM, bacteria that produce mineral phases by a BOB process exert strict control over size, morphology, composition, position, and crystallographic orientation of the particles (Mann et al., 1990; Frankel and Mann , 1993). The archetypical example of microorganisms using BOB processes to produce iron biominerals are magnetotactic bacteria. These bacteria synthesize intracellular, membrane-bounded O, Fe, S, and FeS particles called magnetosomes (Figure 6.2). Various arrangements of magnetosomes within cells impart a permanent magnetic dipole moment to the cell, which effectively makes each cell a self-propelled biomagnetic compass. The study of the biomineralization of magnetite magnetosomes has been aided by the isolation and axenic culture of several different magnetotactic bacteria (Bazylinski, 1990; Meldrum et al. , 1993; Sakaguchi et al., 1993). Unfortunately, most iron sulfide MTB have yet to be isolated and grown in pure culture.

Much of the current research in biomineralization is directed towards identifying, mimicking, or duplicating BOB-type processes in order to produce tailor-made inorganic materials (Mann, 1993). In several species of MTB, the magnetite particles are enveloped in a membrane structure that anchors the mineral particles at particular locations in the cell and provides an enclosed microenvironment for precise biological control of magnetosome size and morphology (Mann et al., 1990; Frankel and Mann , 1994). The most common magnetosome arrangement is one or more

linear chains traversing the long axis of the cell (Mann, 1990; Frankel and Bazylinski , 1994). How the bacteria accomplish this is not presently understood, but the bioarchitectural framework of assemblies of aligned magnetic particles in MTB clearly has artificial counterparts in the manufacture of permanent magnets (Frankel and Bazylinski, 1994). Biomimetics is a new interdisciplinary field that seeks to understand relationships between structures and functions of biological composites in order to design and synthesize new materials, perhaps without the toxic residues characteristic of non-biological modes of industrial mass production (Sarikaya, 1994; Mann, 1993). This research may lead to the synthesis of novel magnetic, electronic, or magnetopharmaceutical materials on a nanometer scale.

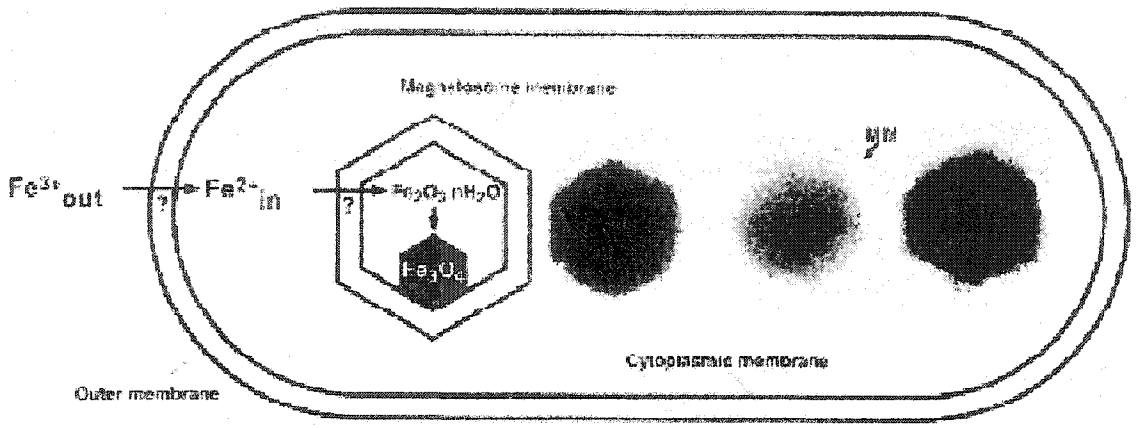

Figure 6.2: Proposed Model for Magnetite Biomineralization in *Magnetospirillum* species. Fe(III) is actively taken up by the cell, possibly via a reductive step. Iron is then thought to be reoxidized to form a low-density hydrous oxide which is dehydrated to form a high-density Fe(III) oxide (ferrihydrite). In the last step, one-third of the Fe(III) ions are reduced, and with further dehydration, magnetite is produced within the magnetosome vesicle. The magnetosome membrane contains specific proteins, which are thought to have crucial functions in the accumulation of iron, nucleation of minerals and redox and pH control. The electron micrograph shows magnetosome particles from *Magnetospirillum gryphiswaldense* (Lowenstam and Weiner, 1989).

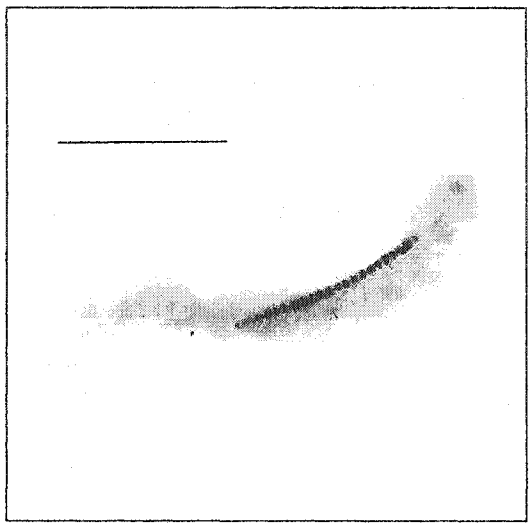

Figure 6.3: Transmission electron micrograph of *Magnetospirillum magnetotacticum* showing the chain of magnetosomes inside the cell. The magnetite crystals incorporated in the magnetosomes have cuboctaheral morphology and are ca. 42 nm long. The magnetosome chain is fixed in the cell and the interaction between the magnetic dipole moment associated with the chain and the local magnetic field causes the cell to be oriented along the magnetic field lines. Rotation of the cellular flagella (not shown) causes the cell to migrate along the field lines. Bar equals 1 micron (Bazylinski, 1990; Sakaguchi et al., 1993).

Why would these bacteria need a compass? Like many other types of bacteria, magnetotactic bacteria don't like oxygen very much. They will move away from areas with high oxygen and toward areas with low or no oxygen. In an aquatic environment, the level of oxygen decreases as one moves deeper into the water. So,

magnetotactic bacteria like to live in the deeper parts of their aquatic environments (Figure 6.4). They use their magnetic compass to tell them which way is down.

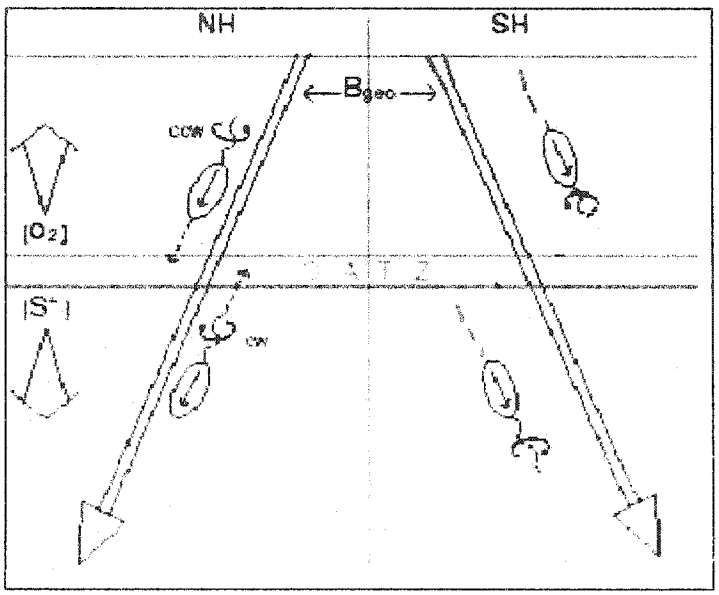

Figure 6.4: Highest number of magnetotactic bacteria found at the oxic-anoxic transition zone (OATZ), located at the sediment-water interface, microaerophilic to anaerobic lifestyle (100,000 to 1 million/ml). By moving North, the bacteria move deeper into the water and into areas with less oxygen, in the Northern hemisphere (NH), in the Southern hemisphere (SH), the bacteria point downward.

How do they do this?

The answer of this question is important for stratigraphers, who need to know factors that control the vertical motion these microorganisms. The bacteria produce an extra

production of biominerals as a weight so that the cellular system drops to the bottom of the sea or lake. The MTB use their magnetic compass to tell them which way is down. In the Northern Hemisphere, the geomagnetic field points down at an angle. So the MTB that are aligned to this field are pointing down. By moving North along this field in the Northern Hemisphere, they move deeper into the water, and into areas with less oxygen. Interestingly, in the Southern Hemisphere, the MTB in this half of the world are "south-seeking", which points them downward. At the Equator, the geomagnetic North doesn't point up or down, so the MTB found there are mixtures of north-seeking and south-seeking bacteria (Figure 6.5). The bacteria's microaerophilic to anaeorobic lifestyle along with stratigraphic and geochemical studies on the processes of their biogenic minerals formation, will help answer further questions.

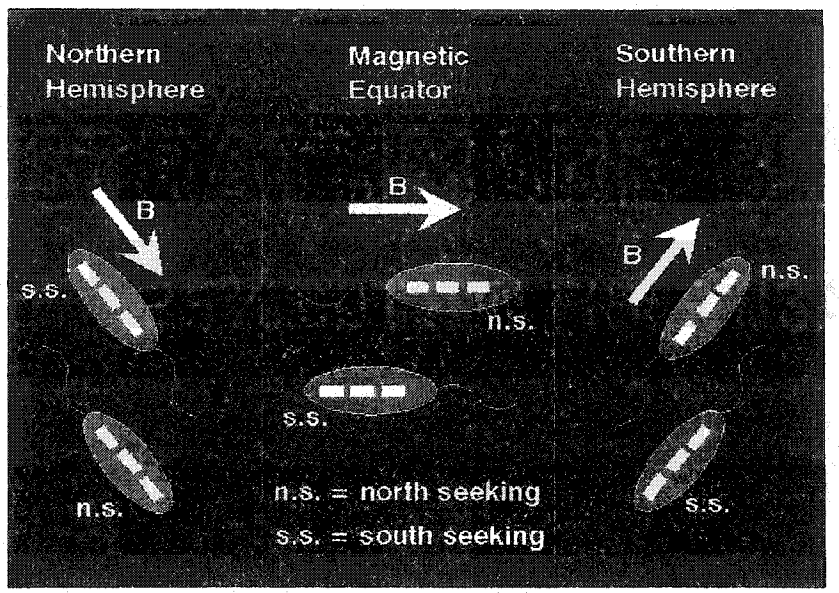

Figure 6.5: Diagram showing north seeking and south seeking MTB in both hemispheres (Blakemore 1975)

The discovery of the magnetotactic was based on the observation of a drop of water and sediment from a pond, lake or marsh on a microscope slide The magnetic field was few gauss, comparable in strength to the geomagnetic field. These observations revealed that bacteria migrated persistently along magnetic field lines in the field direction, corresponding to Northward migration along geomagnetic field lines (Blakemore 1975). The migration speed of individual bacteria along the magnetic field lines depends on the field strength, but can be 90% or more of the forward swimming speed (up to 150 microns per second) of the cell. If the direction of the local magnetic field is reversed, the magnetotactic bacteria execute "U-turns" and continue migrating in the same direction relative to the local magnetic field (Figure

6.6). The migration direction of bacteria in the magnetic field can be reversed by subjecting the cells to a strong (several hundred gauss) magnetic field pulse oriented opposite to the field in which they are migrating (Bazylinski 1994). Magnetotactic bacteria that spontaneously migrate Southward along geomagnetic field lines are found in aquatic sediments and waters from the Southern Hemisphere.

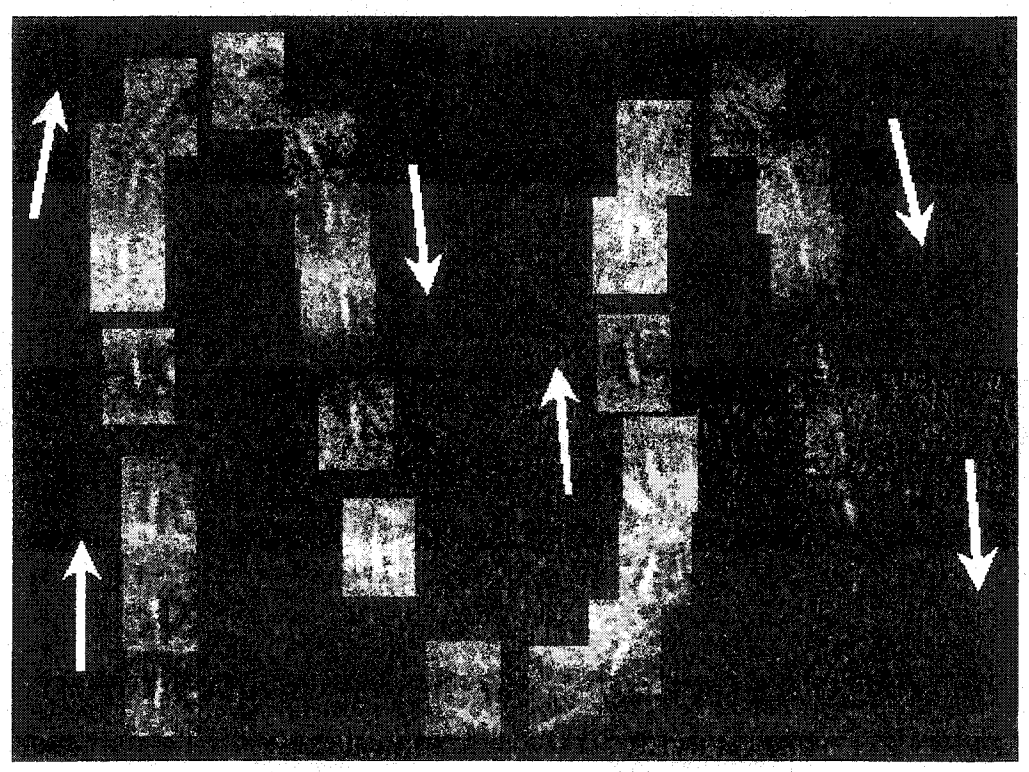

Figure 6.6: The magnetic dipole within a *magnetotactic* bacterium, rotates through 180 degrees when the polarity of the applied magnetic field is reversed. From the time and diameter of the u-turns the magnetic moment may be estimated. The image shows a sequence of video frames capturing the motion of a swimming bacterium during a 3 u-turn, 2 second track. A typical turn diameter is 60 microns, with a

bacterium swimming at approximately 40 μm/s, under an applied field of 7 gauss (0.7 mT) (Bazylinski, 1995).

MTB communities exist in many aqueous systems and have the potential for high levels of activity. In some areas, their activity occurs naturally, whereas in others, it may need to be stimulated through availibility of electron donors or acceptors in the aqueous environment. Further works will determine the factors influencing the rate of accumulation of bioproducts as well as an evaluation of such mechanisms that lead to the biogenic minerals growth. Magnetosome particles remain preserved after the bacterial cells die and thus can be deposited as magnetofossils, which contribute significantly to the magnetization of sediments. Magnetotactic bacteria (MTB) are a heterogeneous group of procaryotes, which are ubiquitous in aquatic environments and cosmopolitan in distribution. Given their high abundance and variety in marine and freshwater habitats, MTB very likely play an important biostratigraphical and ecological role in many types of sediment, as for instance in biogeochemical cycling of iron and other elements. However, their role remains to be fully evaluated.

Fresh water bacteria

Freshwater communities of MTB have been studied by several microscopic, cultural and molecular-biological approaches. Highest numbers of MTB, 10^5 -10^6/ml (Blakemore et al., 1979; Spring et al., 1993) are usually found at the oxic-anoxic transition zone generally located at the sediment-water interface, which is consistent with their microaerophilic to anaerobic lifestyle. Freshwater sediments were found to

contain various morphological types of MTB, including, vibrio-like, coccoid, and helical forms.

Marine environments

In the marine environment, MTB have been mostly found in coastal environments like marshes and estuaries, although some studies have indicate their apparently widespread occurrence in the ocean down to depths of 3000m (Stolz et al., 1986). As in freshwater environments, the occurrence of MTB is usually restricted to the upper layer of the sediment. However, in some chemically stratified estuarine basins, MTB were found to occur in the microaerobic layer of the water-columns (Bazylinski, 1995).

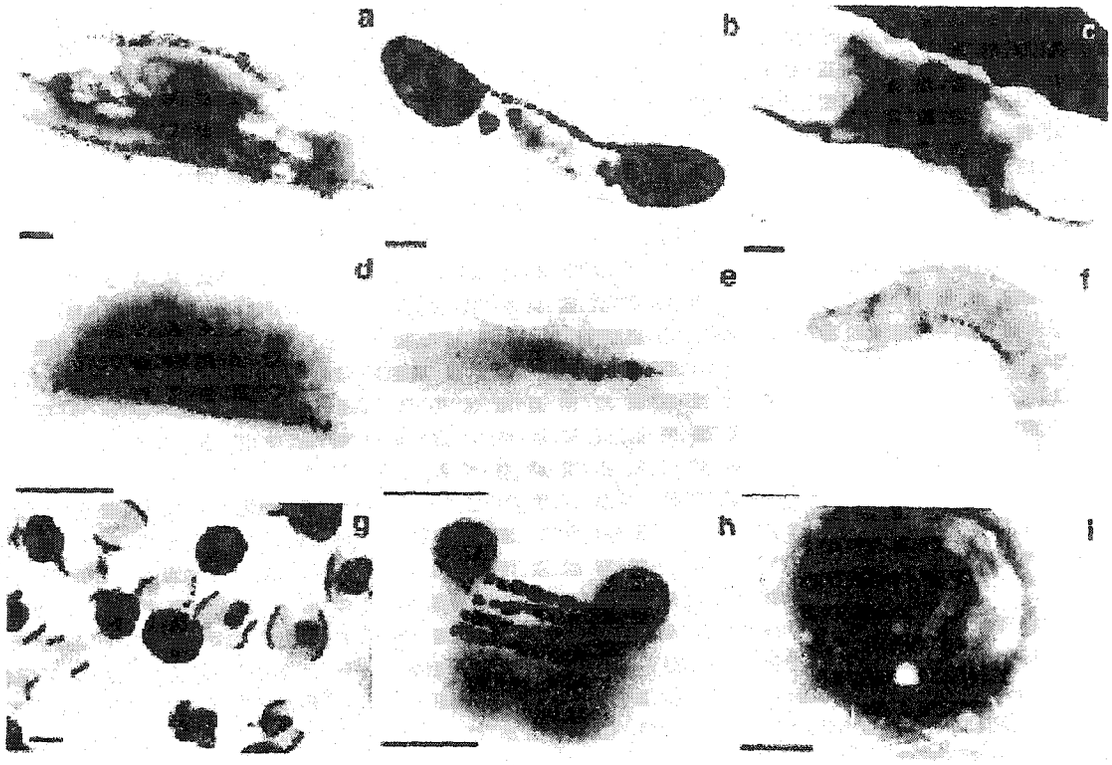

Figure 6.7: Transmission Electron Micrographs (TEM) of Magnetotactic Bacteria. TEM showed whole cells of various magnetotactic bacteria collected from different natural habitats. The diversity of morphological forms include large rods (a, b, c), vibrios (d), spirilla (e, f), and coccoid (g, h, i) cell forms. The bar is equivalent to 0.5 μm (Bazylinski, 1993).

Generally, morphological types similar to freshwater MTB are found in marine habitats, although some sulfidic sediments are characterized by the presence of unique morphological forms, notably a many-celled magnetotactic prokaryote which was identified in marine and brackish sediments (Farina et al. 1990; Mann et al.

1990b) (Figure 6.7). Several MTB from reducing environments with high concentrations of H_2S contain particles of iron-sulfide (greigite and pyrite) instead of iron oxides found in most MTB (Bazylinski et al. 1993; Mann et al. 1990b). It was demonstrated that a freshwater sulfate-reducing bacterium could intracellularly form magnetite (Sakaguchi et al. 1993), suggesting that marine counterparts are most likely abundant given the importance of sulfate reduction in marine systems.

Iron and Sulfate-Reducing Bacteria

The Iron and Sulphur Bacteria are neither morphologically nor physiologically homogeneous, yet they may be characterised by the ability to transform or deposit significant amounts of iron or sulphur, usually in the form of objectionable slime. "Iron Bacteria" are considered to be capable of metabolising reduced iron present in their water habitat and depositing it in the form of hydrated ferric-oxide on or in their secretions. Bacteria of this type obtain energy by the oxidation of iron from the ferrous to the ferric state; the ferric form is precipitated as ferric hydroxide (FeOOH). Iron may be obtained from the aquaeous environments of the microorganism. The amount of ferric hydroxide deposited is large in comparison with the enclosed cell.

Some bacteria that do not oxidise ferrous iron may cause it to be dissolved or deposited indirectly. In their growth, they either liberate iron by utilising organic radicals to which the iron is attached or they alter environmental conditions to permit the solution or deposition of iron. As a consequence less ferric hydroxide is produced, but taste, odour and fouling may be engendered.

Iron Biominerals in Sediments

When magnetotactic bacteria die, their magnetosomes can be deposited and preserved in sediments, resulting in a (post) depositional remanent magnetization. The SD size of magnetosomes makes them excellent recorders of the paleomagnetic field and their unique hexagonal crystal forms provide a means for identifying magnetosomes via electron microscopy of magnetic extracts from sediments. Fossil magnetosomes, sometimes preserving the chain structure, have been identified in sediments spanning the Phanerozoic (Vali and Kirschvink 1990) and references therein].

Although magnetotactic bacteria are ubiquitous in many present day aquatic environments, the eventual fate of magnetosomes and their relative contributions to remanent magnetization and the mineral magnetic record in sediments is not so obvious. Oldfield (1992) summarizes what he calls the ``detrital" and ``biomagnetic" interpretations of the source(s) of fine grained magnetite in Quaternary sediments with emphasis on the mineral magnetic signature of paleoenvironmental change. He argues that, whereas TEM observation of magnetosomes provides proof that a biogenic component is present, new magnetic methods are needed to quantify the biogenic contribution in sediments and establish sediment-source linkages.

The most effective magnetic approach for biogenic identification and quantification should allow whole sediment samples to be measured using magnetic methods sensitive to the SD size specificity, and possibly chain assemblage, of BOB-type biogenic systems. Magnetic methods have the advantage of being rapid and non-destructive but may suffer from an ambiguity in distinguishing biogenic SD particles from detrital SD or small multidomain particles. In addition, BIM-type magnetic

minerals lack the SD size specificity of magnetosomes and, at least for magnetite produced by GS-15, resemble inorganic magnetite particles produced during soil formation (Lovley, 1990). Hence, crystal morphology alone is not a useful criterion for identifying BIM-type magnetite. Furthermore, unless one can show that all SPM particles in sediments or soils are biogenic, magnetic identification of BIM-type particles is also precluded (Moskowitz et al., 1993).

Two approaches to the biogenic problem have recently been presented. In the first approach, Oldfield (1994) suggests using a combination of low-field, frequency dependent, and anhysteretic susceptibilities to isolate a magnetosome magnetic response. The problems posed by an in situ BIM-type magnetic fraction or volume reduction of magnetosomes producing SPM particles by dissolution was not addressed. The method is calibrated with synthetic magnetite and natural samples from several environments where evidence suggests the presence of either detrital or non-detrital (ie., biogenic?) magnetite. However, no electron microscopy was done to check whether magnetosomes were actually present in the sediments yielding the ``biogenic'' signature. The second approach is based on low temperature behavior (20-300 K) of saturation remanence observed in pure cultures of MTB on warming through the cubic-monoclinic phase transition in magnetite near 100 K (Moskowitz et al., 1994). Unlike room-temperature remanence/susceptibility parameters that are sensitive to a specific SD particle volume distribution, the low-temperature results appear to depend on the unique chain arrangement of magnetite magnetosomes in MTB and may be sensitive enough to quantify this fraction in bulk samples.

However, the method has yet to be ``field-tested" on natural samples with known biogenic components.

Several studies reported biogenic minerals in lake, marine, and continental eolian deposits (Snowball, 1994; Hess, 1994; Evans and Heller, 1994; Hawthorne and McKenzie, 1993; McNeill and Kirschvink, 1993; Maher and Thompson, 1992). Two papers dealt with the formation and destruction of biogenic magnetite in lake sediments combining magnetic, TEM, and geochemical methods (Hawthorne and McKenzie, 1993; Snowball, 1994). In a study of Lake Greifen (Switzerland) sediments spanning the past 300 years, Hawthorne and McKenzie (1993) conclude that dissolution and sulfidization of detrital and biogenic magnetite in the upper 30 cm occurred in response to a change in the depositional environment of the lake from aerobic to anoxic due to eutrophication associated with agricultural/industrial development in the area since 1887. In contrast, Snowball (1994) documents a high concentration of biogenic magnetite in the upper sediment levels with progressive dissolution of biogenic magnetite at depth from lake sediments in Sweden. Biogenic magnetite was confirmed based on TEM observations and comparative magnetic studies on catchment and sediment samples.

Hess (1994) reports abundant fossil magnetosomes in oxic to suboxic hemipelagic sediments from the southwest Pacific Ocean. He concludes that biogenic magnetite is the dominant fraction in these sediments and that down-core magnetic variations represent paleoenvironmental changes affecting bacterial paleoecology. Finally, Evans and Heller (1994) suggest that the magnetic enhancement observed in paleosols from the loess plateau of China is due to in situ formation of both BOB-

type (SD) and BIM-type (SPM) biogenic magnetites. Although this is an intriguing idea, neither TEM identification of soil magnetosomes nor observation of extant species of MTB or dissimilatory iron-reducing bacteria in modern soils in the area were documented. Instead, biogenic confirmation was based solely on the similarity of magnetic parameters with deep-sea sediments containing fossil magnetosomes. In contrast, Maher and Thompson (1992) found magnetite particles resembling magnetosomes in paleosol based on TEM observations of extracts, but they conclude that this biogenic(?) fraction is a minor magnetic component of the paleosol.

Iron Sulfides

Greigite is isostructural with magnetite and is also ferrimagnetically ordered at room temperature. The greigite particles are characterized by narrow particle size distributions and species-specific crystal forms (Heywood et al., 1991). Electron microscopy of the greigite particles in several organisms has revealed at least two idealized particle morphologies: cubo-octahedral and elongated cubic with the axis of elongation along the <100> direction (Heywood et al., 1991; Bazylinski et al., 1994). The intrinsic magnetic properties of greigite are poorly known, but the biogenic particles provide some useful information. First, greigite magnetosomes, which should theoretically fall within the SD range for magnetotaxis, have dimensions between 67-100 nm. These particle dimensions observed for greigite magnetosomes are consistent with some simple calculations for the SD size limit in FeS (Ricci and Kirschvink, 1991). Second, the greigite magnetosomes are oriented with their <100> axes aligned along the chain axis (Heywood et al., 1990; 1991), instead of <111>

directions as observed in their magnetite cousins, implying that the <100> direction is the magnetic easy axis in greigite. Although the magnetocrystalline anisotropy constant (K) has never been measured for greigite, the chain arrangement of the biogenic particles indicates that the sign of K must be positive at room temperature. Micromagnetic calculations for greigite should therefore be consistent with a positive anisotropy constant.

Although particular species of MTB are usually characterized by a unique magnetosome morphology and mineral composition, the magnetotactic bacteria found in sulfidic habitats are interesting exceptions. The MMP contains single or double chains of greigite and pyrite particles, each exhibiting several different crystal morphologies, but all within a narrow size range of 50-90 nm (Bazylinski and Frankel, 1992; Bazylinski et al., 1994; Heywood et al., 1990). The pyrite particles seem to be the dominant phase but the arrangement of the greigite/pyrite particles within the chains or the functions of the pyrite particles are unknown (Heywood et al., 1991). In addition, copper has been identified in association with some of the greigite-pyrite particles in the MMP and is the first evidence that a transition metal other than iron could be biomineralized by MTB (Bazylinski et al., 1993b). Lastly, the MTB described by Bazylinski et al. 1993, produce both magnetite and greigite magnetosomes. Both ferrimagnetic mineral phases are co-organized in the same magnetosome chain, but each phase has a distinct crystal morphology and crystallographic orientation. The magnetite magnetosomes are arrowhead-shaped, whereas the greigite ones are rectangular. Furthermore, the magnetite and greigite

crystals are aligned with their respective <111> and <100> easy axes along the chain direction.

Magnetosomes

The hallmark feature of all MTB is the presence of unique intracellular structures, known as magnetosomes, which consist of magnetic iron-mineral particles enclosed within membrane vesicles (Balkwill et al., 1980). With the exception of the aforementioned MTB producing iron-sulfide crystals, the iron mineral particles generally consist of magnetite (Fe_3O_4). Magnetite is an inverse spinel ferrite of structural formula Fe^{3+} [Fe^{2+}, Fe^{3+}]O_4, which has ferrimagnetic properties (Banerjee and Moskowitz, 1985). Unlike magnetite found in inorganic systems or produced extracellularly by the metabolic activities of dissimilatory iron-reducing bacteria (Moskowitz et al., 1989), the intracellular magnetosome crystals are characterized by narrow size distributions and uniform, species-specific crystal habits.

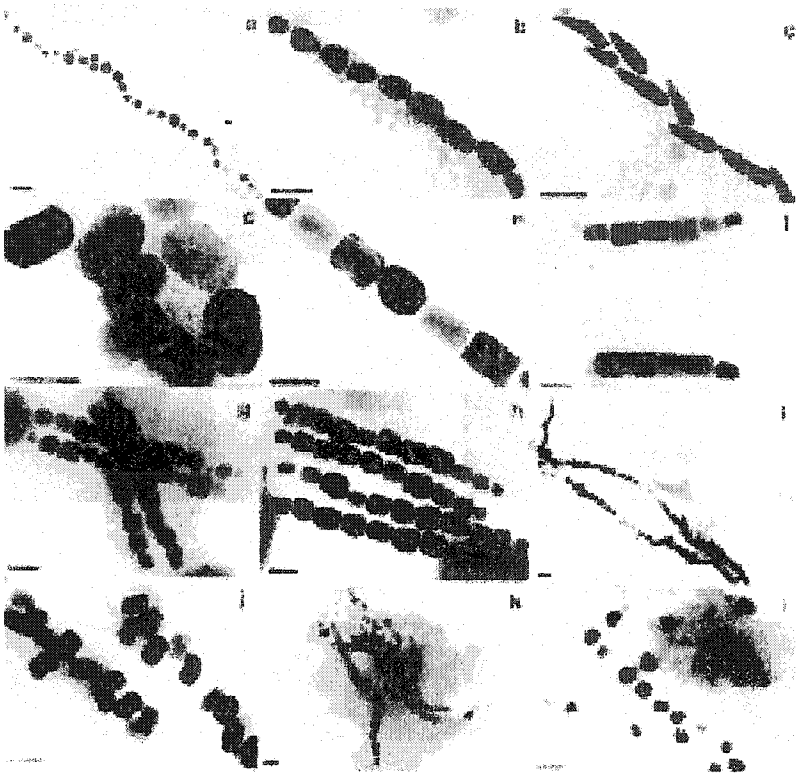

Figure 6.8: TEM PHOTOGRAPHS OF MAGNETOSOMES SHOWING VARIOUS SHAPES: CUBO-OCTAHEDRAL (a), BULLET-SHAPED (b, c), ELONGATED PRISMATIC (d,e, f, g, h, I, j, k), RECTANGULAR MORPHOLOGY (l), ARANGED IN ONECHAIN (a, b, c, e), TWO CHAINS (f, I), MULTIPLE CHAINS (g, h), IRREGULARLY CHAINS (j, k, l), THE BAR IS EQUIVALENT TO 0.1μm (Moskowitz, 1995).

All habits can be derived from various combinations of the octahedral {111}, dodecahedral {110}, and cubic {100} forms compatible with magnetite (Fd3m) symmetry (Devouard et al., 1998). The particle sizes are typically 35-120 nm, which is within the permanent, single-magnetic-domain-size range for magnetite (Moskowitz, 1995) (Figure 6.8). The magnetosomes are usually organized in chains, resulting in a permanent magnetic dipole sufficiently large so that it will orient the entire bacterium along the geomagnetic field at ambient temperature. This passive orientation results in the migration of the cell along the magnetic field lines as it swims ("Magnetotaxis"; Blakemore and Frankel, 1981).

Problems in isolation and cultivation of these bacteria arise from their lifestyle, which is adapted to sediments and chemically stratified aquatic habitats. As typical gradient organisms, MTB depend on complex patterns of vertical chemical and redox gradients, which are difficult to mimic under laboratory conditions. Since no strictly selective media and growth conditions are known for the cultivation of MTB, the effective separation of magnetotactic cells from non-magnetic contaminants is crucial in their isolation. This can be achieved by exploiting their active migration along magnetic field lines in a capillary "racetrack" method (Wolfe et al., 1987). Growth media involving sulfide and redox gradients have proven useful in the isolation of MTB (Schüler et al., 1999). Only a limited number of MTB has been isolated in pure culture so far and most of the isolates are poorly characterized in terms of growth conditions and physiology. Examples of isolates, which can be grown under laboratory conditions, include several freshwater species of *Magnetospirillum*

(Blakemore et al., 1979; Burgess et al., 1993; Schleifer et al., 1991; Schüler and Köhler, 1992; Schüler et al., 1999).

MTB *Magnetospirillum* microaerobically grown on simple media that contain short organic acids as a carbon source used by Blakemore et al., 1979; Matsunaga et al. 1990; Schleifer et al. 1991; Schüler and Köhler 1992) and have a oxygen-dependent respiratory type of metabolism. Nitrate is used as an electron acceptor microaerobically in some strains as Bazylinski and Blakemore (1983) studied their phylogeny. *Magnetospirillum magnetotacticum* was the first magnetotactic bacterium available in pure culture they used in initial studies. They found that one of the reasons for oxygen sensitivity in this organism may be the lack of the oxygen-protective enzyme catalyzer, as addition of catalyzer to the growth medium resulted in increased oxygen tolerance.

Because of the large amounts of iron required for magnetite synthesis, magnetotactic bacteria can be anticipated to use very efficient uptake systems for the assimilation of iron. Although several studies have focused on iron uptake, the exact mechanisms and components involved are not well understood. The initial finding of Paoletti and Blakemore (1986) that cells of *Magnetospirillum magnetotacticum* produced a hydroxamate type siderophore under high iron condition, has not been replicated in other studies and no unequivocal evidence for the involvement of siderophores in the formation of magnetite has been found so far. Nakamura et al. (1993) hypothesized that ferric iron was taken up in *Magnetospirillum* AMB-1 by a periplasmic binding protein-dependent iron transport system. In *Magnetospirillum gryphiswaldense*, the major portion of iron is taken up as Fe(III) in an energy-dependent process with a

V_{max} and K_m of 0.86 nmol min^{-1} (mg dry weight)$^{-1}$ and 3 μM, respectively (Schüler and Baeuerlein, 1996). The high rates of ferric iron uptake may reflect the extraordinary requirement for iron in these bacteria. Both the amount of magnetite formed and the rates of iron uptake were close to maximum at extracellular iron concentrations of 15-20 μM Fe, indicating that this bacterium is able to accumulate copious amounts of iron from relatively low concentrations.

While size and morphologies of mature magnetite crystals are largely unaffected by environmental conditions, the number of magnetosome particles per cell can vary considerably and strongly depends on the growth conditions. Besides the availability of micromolar amounts of iron, microaerobic conditions are required for magnetite formation in *Magnetospirillum* species (Blakemore et al., 1985; Schüler et al., 1995; Schüler and Baeuerlein, 1998). Cells of *M. gryphiswaldense*, which are non-magnetic during aerobic growth, start to produce Fe_3O_4 when shifted to microaerobic growth conditions corresponding to an oxygen concentration of about 2-7 μM O_2. The accumulation of iron during growth is tightly coupled to the induction of magnetite biomineralization. While the intracellular iron content in pre-magnetic cells is relatively low and in the same range as reported for other, non-magnetotactic bacteria, magnetic spirilla can accumulate more then 2% iron on a dry weight basis (Blakemore et al., 1979; Schüler and Baeuerlein, 1998).

Magnetosomes: Magnetite

The characteristics of magnetosomes are their size specificity and distinctive crystal morphologies (Mann et al., 1990b; Frankel and Bazylinski, 1994). Although variations exist between species, almost all magnetosomes, regardless of composition, fall within a narrow size range of 35-120 nm when measured along their long axes (Vali and Kirschvink, 1990; Heywood et al., 1990; 1992; Bazylinski et al., 1994). This size specificity of magnetosomes is significant because within this size range the particles are uniformly magnetized, permanent single magnetic domains (SD). In addition, the particles are arranged along the chain axis such that the crystallographic magnetic easy axes are also aligned (Frankel and Bazylinski, 1994). The size specificity and crystallographic orientation of the chain assembly is optimally designed for magnetotaxis in the geomagnetic field.

For a given cell type, magnetosomes usually have a uniform size, shape, crystal morphology, and arrangement within the cell (Mann et al., 1990b; Frankel and Bazylinski, 1994). Magnetosomes occur in at least three different crystal forms determined using transmission electron microscopy. The simplest form, found in *Magnetospirillum magnetotacticum*, is cubo-octahedral, which preserves the cubic crystal symmetry of magnetite (Mann et al., 1990b). A second type, found in coccoid and vibrioid strains, is an elongated hexagonal prism with the axis of elongation parallel to the <111> crystal direction (Meldrum et al., 1993). A third type, observed in some uncultured cells, is an elongated cubo-octahedral form producing unique bullet-shaped, tear-drop, and arrowhead particles (Vali and Kirschvink, 1990; Mann et al., 1990b). The growth mechanisms for these forms are unknown but particle

shapes may be related to anisotropic ion flux through the magnetosome membrane or from constraints imposed by the surrounding membrane structure (Mann et al., 1990b; Frankel and Mann, 1994). Whereas the cubo-octahedral form is common in inorganic magnetites, the prevalence of elongated hexagonal forms in magnetosomes appears to be a unique feature of the biomineralization process in MTB (Frankel and Mann, 1994; Frankel and Bazylinski, 1994). This aspect of magnetosome morphology forms the basis for distinguishing magnetosomes from detrital or BIM-type magnetite using electron microscopy.

The variability of magnetosome design and chain assembly is apparent in a study by Vali and Kirschvink (1990) on several types of uncultured magnetotactic bacteria. In one microorganism, an estimated 1000 bullet-shaped magnetite crystals were assembled into 5 rope-like bundles traversing the cell's long axis. Another bacterium was found to contain magnetosomes with three different crystal shapes, while yet another produced highly elongated (up to 300nm x 30 nm), but still SD, magnetosomes. Farina et al., 1994, report finding unusual marine MTB that produce chains of ``large" magnetosomes (200 nm). The magnetosomes are considered large because their crystal dimensions places them outside the theoretical SD size range and within the non-uniformly magnetized two domain (TD) size range for magnetite. If confirmed, the ``large" magnetosomes raise some interesting questions about their biological function (magnetotaxis?) and may provide an opportunity to study the micromagnetic structure of non-SD particles.

Magnetosomes and Fine Particle Magnetism

Biogenic magnetic minerals provide a novel source of material for fundamental studies of magnetism. For example, biogenic magnetite has been used to study the effects of magnetic interactions on isothermal (IRM) and anhysteretic (ARM) remanent magnetization. Because magnetosomes are of uniform size and shape, one does not have to untangle these effects from magnetic interaction effects, a common and often limiting problem in fine-particle studies using synthetic samples. An interaction test based on IRM and ARM behavior and ``calibrated" against whole cells was used to study compaction, cementation, and dolomitization of platform carbonates (Diaz et al., 1991; McNeill and Kirschvink, 1993). Proksch and Moskowitz (1994) used a variation of the Wohlfarth-Cisowski interaction test in which intact chains and extracted magnetosomes were prepared in different initial remanent states before the IRM acquisition curve was measured. By analyzing a series of IRM curves, it was possible to separate the effects of both positive interactions along a chain and negative interactions among chains or clumped magnetosomes. This approach may prove useful for detecting biogenic chain fractions in sediments.

As mentioned previously, some magnetotactic bacteria produce ``large" magnetosomes (up to 200 nm) with particle dimensions that are larger than the theoretical SD size range for magnetite (Farina et al., 1994). Neglecting the biological implications of non-SD magnetosomes and engaging in some speculation, the existence of these magnetosomes has several fascinating magnetic implications. Either the magnetosomes are indeed two domain; or (1) the magnetosomes are really

SD and the theoretical groundstate SD-TD transition size needs to be slightly revised; or (2) the magnetosomes are uniformly magnetized in an SD state but it is a higher energy metastable SD state within the equilibrium TD range. Possibility (2) is the most intriguing and, if true, these bacteria can provide validation of micromagnetic models as well as provide a source of metastable SD magnetite particles for study. Interestingly, the magnetosome dimensions are consistent with recent theoretical grain size limits for metastable SD magnetite particles (Dunlop, 1990).

Contact and non-contact scanning force microscopy with a magnetic tip (MFM) was used to simultaneously image topography and magnetic forces from the magnetosome chain assembly in a single MTB cell (Proksch et al., 1994; Farina et al., 1994). The MFM estimate of the dipole moment of a single cell agreed well with the average dipole moment of the cell population from which the cell came, as determined with a superconducting (SQUID) magnetometer. However, the MFM result is a direct magnetic measurement of a single cell that represents a higher improvement in sensitivity over conventional SQUID magnetometers.

The MFM can also be a useful magnetic probe to study individual SD and ``large" magnetosomes. It should be possible to decide among the alternative micromagnetic explanations for ``large" magnetosomes discussed above by either directly imaging a domain wall, spin vortex structures, or inducing the nucleation of a domain wall from the field of the MFM tip. The ``conventional" SD magnetosomes also can provide a useful magnetic system for studying single particle switching behavior and time-dependent phenomena. Finally, MFM studies of magnetosomes can be useful for comparison with current computer modelling of the micromagnetic spin structures of

fine magnetic particles from first-principle calculations and quantitative predictions based on those models (Dunlop, 1990). One potential payoff of these models will be to predict the grain size dependent behavior of remanence, coercivity, and susceptibility (ie., hysteresis properties) for the different magnetic minerals found in nature. Most importantly, as ``grain-size proxies," these magnetic parameters form the basis for interpreting the magnetic record of paleoclimate change and the magnetic fingerprinting of remagnetization in limestones. The study of biogenic magnetic minerals can provide critical experimental validation of these micromagnetic models and advance our understanding of the magnetic behavior of magnetite.

Cellular Magnetic Dipole

Whether the mineral particles are magnetite or greigite, the chain of magnetosome particles constitutes a permanent magnetic dipole fixed within the bacterium [3]. The magnetic dipole moment is generally sufficiently large so that it, and consequently the bacterium, is oriented in the geomagnetic field so that $\langle \cos\varnothing \rangle$ 0.9, where $\varnothing$ is the instantaneous angle between the magnetic dipole moment and the field direction. Magnetotaxis is a passive process in which the orientation of the magnetic dipole in the ambient magnetic field as the organism swims causes it to migrate along the magnetic field lines (Figure 6.9).

Magnetotactic bacteria have two possible magnetic polarities, depending on the orientation of the magnetic dipole within the cell. The polarity can be reversed by a magnetic pulse which is greater than the coercive force of the chain of particles. As noted above, bacteria with reversed polarity migrate along magnetic field lines in the

direction opposite to that of bacteria with the original polarity. In natural habitats, the predominant polarity type in the population of a given bacterial species is determined by the sign of the inclination of the geomagnetic field.

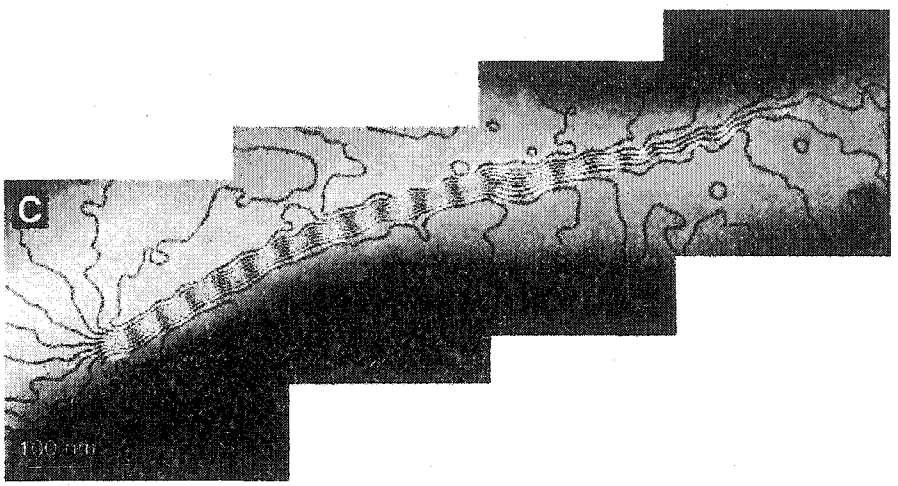

Figure 6.9: Magnetic flux lines associated with a MTB cell,superposed on the magnetosome chain (shown in white) Dunin-Borkowiski and al, 1998.

Biotechnological Applications

Magnetosome formation in bacteria has the potential to yield useful biomaterials. The synthesis of nano-sized magnetite particles by a biological process promises advantages in terms of controlling crystal growth and structural properties. By comparison, synthetic magnetic particles are non-uniform, often not fully crystalline, compositionally nonhomogeneous, and in an agglomerated state which imposes problems in processing. Moreover, biomineralization provides a way to produce highly uniform magnetite crystals without the drastic regimes of temperature, pH and pressure which are often needed for their industrial production (Mann et al., 1990). Accordingly, numerous biotechnological applications of the small magnetic crystals have been contemplated (Schüler and Frankel, 1999). The small size of isolated magnetosome particles provides a large surface-to-volume ratio, which makes them useful as carriers for the immobilization of relatively large quantities of bioactive substances, which can then be separated by magnetic fields. In several studies, bacterial magnetosomes were used for immobilizing enzymes and antibodies (Matsunaga and Kamyia, 1987; Nakamura et al., 1991; 1993b). The presence of the magnetosome membrane resulted in dispersion and handling properties superior to those of synthetic magnetic particle conjugates. Using phagocytosis and polyethylene glycol fusions, bacterial magnetite particles were incorporated into eucaryotic cells, which could be manipulated by magnetic fields (Matsunaga et al., 1989).

Another application of bacterial magnetosomes may lie in their potential use as a contrast agent for magnetic resonance imaging and tumor-specific drug carriers based on intratumoral enrichment. Synthetic liposomes containing superparamagnetic iron

oxide particles have already been used into biomedical applications of this type. Other suggested applications of MTB involve the use of living, actively swimming cells. Proposed examples include the application of MTB in the analysis of magnetic domains in magnetic materials (Harasko et al., 1993; 1995) and the use of MTB for the removal of heavy metals and radionuclides from wastewater (Bahaj et al., 1994; 1998).

As yet, no application of MTB has attained commercial scale, however. This situation is in part due to the problems related to mass cultivation of these bacteria. Another reason for the limited practicability of many systems is the lack of a basic understanding of bacterial magnetite biomineralization at a biochemical and molecular level. Thus, more research in this field is clearly required. Genetic approaches are offering promising ways for engineering bacterial magnetosome formation and the biomineralization process providing new materials.

Questions in further research could be addressed in relatively well-studied systems, while at the same time increased effort needs to be spent to exploit the metabolic potential of the vast biodiversity of natural occurring MTB, including largely unexplored habitats such as the marine environment.

CHAPTER 7: ENVIRONMENTAL SCIENCE

A PROPOSED METHOD OF BIOGENIC MAGNETITE REMOVAL FROM AQUIFERS USING APPLIED MAGNETIC FIELD

Intorduction

Biogenic magnetites are produced by magnetotactic bacteria or iron-reducing bacteria, intracellularly or extracellularly. They are well-ordered crystals that exhibit narrow size distributions and specific morphologies. The biogenic minerals in the magnetotactic bacteria are within the single-domain size range, 35 to 120 nm in length, (Butler and Banerjee, 1975) and are usually arranged in a chain motif, providing the cell with a permanent dipole moment. This arrangement causes the cell to align along Earth's inclined geomagnetic field lines, functioning as an efficient means of locating and maintaining an optimal position in vertical chemical gradients (Blakemore et al., 1993).

The author's hypothesis is that the magnetotactic bacteria respond to magnetic fields to guide tactic movement as described in the studies of Doyle and Wachtel, 1999. Owing to its internal magnetite particles, cells can also be moved and guided by externally applied magnetic fields, which can be combined in various ways with the gravity vector. These microorganisms therefore provide an opportunity to test if they can be isolated or suspended and removed from the medium to prevent their sedimentation, by using a modified magnetic field.

The objectives are:

- To find the magnetic susceptibility of a known magnetotactic bacterium. This parameter is an important clue in the application of any modified magnetic field that induces the reorientation of the bacteria trajectory (calcultaion at APPENDIX D) ;
- To find the bacterial magnetic moment, which measures the torque that the Earth Magnetic Field applies to the magnetotactic bacteria to align them along the field (method and calculations at APPENDIX E);
- Construct an experiemntal design that allows magnetotactic bacterial reorientation by imposing to them a field intensity greater than the Earth Magnetic Field's intensity;
- To obtain a field mapping region in laboratory jars that show a vertical trapping region where the bacterial accumulation can be quantified.
- From results draw graphs and identify the different correlation between various magnetic field intensities/bacterial moment/bacterial accumulation

METHODS

A. Sample Collection: Bacterial Cultures

A bacterial collection was completed during field work at a pond located in a low plain north to Anthony' Nose, Westchester New York. The pond lies along New York Route 172 at the southbound exit from Interstate 684. There is no local name assigned to this pond. The method and materials used for collection are detailed at APPENDIX E.

B. Determination of the magnetic susceptibility of a magnetotactic bacteria

The Spencer and Zare's method was used at the NJ-J. Ferris HS Laboratory in New Jersey. The design is a photgate-pendulum apparatus that determines the magnetotactic bacteria (MTB) 's magnetic susceptibility (Figure 7.1). It is essential to know this parameter which is an important clue for the application of any modified magnetic field that induces bacterial reorientation. The magnetic susceptibility of MTB is calculated and compared to two known paramagnetic compounds. A calibration curve was plotted for reference.

The most common methods of measuring magnetic susceptibility include the Gouy, Faraday, and Rowland methods (Eaton et al., 1979). All these involve the use of large, expensive magnets and fragile, time-consuming suspension of the sample. So, the author used the Spencer and Zare's method, 1999. They developed a simpler, more affordable alternative to these methods using a laser-pendulum apparatus (figure 7.1) which is also easy to reproduce. By comparing the period of oscillations for different materials, the molar susceptibilities at room temperature can be readily

determined (Spencer et al., 1988).

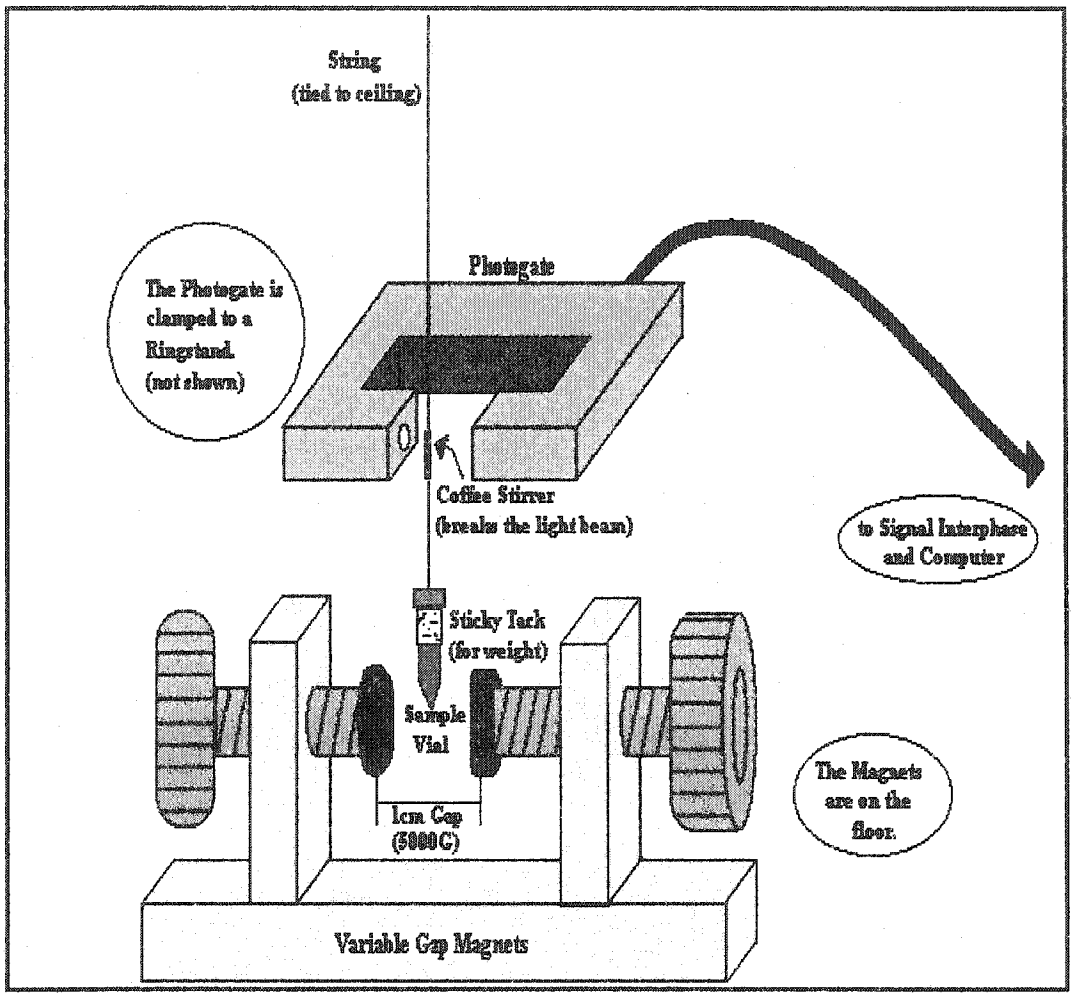

Figure 7.1: Schematic description of the Laser-pendulum apparatus reproduced by the author in this research. The detailed of procedures and experiment are described in APPENDIX C.

From these experiments and calculations, our results showed magnetic susceptibilities of various paramagnetic compounds determined with a reasonable degree of accuracy using the photogate-pendulum apparatus. Furthermore, it was determined that magnetotactic bacteria (MTB) have a susceptibility of 6343×10^{-6} cgs, and the the ratio density/Molar (χ/M) was found to be 0.008514 $[cm^3]^{-1}$. The null hypothesis was therfore rejected, and all the criteria stated in the problem were met. For Methodology and Experiments, see APPENDIX C.

C. Bacteria Magnetic moment

See APPENDIX D for caculation of the magnetotactic bacteria's magnetic (MTB) moment.

MATERIALS

Introduction

A current-carrying wire coil is constructed to have a magnetic field capable of inducing magnetic forces greater than the Earth's gravity in magnitude. Field mapping showed a vertical (or horizontal) trapping region with a calculated magnetic field strength. This opposes, to the extent possible, a new and greater gravitational force on the bacteria (Figure 7.2).

Such a design is used as a basis for space flight experiments by NASA, in which, rather than being quiescently suspended, bacteria would be subject to a gravity-like force, in which a magnetic field can be used, on one hand, to establish functional weightlessness and on the other, magnetopseu-

do-gravity (Figure 7.3).

The author's main idea is to isolate the microorganisms and to precipitate the biologically produced magnetite before sedimentation by applying conditional variability such as gravity and the microorganisms magnetic moment (APPENDIX D), in either an aerobic or anaerobic system.

Experimental Design Apparatus

- Non-magnetic tangent galvanometer ammeter
- Knife-switch magnetic compass
- Heavy insulated copper wire (about 10 meters)
- Electric power supply
- Rheostat

- Polar coordinate graph paper
- Sample of Sediment/MTB and Water

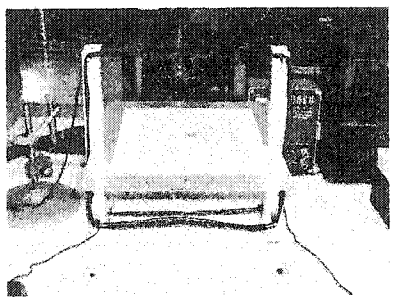

A

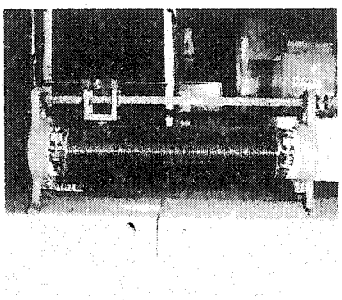

B

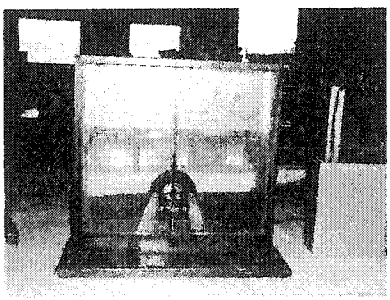

C

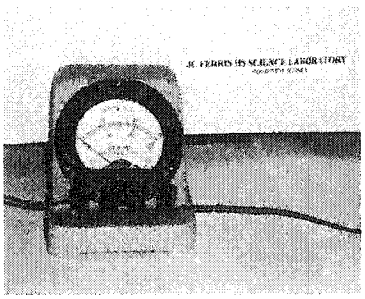

D

Figure 7.2: Materials used for experiments. A = Support Polar coordinateAmperemeter, B = Rheostat, C = Galvanometer, D = Amperemeter. These materials are used to make the apparatus that induces a variable magnetic field intensities to bacteria culture.

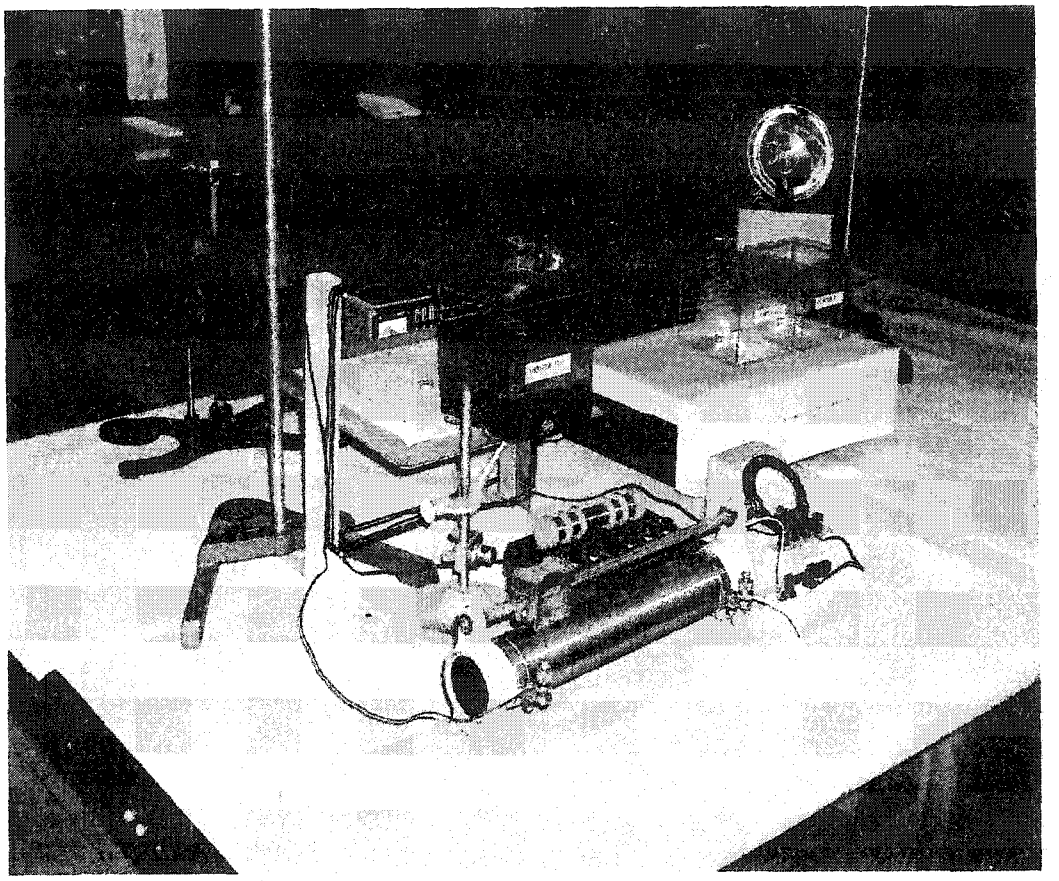

Figure 7.3: Picture of the experimental setting with the reheostat used to vary the electricity that changes the magnetic induction intensity.

Schematic design

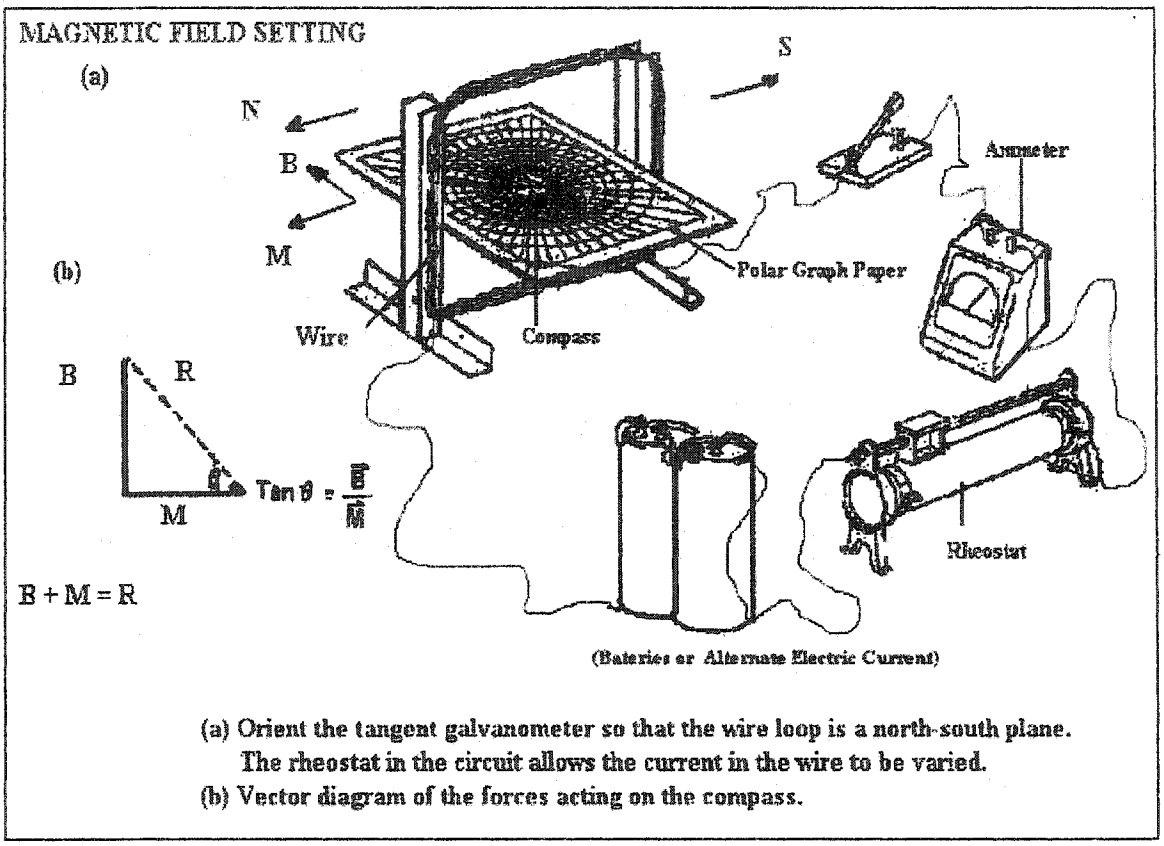

Figure 7.4: (a) orient the tangent galvanometer so that the wire loop is in a north-south direction. The rheostat in the circuit in the wire allows the current to be varied. (b) Vector diagram of the forces acting on the compass needle.

The schematic arrangement of the apparatus is shown in Figure 7.4. The strength of the induced magnetic field around the insulated wire increases if the eletcric current through the wire increases. The rheostat in the circuit allows the current in the wire to be varied. This will permit to impose the MTB various madnetic field intensities. Our support frame is lined-up in the north-south (magnetic) direction. When the knife switch is opened, no current flows through the wire. Therefore, no induced magnetic field exists around the MTB. The compass, in this case, is acted upon only by the Earth's Magnetic Field (EMF). Thus the needle of the compass points in the direction of the magnetic north, as indicated by the vector M. When we close the electrical circuit, the current flows through the wire, a new magnetic field, due to the current, appears around the bacteria's environment. This magnetic field acts in the direction given by B. If the Earth Magnetic Field (EMF) was nonexistent, the MTB could all point in the direction of B. However, under the influence of the two magnetic fields, B and M, the MTB takes the direction of their resultant R. The EMF, M, is a constant. The imposed and new magnetic force B, changes. The resultant R gives the direction of the MTB and it represents the sum of M and B (Figure 7.4). The angle θ is the angle between M and the direction of the MTB. Looking at the diagram, we can see the following relationship between B and M:

$\text{Tan } \theta = B/M$

Because M does not change, the tangent of the angle θ is directly proportional to B.

Experiment of set up test

We made an easy setting using a standard laboratory jar, preferably rectangular identified as (LJ-1). In the assay, we add our bacteria culture in a laboratory t-jar suspended in a o-ring, next to the support frame, where lies a polar coordinate graph (Figure 7.3). We designed this setting so that the axis of the magnetic field (B) is parallel to the plane of of the sediment/water surface and passes through the center of the strain. The magnetic field (B) at the water should be at least a few gauss. The support frame is initially oriented so that the northern magnetic pole (the pole that attracts the North-indicating end of the magnetic compass needle) is nearest the water/sediment. Magnetotactic bacteria in the rectangular jar can be seen swimming persistently in the direction of the resultant R, which is north /east in our setting test experiment (Figure 7.5). The MTB accumulate at the north-eastern side along that edge of the jar. If the support table is now rotated 180°, the bacteria will rotate and swim away from the edge, i.e., they swim in the same direction relative to B. Another 180° rotation of the bar magnet will cause the bacteria to return to the same edge of the jar.

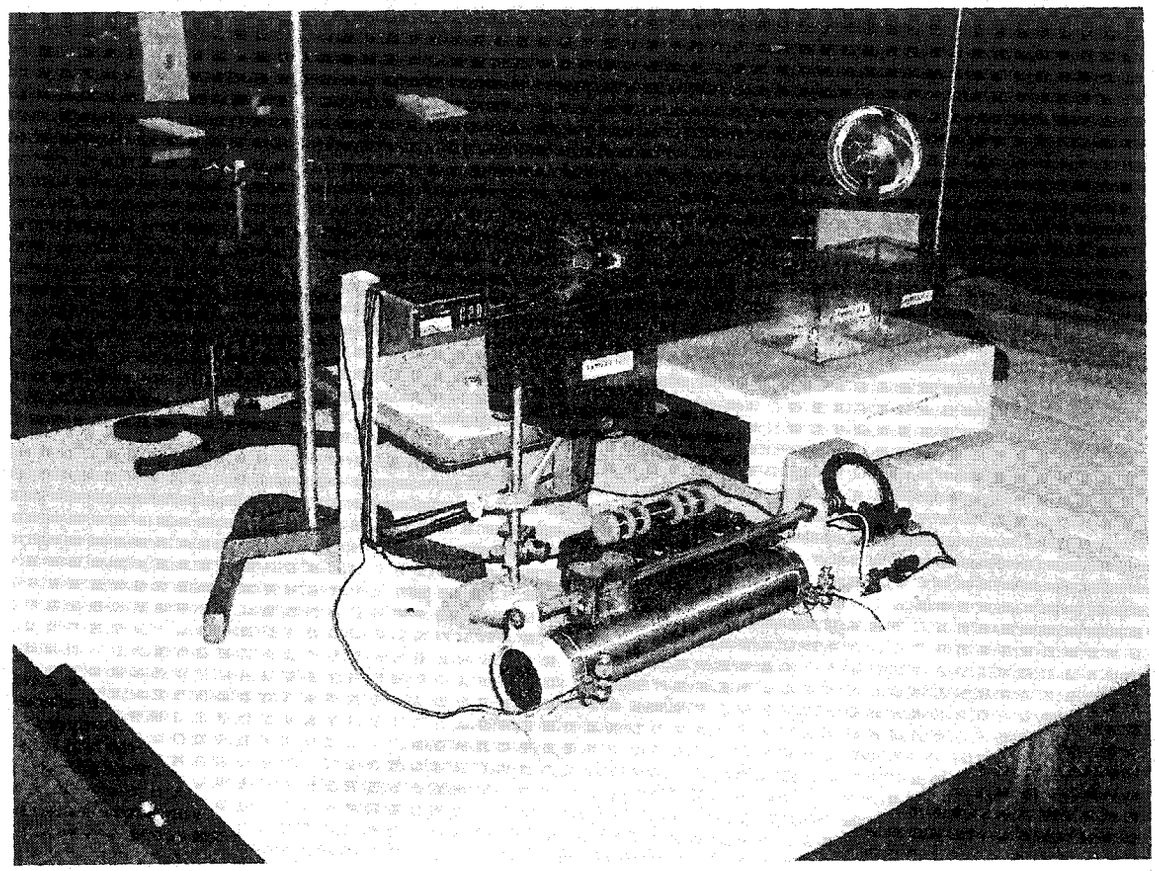

Figure 7.5: Photography of the setting at the BOED J. Ferris HS Science Lab in New Jersey. The laboratory jar JL-T is placed outside the support frame to minimize the new applied magnetic fields.

Bacteria that swim toward the southern Earth magnetic pole of the magnetic field, i.e., when the support frame induced magnetic orientation parallel to B (EMF), are said to have north-seeking (NS) polarity because they would swim northward in the geomagnetic field; bacteria that swim away from the southern magnetic pole (or toward the north magnetic pole), i.e., swim antiparallel to B, are said to have south-seeking (SS) polarity (see background on Magnetotactic Bacteria, chapter 5).

Modified Experimental setups

One modification of the previous assay is to magnetically upgrade the water/sediment sample with a more sophisticated setup by using a current carrying coil that will permit variation of the intensity of the imposed magnetic field B (Figures 7.6). The rheostat controls the quantity of electricity send into the setup. Another rectangular laboratory jar (LJ-2) is placed on the frame table, where a variable and calculated magnetic field is induced into its environment. The new induced magnetic field values are called B1, B2, and B3. The rectugular jar LJ-2 is placed on a table stand perpendicular to the electric current coil setup plan A cover slip permits the elimination of perturbation by other electric devices in the room and the ressessing reduce evaporation of the water. It also allows sediment in the jar LJ-2 to fall to the bottom, leaving the edge of the water clear to view the bacteria. If the induced magnetic fields (B1, B2, and B3) are directed adjacent to the outer surface of the water/sediment sample, the axis of the resultant R induced magnetic field will be perpendicular to the surface water. The MTB will accumulate at in a direction north-

east inside the t-jar, identified by their dark color. They can then be easily removed with a Pasteur pipette and quantified (see data tables graphs, and figures).

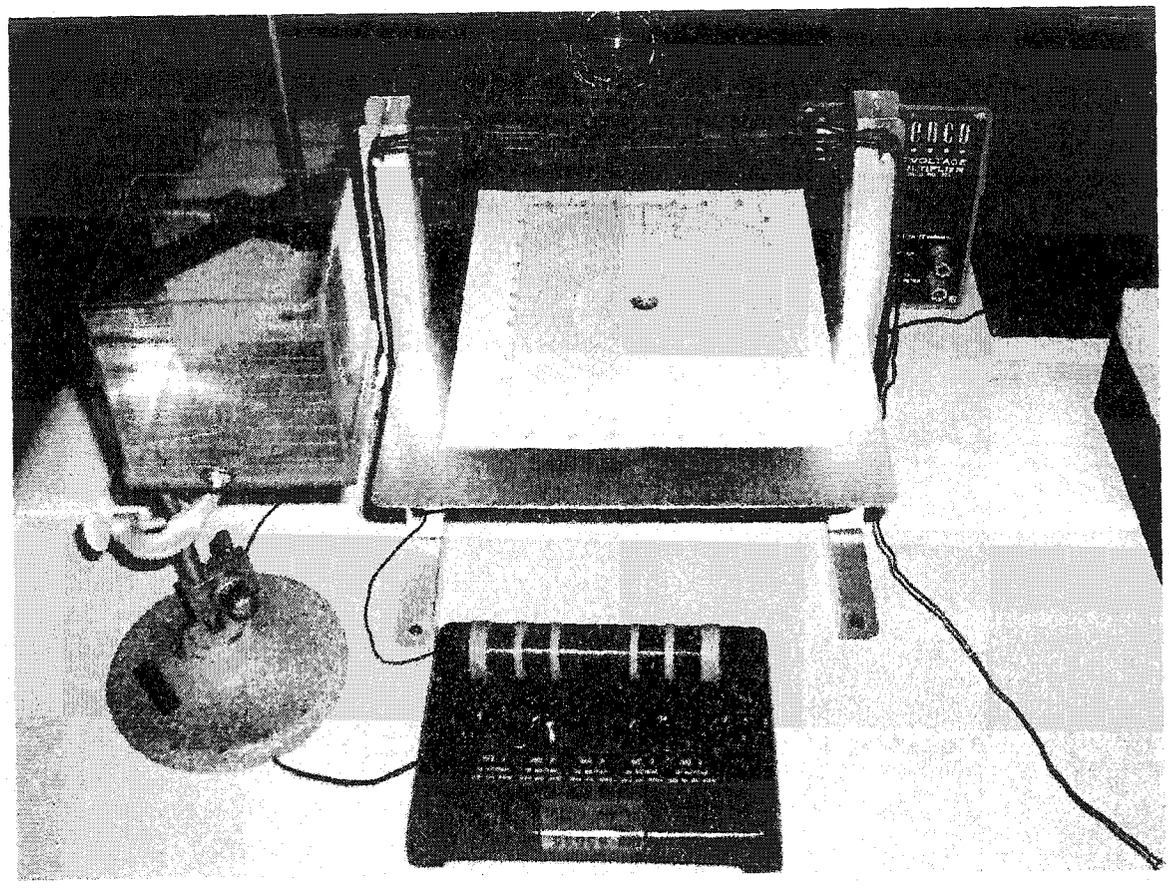

Figure 7.6: Photography showing the setting of the rectangular jar, the compass and the electric current alternator.

Other setups would simply utilize either a current carrying coil wound on a soft iron nail or a Helmholtz coil pair with a reversing current.

The magnetobacterium used in this experiment is from fresh water and is facultative anaerobe that uses either oxygen or nitrous oxide as terminal electron acceptors (Bazylinski et al. 1988; Meldrum et al. 1993).

A capillary "race track" can be added to the setup and placed inside the rectangular jar (at its end corner), where bacterria, subject to the direction of the new induced magnetic field, will accumulate.

A second strain of a culture of fresh water bacteria is set as test in a laboratory jar identified as J-L-T. J-L-T was not submited to any magnetic induction (except that of the Earth's magnetic field).

Our experimental design was not focused on the biotechnical approaches of microbial growth or the study of the bacteria activities. Our research emphasized only one of the different variables or parameters that can affect the accumulations of the microorganisms' bioproducts. The parameters affecting the MTB growth is the author's further post-doctoral research.

RESULTS

The new induced magnetic fields are greater than the Earth's local magnetic field (EMF). This is necessary to reorient the bacteria in the rectangular jars (Figure 7.7). The resultant magnetic force R, applied to the microorganisms, needs to be known. The value of the resultant R was obtained by the calculation of the magnetic moment of the bacteria (APPENDIX D).

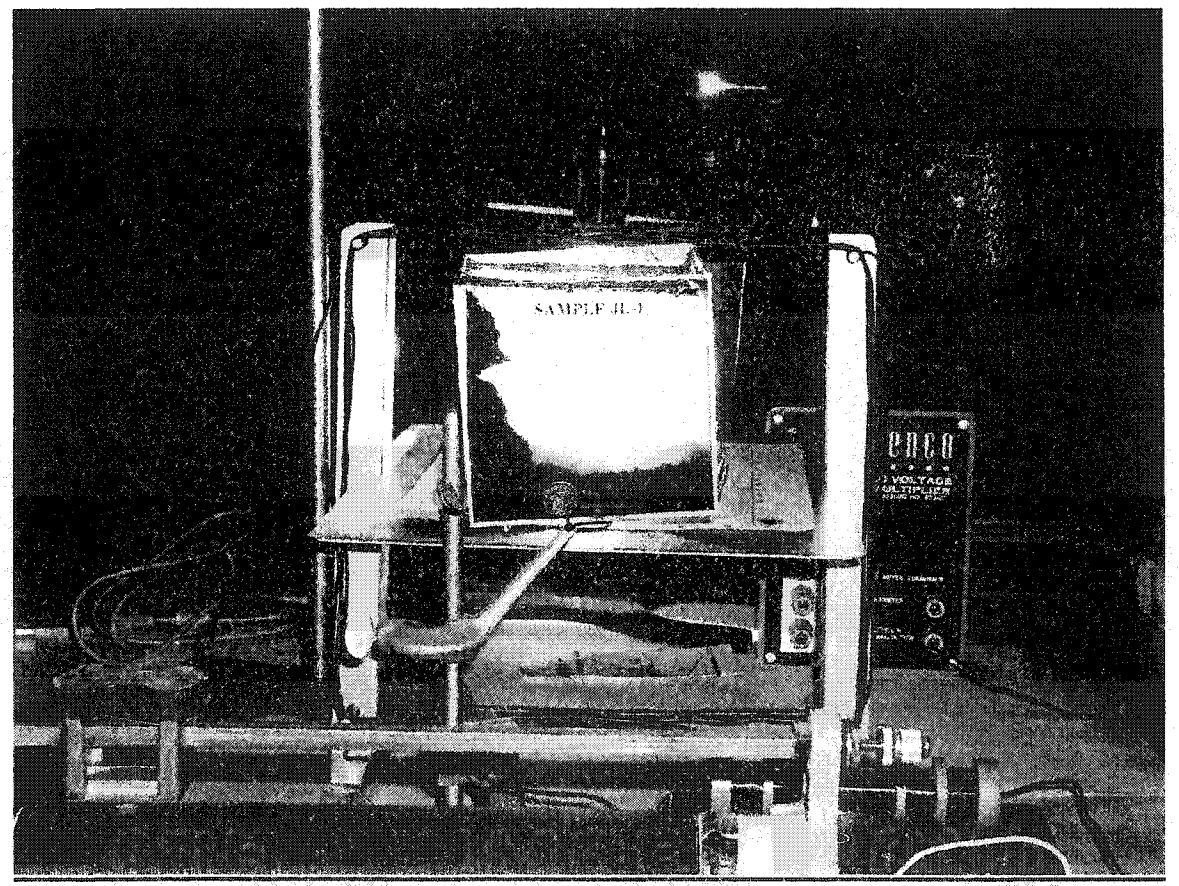

Figure 7.7: Sample JL-1 after 24 hours of magnetic induction in the BOED J. Ferris HS Science Lab.

Accumulation Graphs:

The following graph shows the number of cells accumulated at an increasing bacteria magnetic moment during a period of time of 1 to 24 hours.

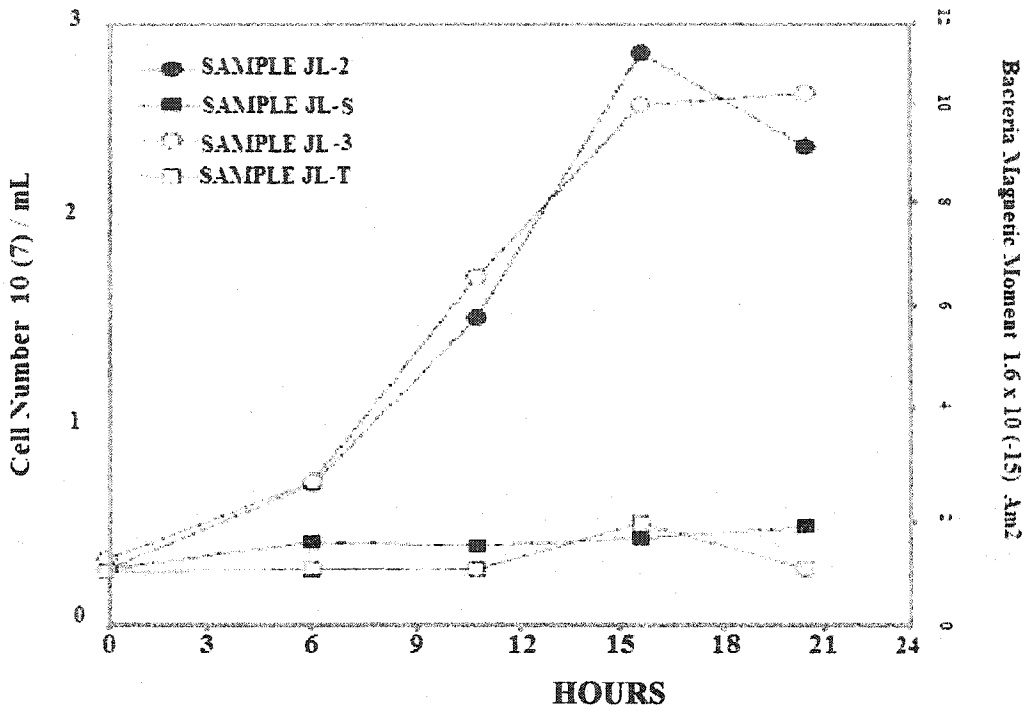

Figure 7.8: This graph shows the concentration of magnetotactic bacteria at various magnetic field intensities that increase the microorganism,s magnetic moment. These results were obtained from estimated cell counts in the laboratory jar-samples JL-1, JL-2, JL-S, and JL-T after 6, 9, 12, 15, 18, and 21 hours of applied magnetic inductions

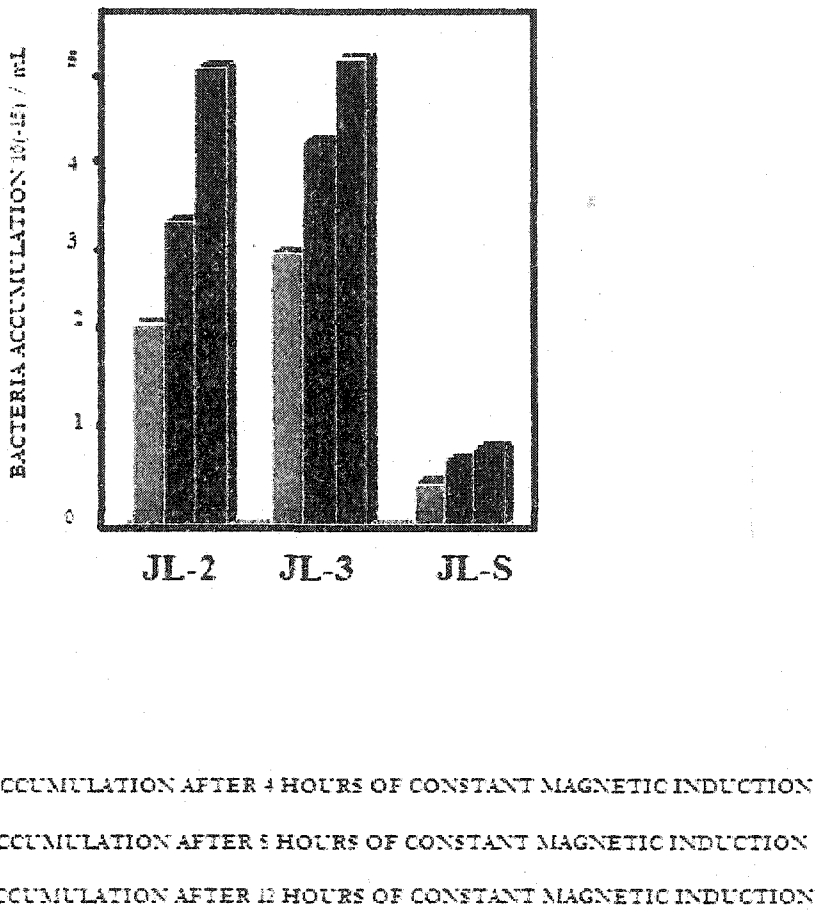

Figure 7.9: Bacterial accumulation measured from laboratory jars JL-2, JL-3, and JL-S after they have been submitted to a constant magmatic induction of 20x10(-6) Emu.

ESTIMATED CELLS NUMBER CURVE AT A CONSTANT MAGNETIC INDUCTION FOR 24 HOURS OF JARS JL-3, JL-2 COMPAREDTO THE JARS JL-S AND JL-T

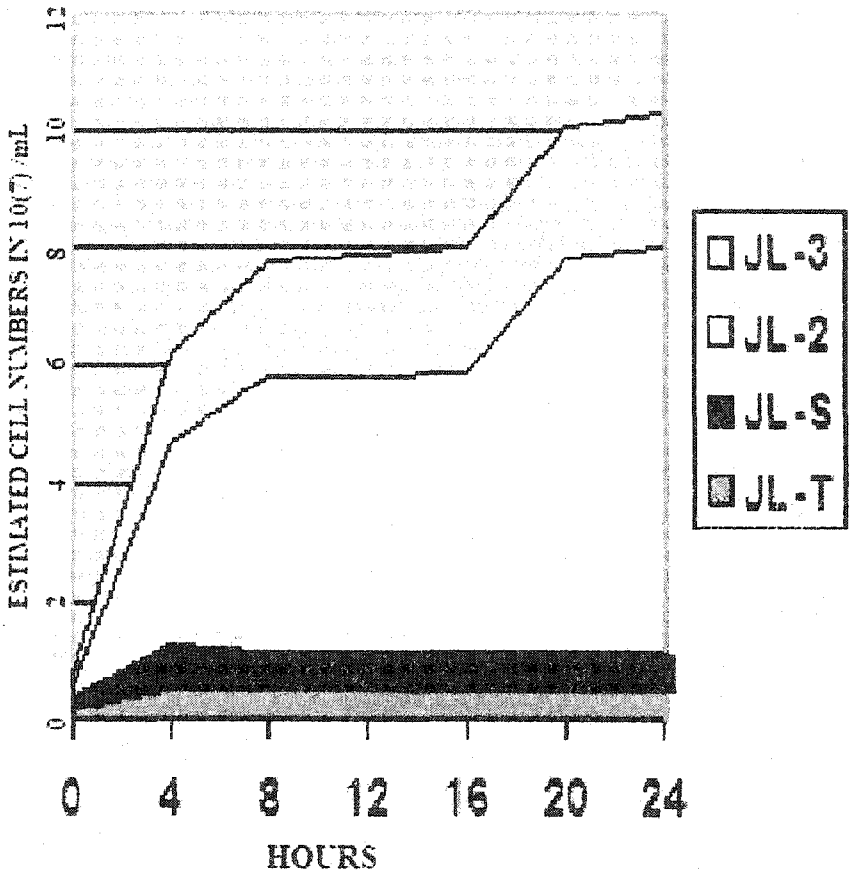

Figure 7.10: The curves show accumulations of bacterial cells during 24 hours in laboratory jars JL-2 and JL-3 compared to the setup test jar (JL-T) and setup sample jar (JL-S).

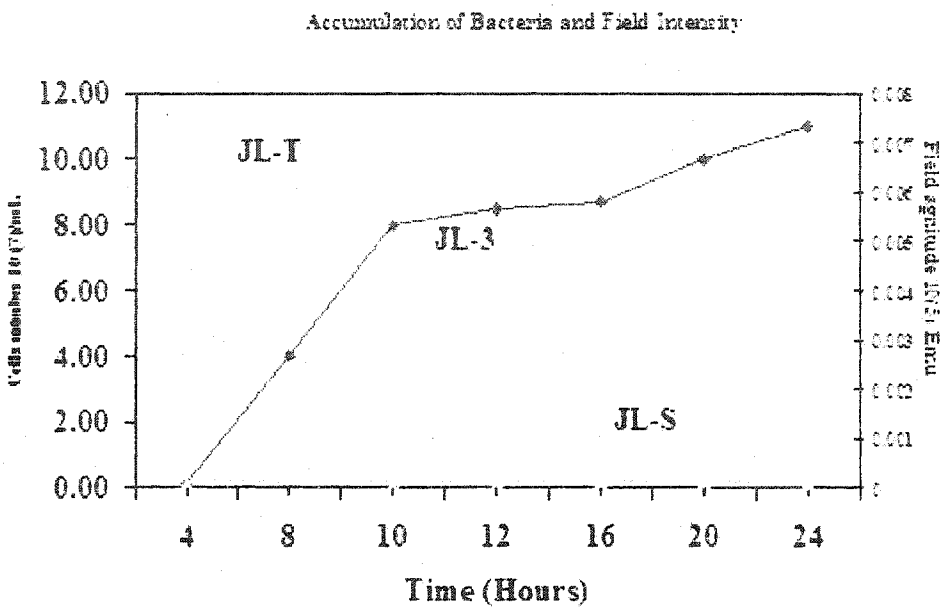

Figure 7.11: Graphs of bacterial accumulations in laboratory jars JL-3, JL-T and JL-S after 24hours of increasing magnetic field intensities. The lab jar JL-S, subjected to the Earth's magnetic field only, did not show any bacterial fluctuation. JL-3 was placed in the support frame and received the variations of applied magnetic intensities. Its curve showed a significant increase of cell numbers.

Field Magnitude: 10.10^{-6} Emu

Time	JL-2 (10^7/mL)	JL-S (10^7/mL)	JL-T (10^7/mL)
2 Hour	19	19	19
10 Hours	38	25	35
24 Hours	89	24	34
36 Hours	89	24	35
48 Hours	78	24	21

Table 7.1: Table showing the accumulations of cells in laboratory jars JL-2, JL-S and JL-T under a constant magnetic intensity of $10x10^{-6}$ Emu, induced from 2 to 48 hours.

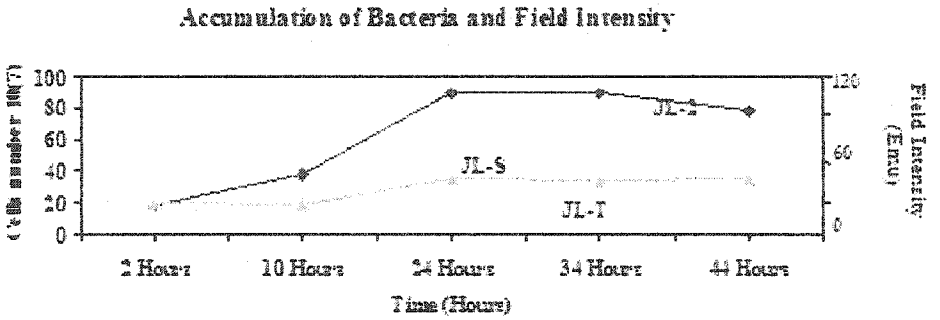

Figure 7.12: Graph constructed from table 7.1 data, showing bacterial accumulation and cells accumualtion in laboratory jars JL-2, JL-S, and JL-T at a constant magnetic induction of 10.10^{-6} Emu.

Field Magnitude: 20. 10^{-6} Emu

Time	JL-2 (10^7/mL)	JL-S (10^7/mL)	JL-T (10^7/mL)
2 Hour	19	19	19
10 Hours	48	46	65
24 Hours	98	44	66
36 Hours	100	46	63
48 Hours	95	38	56

Table 7.2: Table showing the accumulations of cells in laboratory jars JL-2, JL-S and JL-T under a constant magnetic intensity of 20x10^{-6} Emu, induced from 2 to 48 hours.

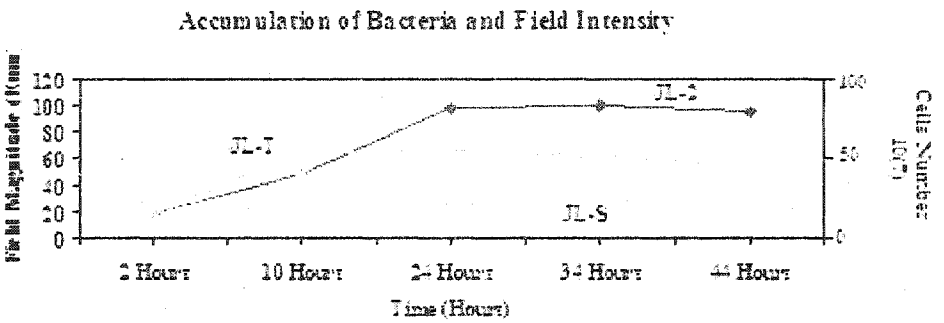

Figure 7.13: Graph constructed from table 7.2 data, showing bacterial accumulation and cells accumualtion in laboratory jars JL-2, JL-S, and JL-T at a constant magnetic induction of 20x10^{-6} Emu.

Field Intensity: 30. 10^{-6} Emu

Time	JL-2 (10^7/mL)	JL-S (10^7/mL)	JL-T (10^7/mL)
2 Hour	19	19	19
10 Hours	52	56	60
24 Hours	79	67	69
36 Hours	89	89	89
48 Hours	99	98	89

Table 7.3: Table showing the accumulations of cells in laboratory jars JL-2, JL-S and JL-T under a constant magnetic intensity of $30x10^{-6}$ Emu, induced from 2 to 48 hours.

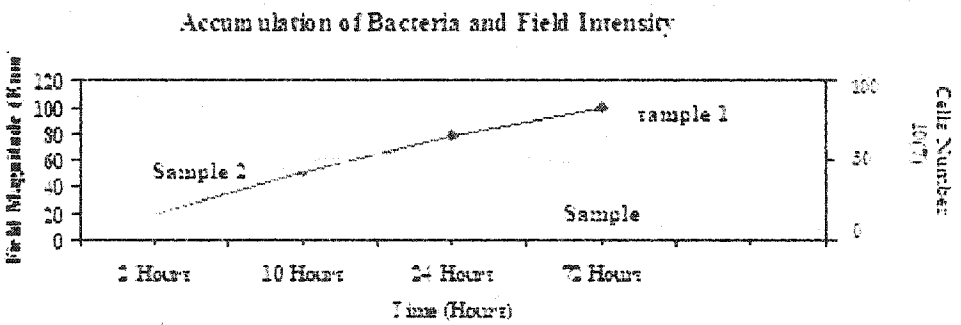

Figure 7.14: Graph constructed from table 7.3 data, showing bacterial accumulation and cells accumualtion in laboratory jars JL-2 (sample 1), JL-S (sample), and JL-T (sample 2) at a constant magnetic induction of 30. 10^{-6} Emu.

DISCUSSION OF RESULTS

Introduction

Quantitative aspects of biogenic magnetite isolation were conducted using the author's experimental setup and a variety of MTB (*Aquaspirillum magnetotactum*). The initial rate, short and long-term extent of bacterial accumulation were linearly correlated with field magnetic intensities. Accumulation rates reached an asymptote at cell concentrations in excess of 2.9 $x10^7$/ mL of aggregates MTB and biogenic iron.

These results demonstrated that the accumulations of MTB cells can be controlled by increasing values of induced magnetic-field intensity. The MTB Strain growth was not the focus in this research. So, we did not monitor their growth rate, which could be further postdoctorate research topics. The count of cells produced per micromole of biogenic minerals was estimated using the cells count method of Lovley and Phillips (1986). During our experiments, the MTB growth, compared to results obtained from previous researches, are estimated from 2 to 4% of their initial number (minimal).

These findings indicate that MTB accumulations may be able to increased significantly in an greater and magnetically induced environment where the biogenic iron are forms of minerals produced from microbial activity. Results suggested that the potential for cell accumulation can be determined by the intensity of the applied magnetic field (the local Earth magnetic field (EMF) or an imposed magnetic field) and the cells' magnetic moment and susceptibility in their environments.

Discussion of the Analytical Techniques

Total MTB in the cultures was determined using the extraction procedure of Erice and Zachara (1996). The extraction from short term magnetic induction (1-2 h), was first performed in a test sample (Sample JL-T) with 0.5 M HCl and measurement of biogenic magnetite was done using a 0.2-*l*m membrane-filtered portion of the extract with 5-10 mL of FerroZine (1 g L-1) in 50 mM HEPES buffer (pH 7) (*5*). Biogenic magnetite were determined by passing a portion of culture through a 0.2-*l*m membrane filter directly into 5-10 mL of FerroZine. Total magnetite was determined by adding a portion of filtered culture to 5-10 mL of FerroZine followed by the addition of 0.25 mL of 10% hydroxylamine hydrochloride so all other Fe(II) are reduced to Fe(III). This facilitates their quantification. The amount of magnetite was estimated by adding a sample (0.5mL) of culture (containing ferrous iron) to 2 mL of N2-bubbled 1M sodium acetate (pH 5) contained in a sealed N2-flushed serum vial. Then, the mid-term analysis after 24-h of magnetic induction was performed, immediately followed by the long term expriment. The cell counts, with variable magnetic field intensities, reached a maximal concentration around the $30x10^6$ cells /mL. All graphs have shown large concentrations of MTB and biogenic iron at the side of the rectangular lab jars, at the direction of the magnetic resultant R (B+M).

In all of extraction series of MTB conducted, unwashed and undiluted N_2-sparged cell suspensions were prepared directly from the MTB cultures under sterile conditions. This approach allowed an acquisition of a large number of cells that were present in sediment-water. For some experiments, MTB collected did not show expected results of accumulation. Unless specified otherwise, the initial count of cell

density in the samples $0.25x10^7$ /mL, as estimated by the relationship between JL-2 and JL-3 in direct cell counts (figures 7.8, 7.9, 7.10, 7.11, 7.12, 7.13, and 7.14. Collection of MTB, in the different water/sediment samples in jars, were performed with sterile syringes and needles that had been flushed with sterile, O2-free N2.

Control Experiments

We checked for the presence of current in the room by placing a jar outside the support frame. This jar contains the same water/sediment mixtures in other samples. This is for the purpose of evaluating a local magnetic induction that could be added to our experimental setup. We checked as well any organic iron coumpounds in the solution that could potentially affect the rate/extent of microbial iron(III) oxide reduction. JL-S is our standard sample (Figure 15).

To check whether or not increasing magnetic moment of MTB could promote the bacterial orientation in the rectangular jar in a manner analogous to that of the EMF, we compared the jars LJ-1 and the standard jar LJ-S, outside the frame. Initial rate of accumulation in the LJ-S were not significantly different from one another (LJ-1, LJ-2, and LJ-T). The amount of MTB accumulation after 5 hours was also similar in the four rectangular jars.

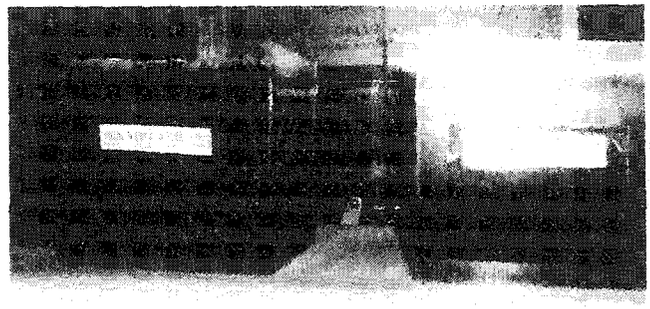

Figure 7.15: Experimental jars setting JL-S and JL-T.

A preliminary comparison of MTB accumulation in all jars showed 40 times more cells in LJ-2 than in JL-S and 10 times more in LJ-1. This could result to the variations of the bacteria different magnetic moments by new and greater magnetic field intensities, or most importantly by the presence of additional amorphous Fe (both from organic and inorganic origin) present in the laboratory jar LJ-2.

This trend was qualitatively consistent with the trend of increasing cells acumulation and field magnetic intensity as shown in graphs. The induced magetic field intensity is a parameter that influences rate of bacteria accumulation (JL-2). The cells accumulation in the water-sediment mixture, over two hours period present in the laboratory jar JL-2, is almost 10 times than that in the lab JL-T. The cells are seen on the side of the jar where the new magnetic field resultant is pointed (Figure 7.16).

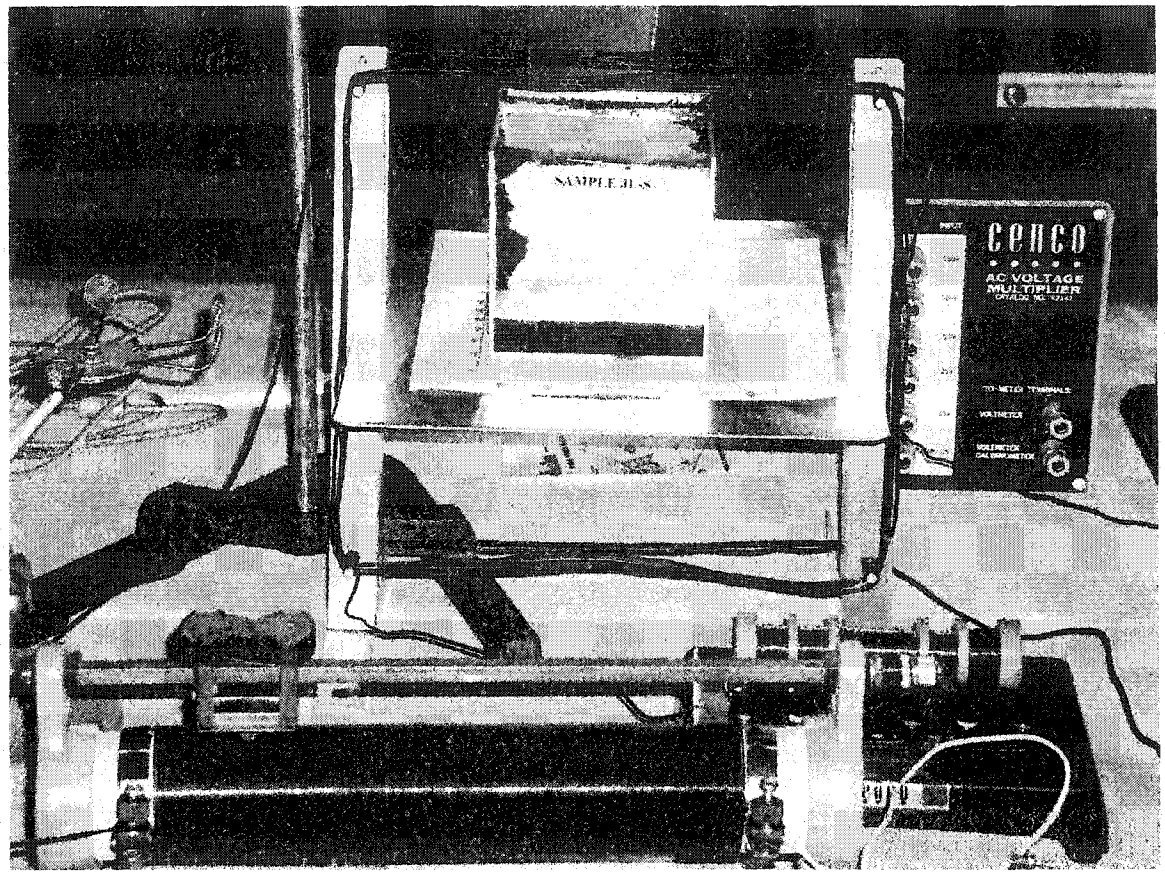

Figure 7.16: Picture of JL-S after short term magnetic induction. The dark place represents the point of cells and iron accumulation in the laboratory jar.

For each of the samples, the accumulation of MTB was proportional to the intensity of field magnetic. Complete saturation of MTB accumulation with respect to the magnetic-field intensity was observed on all sample graphs. Accumulation rates began to level off at the highest magnetic field values.

These results are reflected by the linear correlation between initial accumulations rate and bacterial magnetic moment. All samples were present at the same starting concentration (10-100mmol of Fe L-1). Because of the relationship between accumulation and MTB and cell magnetic moment, a logarithmic relationship

between initial MTB and induced magnetic field intensity was evident (data not shown).

The relationship between MTB accumulation and field magnetic intensity (and the rate of cell density in JL-2) approximated a hyperbolic function. The rate of accumulation leveling off as cell density approached an asymptotic value. The cells' density corresponded to the maximal accumulation. We can then assume that any further increase is simply due to biological activity (proliferation of new cells - growth).

Based on these results, for the range of accumulation included in the calculation of magnetic moment (Tables 7.1, 7.2, and 7.3) , the magnetic field values ranged from 15 to 35% of their maximum intensity. This indicates that an excess of cell accumulation may not have been present at the highest induced magnetic field. We suggest that this is consistent with the fact that accumulation of MTB ratios showed in some cases a modest (up to 10%) decrease within the region of the plots chosen for magnetic field/MTB accumulation.

Effect of MTB accumulations at long-term extent of constant magnetic field intensity

MTB concentrations were measured in jar JL-LT after 48 hours of magnetic induction to determine the longterm effect (Figure 7.17), as a percentage of the initial accumulation of MTB is the same as in the other samples. We also set up a standard sample JL-S and a test sample JL-T for comparison. The bacterial magnetic moment was maintained at a constant value.

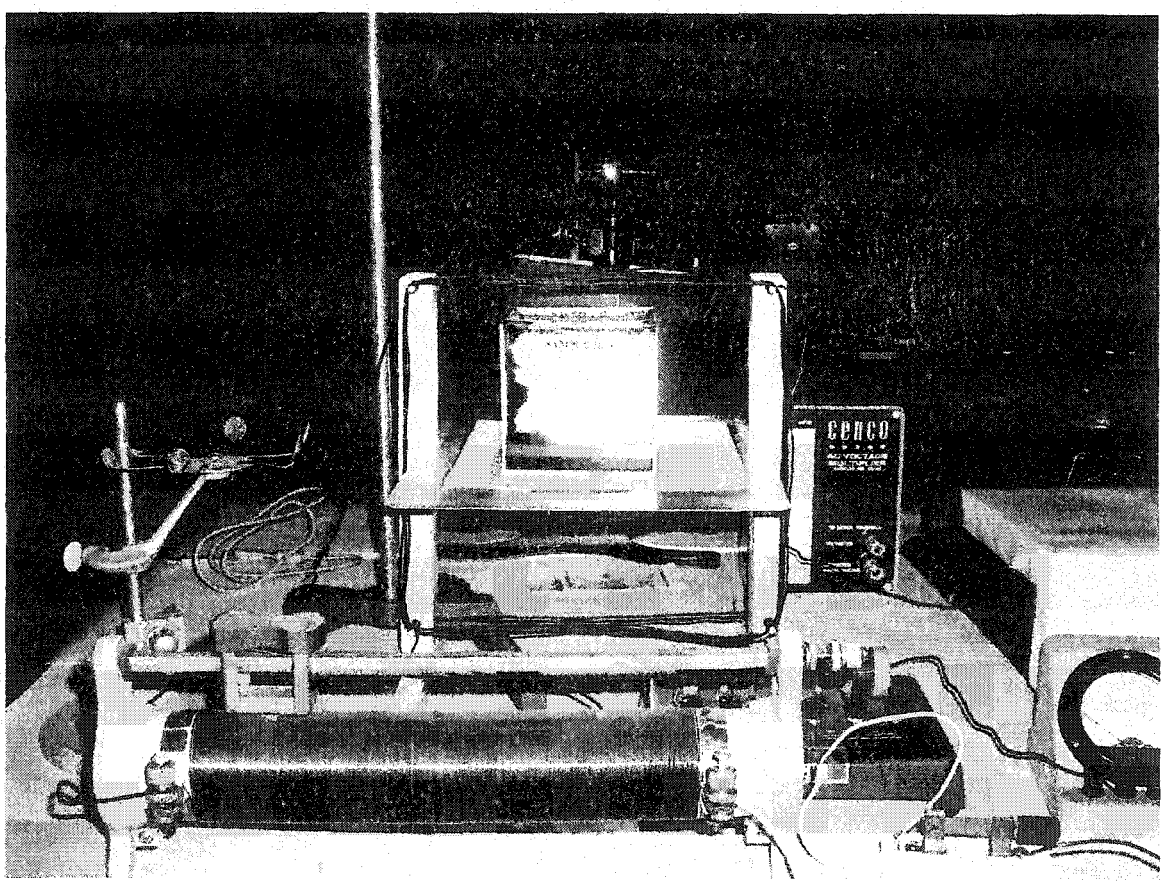

Figure 7.17: Photography of JL-3 after 48 hours of constant magnetic induction.

For a given sample, a consistent fraction of MTB accumulation present in the water/ sediment was slow after 6 hours of magnetic induction (figure 7.18), as reflected by the linear correlations between total accumulation and initial one. The intensity of the induced magnetic field is maintained at a constant value around the jar JL-LT. Other jars, JL-T and JL-S, were subjected only to the EGM. An uncertainty in the MTB accumulation results deserves mention in this regard. The long-term extent of accumulation in JL-LT having same initial MTB concentrations did not follow the rapid linear relationship as observed during the short term induced magnetic field. As shown in the figure 7.9, 7.12, and 7.14, the line graphs did not fall lower after18 hours of magnetic induction. This means that a continuation of a steady magnetic field produce more biogenic magnetite accumulation. This change may have resulted from the following effects:

- dead bacteria due to environmental conditions;
- damage incurred to the cells during collision between each other;
- bacteria attached to biogenic magnetite from dead bacterial;
- the walls of the rectangular lab jar during silmutaneous increase of field magnetic intensity;
- shaking prior to sample removal for MTB counts.

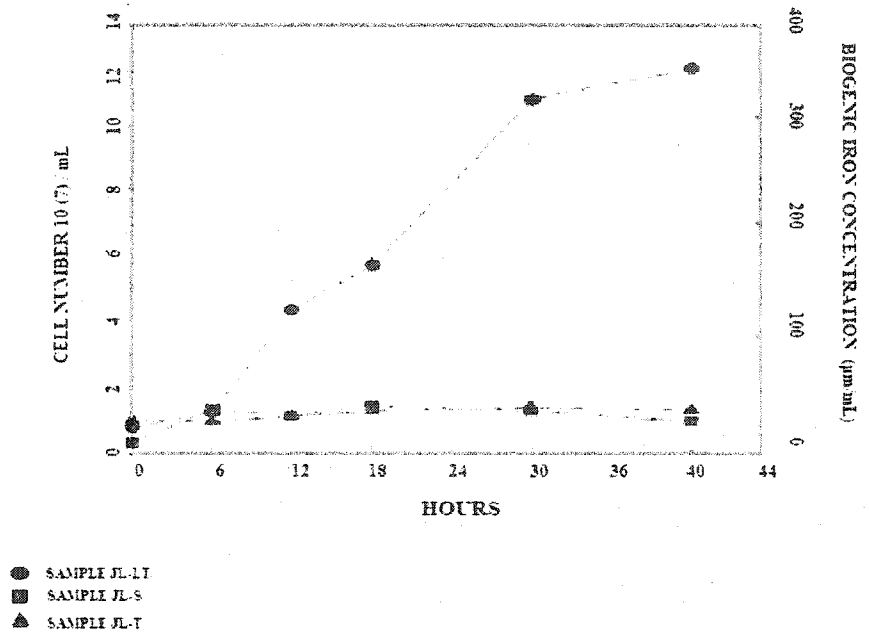

Figure 7.18: The accumulation of biogenic and / or MTB still growing (lightly) after 30 hours of constant magnetic induction during the long term experimental phase. As shown for the other samples JL-T and JL-S, the only magnetic induction was the Earth Geomagnetic field. So, there wasn't major accumulations of MTB or biogenic iron.

Results interpretation

Accumulations in the JL-2 and JL-3 experiments were linear for the first 15 hours, but declined considerably thereafter. In contrast to the standard test sample JL-S and JL-T, accumulation were not significant. These two jars are mgnetically induced by only the EMF. After an induction of 15 hours, the sample JL-T shows a considerable linear regression. A slightly progressive regression in the jar JL-S can be seen. We could not explained the light regression after 15 hours in the JL-S jar (figure 7.19).

The results from long term extent induced magnetic field was in agreement with what would be expected based on the accumulation, indicating that its initial slow rate of accumulations was not reflective of a long-term resistance to the maintained induced-magnetic field. Only a small fraction (<10%) of total MTB was accounted in JL-LT after 48 hours of imposed and constant magnetic field. On a shorter time scale (24-h incubation), the ratio of accumulation declined from 10-25% in MTB and biogenic magnetite.

The addition of any 10% increase of magnetic field intensity to all samples shows only a minor amount of MTB accumulation. Considering this low degree of magnetic enhancement, it is likely that the modest accumulation of MTB (12-16%) observed, was due to a bacterial proliferation, rather than the new imposed magnetic field effects. The EMF was not taking effect due to the higher magnetic intensities from our experiment.

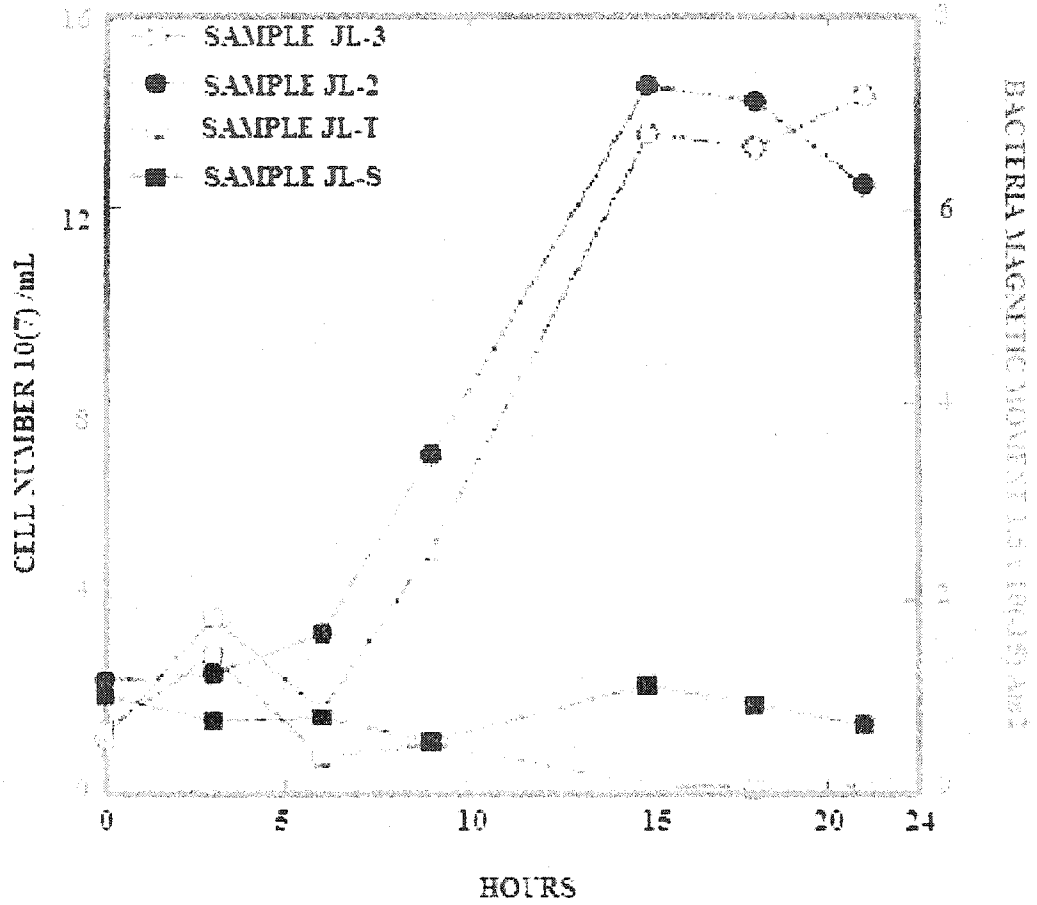

Figure 7.19: Samples Jl-2, JL-3, and JL-T show an initial increase of accumulation due to induced magnetic field afer 3 hours. We assume that the linear regression of samples JL-3 and JL-S could be an unexplained sudden decrease of the induced magnetic field 5 hours after. The standard sample JL-S was only submitted to EMF, so we did not expect any high accumulation. However, the stronger induced magnetic field imposed to JL-2 and JL-3 enhance bacteria accumulation as shown in this figure.

Our investigations demonstrate that the initial rate of accumulation was dependent on the amount of the magnetic intensity. Thus, patterns of microbial concentrations observed in this study can be attributed primarily to interactions of the bacteria with the induced magnetic force.

Collectively, these findings are not unexpected if one assumes that something approaching an excess of cells accumulation, relative to available

growth conditions, was present in the samples, based on results shown.

FTIR Spectromicroscopy

The author used the new Fourier-transform infrared (FTIR) spectromicroscopy beamline (Beamline 1.4.3) at the Hackensack Environmental Center X-Ray Laboratory to obtain spatially resolved magnetic field intensity-dependent evidence for biogenic iron. This procedure was used by Holman et al. , 1999, at the Berley University Laboratory, to demonstrate the Microbial Reduction of Hexavalent Chromium by microorganisms aerobically reducers of Cr6+ (Geomicrobiology Journal 16/307, 1999).

Previously, two results of a short term and long term bacteria and magnetic induction were shown. We postulated that the bacteria require a magnetic field, greater than the Earth's magnetic field (EMF), to be reoriented to their trajectory. The bacterial magnetic moment is directly dependent to the number of cells that can be moved from the medium, in a certain amount of time.

The author conducted FTIR experiments with synchrotron radiation (SR-FTIR) to distinguish the relative significance of these accumulations of biogenic and MTB.

Computer Modeling

The rate of accumulation of MTB can provide a useful informations for environmental studies, switching magnetic susceptibility/moment behavior and time-dependent phenomena. We use current computer modelling to monitor these relationships using calculations and quantitative predictions based on those data as described by Dunlop, 1990 (Figure 7.20). One potential payoff of these models will be to predict the cell accumulation dependent behavior of magnetic moment, coercivity, and susceptibility (ie., hysteresis properties) for the different biogenic iron from microorganisms. Most importantly, these parameters form the basis for interpreting the paleoenvironmental setting at our research site. They could provide the basis for interpreting the magnetic record of paleoclimate change and the magnetic fingerprinting of remagnetization in sediments. These results showed experimental validation of these micromagnetic models and advance our understanding of the magnetic behavior of biogenic magnetite and iron sulfide.

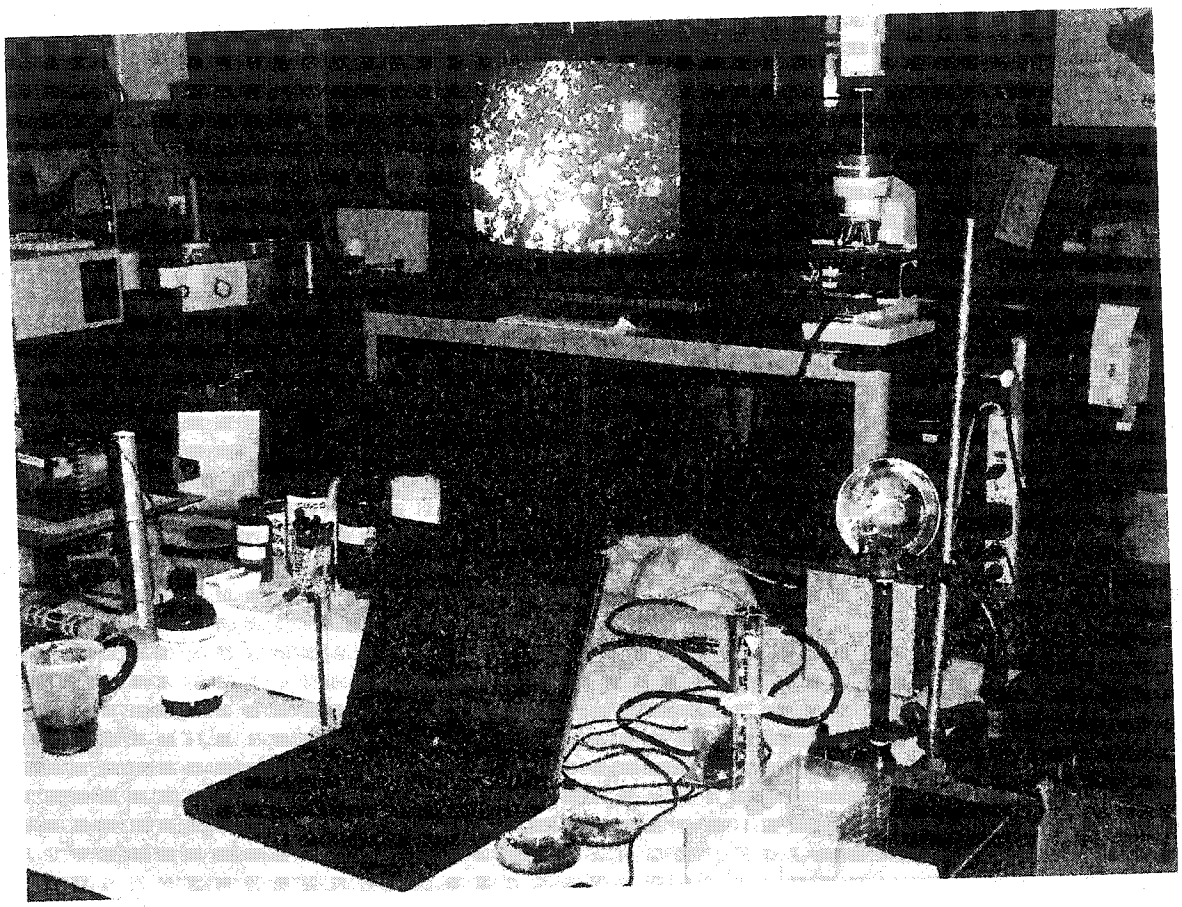

Figure 7.20: Picture showing the computer modelling setting used in this reasearch for MTB accumulation studies.

3-D Graphs Of Short term and long term from computer modeling

The brightness of the infrared radiation made at the HSK EC X-Ray E.lab spatially resolved the spectromicroscopy. Imaging of the surface at characteristic absorption bands showed a strong correlation between peak magnetic moment and time and peak accumulation and cells number (Figures 7.21 and 7.22).

SHORT TERM MAGNETIC INDUCTION (24hrs)

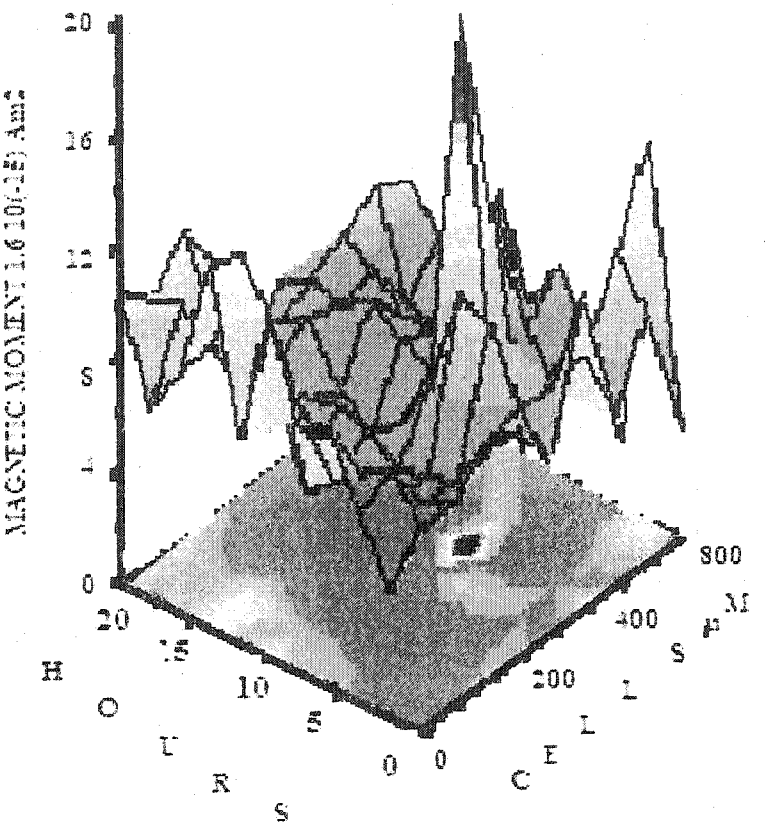

Figure 7.21: Short term magnetic induction from computer modeling results with a 3-D presentation. Imaging of the surface at characteristic absorption bands showed a strong correlation between peak magnetic moment and time and peak accumulation and cells number

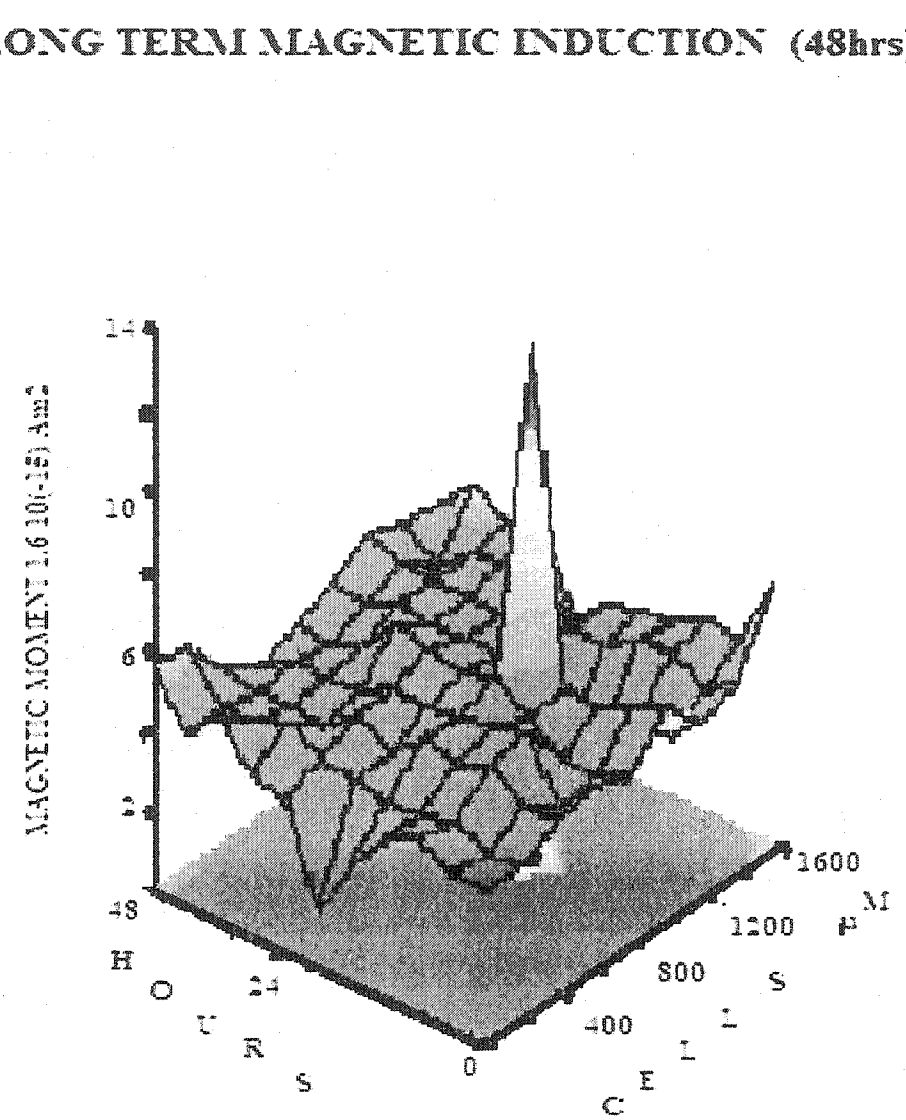

Figure 7.22: Long term magnetic induction from computer modeling results with a 3-D presentation. Imaging of the surface at characteristic absorption bands showed a strong correlation between peak magnetic moment and time and peak accumulation and cells number

In addition, we evaluated effects of environmental conditions such as the bacterial growth in their cultures, the local magnetic field, and the room electric circuit that can induce an added magnetic field. Experiments with increasing cells magnetitic moment showed evidence of accumulation with both when microorganisms were in life and after their die, leaving their biogenic magnetic products in the jars. The accumulation was significantly enhanced when the samples were submitted to higher magnetic field intensities.

Problems

A critical aspect of this project is that despite their ubiquitous occurrence and high abundance, cultivation of MTB in the laboratory has proven difficult. Problems in isolation and cultivation of these bacteria arise from their lifestyle, which is adapted to sediments and chemically stratified aquatic habitats. This make it difficult to carry longer research terms.

As typical gradient organism, MTB depends on complex patterns of vertical chemical and redox gradients, which are difficult to mimic under laboratory conditions. Since no strictly selective media and growth conditions are known for the cultivation of MTB, the effective separation of magnetotactic cells from non-magnetic contaminants is crucial in their isolation (see APPENDIX: Bacteria culture). This can be achieved by exploiting their active migration along magnetic field lines (Wolfe et al., 1987). Growth media involving sulfide and redox gradients have proven useful in the isolation of MTB (Schüler et al., 1999).

Conclusion

These findings, along with our results with MTB accumulation produced by magnetic field, indicate that factors such as field intensity and MTB concentrations in aqueous medium have an important influence on rates of microbial accumulation. Together these considerations lend credence to the cautionary statements of the author regarding the use of variable magnetic field intensity as an important parameter to remove the MTB in a aqueous system.

Inspite of the above caveats, our results suggest that specific increase of magnetic field strenght provides at least a gross indicator of the relative accumulation of MTB. This apparent dependence on magnetic intensity is functional explanation for the major uniformity of biogenic magnetite deposition in sediments.

Both the concentration of cells and field magnetic intensity correlate positively with the accumulation of MTB. We did not quantitatively differentiate their relative role in controlling initial MTB accumulation. However, our results indicate qualitatively that field magnetic intensity is the most significant factor as shown in the following summary tables of bacterial accumulation/field intensity and time.

TABLES OF BACTERIAL ACCUMULATIONS

FIELD MAGNITUDE: 10.10(-6)

Time	JL-2 10^7/mL	JL-S 10^7/mL	JL-T 10^7/mL
2 Hour	19	19	19
10 Hours	38	25	35
24 Hours	89	24	34
36 Hours	89	24	35
48 Hours	78	24	21

Field Magnitude: 20.10 (-6) Emu

Time	JL-2 10^7/mL	JL-S 10^7/mL	JL-T 10^7/mL
2 Hour	19	19	19
10 Hours	48	46	65
24 Hours	98	44	66
36 Hours	100	46	63
48 Hours	95	38	56

Field Intensity: 30.10 (-6) Emu

Time	JL-2 10^7/mL	JL-S 10^7/mL	JL-T 10^7/mL
2 Hour	19	19	19
10 Hours	52	56	60
24 Hours	79	67	69
36 Hours	89	89	89
48 Hours	99	98	89

Water quality and Magnetic Remediation Application

The fouling of groundwater or drainage pumping systems by iron bacteria is a worldwide problem resulting in impaired hydraulic performance, increased pumping costs, maintenance and corrosion. Naturally occurring bacteria such as the commonly called Iron Bacteria: Magnetotactic Bacteria and Sulfate-Reducing Bacteria, given suitable chemical and physical environment can thrive and through their metabolic processes convert soluble ferrous iron into its insoluble ferric form. The result is the familiar reddish brown gelatinous mass of bacteria, iron hydroxides and water. Since the occurrence of these bacteria is due to a combination of physical, chemical and microbiological factors, successful measures must address all of these.

Our research proves that such a problem can be resolved by using the author's magnetic remediation method to remove magnetotactic and other iron bacteria from contaminated mediums. The procedure as describe in this research uses an externally magnetic field greater than the Earth's geomagnetic force. If this new magnetic field is imposed the bacteria, it will reorient their trajectory. We did not emphasize on the cost per unit element. But assumptions are that this technique can be less expensive than those used now in industry.

APPENDIX A: MINERALS OF ANTHONY'S NOSE

AMPHIBOLE: (Ca, Na, Mg, Fe, Al Silicates) The amphibole family includes mostly dark colored minerals that form crystals and fibers. A common example is hornblende which is usually dark green or black. Amphiboles have prismatic cleavage at an oblique angle.

BIOTITE: (Hydrated K, Mg, Fe Silicate) Biotite mica is found in thin, flexible, black sheets. Local crystals are commonly 1/4 to 1 cm across, but much larger in pegmatites.

CALCITE: ($CaCO_3$) Calcite is the most common mineral in marble and limestone. Calcite may form white or clear crystals that sometimes weather to a sugary powder. Susceptibility to chemical weathering can make outcrops relatively scarce.

COPPER and lead minerals including galena, cerussite, pyromorphite, vanadinite, anglesite, vauquelinite, chalcopyrite, azurite, and malachite. The occurrence of vauquelinite was the first reported in the United States.

FELDSPAR: (Al, Ca, Na Silicates) This is the most common family of minerals in the local rocks at Anthony's Nose Westchester. Two varieties are commonly recognized: plagioclase and potassium feldspar. Potassium feldspar is white to pink. Plagioclase is commonly white to green. Both are opaque to translucent, and

relatively hard, with cleavage at nearly right angles. Plagioclase shows striations on some cleavage surfaces (Beck, L. C., 1842).

GARNET: (Ca, Mg, Fe, Mn Silicates) Commonly dark red with a glassy or waxyluster,

MUSCOVITE: (Hydrated K, Al Silicate) The mica minerals readily split into thin, flexible, transparent sheets. In reflection muscovite mica may look silver. Local muscovite crystals are commonly 1/4 to 1 cm across, but much larger in pegmatites (Fleischer, M., 1987).

PEGMATITES exposed during quarrying yielded the only significant crystals of the blue-green amazonite variety of microcline ever found in Anthony's Nose Westchester New York. These microcline crystals reached a maximum size of about 20 cm, but the amazonite color was usually confined to the outer 5 to 6 mm of the crystals with the interior being grayish-green. These and associated peristerite (albite) yielded fine gemstones early in the 20th century (Luquer, L. M., 1896).

PYRITE: (FeS2) Pyrite is fairly common in local marbles as small, shiny metallic yellow crystals, which can be cubic in shape. Pyrite is popularly known as fool's gold. It weathers to a rusty residue.

PYROXENE: (Ca, Mg, Fe Silicates) The pyroxenes are a family of dark colored minerals that form stubby crystals and granular masses. Augite is a common example. Pyroxenes display prismatic cleavage at nearly right angles.

PYRRHOTITE was mined for a number of years at Anthony's Nose, about a mile east of the Bear Mountain Bridge, south of Manitoga Road. Number of minerals are collected from the dumps including albite, amphibole, apatite, aragonite, barite, biotite, calcite, chalcopyrite, copiapite, epidote, goethite, gypsum, hematite, langite, magnetite, melanterite, oligoclase, opal, orthoclase, pyroxene, pyrrhotite, quartz, serpentine, and titanite. The dumps are extensively weathered due to the decomposition of the sulfides. Other localities in the vicinity may be the source of some older specimens labeled Anthony's Nose. Of these, the most interesting specimens were excavated many years ago and consist of plates of interlocked tabular calcite crystals coated with drusy colorless quartz crystals.

QUARTZ: (SiO_2) Quartz is usually clear to milky, but it can also be gray, pink, or almost any color. Fresh faces show a glassy luster and it usually splits along curved (concoidal) surfaces. Quartz weathers slowly and often forms rounded pebbles (Dana, J. D., 1892).

SERPENTITE and associated minerals, such as brucite, chromite, magnesite, titanite, calcite, magnetite, microcline, olivine, spinel, tourmaline, and tremolite (Friedman, G. M., 1952).

SPECIES LISTING: NOMENCLATURE OF FLEISCHER, M., 1987, AND ROBERTS AND AL., 1990, 5TH EDITION, MINERALOGICAL RECORD, INC., TUCSON :

Albite (NaAlSi3O8): cleavelandite, Bedford quarries; peristerite, granite quarry at Valhalla (Black, D., 1948).

Allanite (Ce) [(Ce,Ca,Y)2(Al,Fe)3(SiO4)3(OH)]: Bedford quarries; emery mines in Cortlandt Township; near Peekskill.

Amphibole group Anthony's Nose pyrrhotite mine; hornblende, tremolite, Peekskill;

Analcime [NaAlSi2O6H2O]: excavations on aqueduct.

Andalusite [Al2SiO5]: emery mines in Cortlandt Township.

Anglesite [PbSO4]: old copper mine at Sparta.

Apatite group Anthony's Nose pyrrhotite mine; Bedford quarries;

Barite [BaSO4]: Anthony's Nose pyrrhotite mine.

Bertrandite [Be4Si2O7(OH)2]: Bedford quarries.

Beryl [Be3Al2Si6O18]: common, yellow, golden, aquamarine, Bedford quarries

Bismuthinite [Bi2S3]: Bedford quarries.

Calcite [CaCO3]: Anthony's Nose pyrrhotite mine

Cerussite [PbCO3]: old copper mine Phyllips Mine.

Chalcopyrite [CuFeS2]: Anthony's Nose pyrrhotite mine

Chlorite group: emery mines in Cortlandt Township

Copiapite [Fe+2Fe+34(SO4)6(OH)2 [20H2O]: Anthony's Nose pyrrhotite mine.

Cordierite [Mg2Al4Si5O18]: emery mines in Cortlandt Township.

Corundum [Al2O3]: Crugers; emery, emery mines in Cortlandt Township; emery, Peekskill.

Datolite [CaBSiO4(OH)]: in veins near Yonkers.

Dolomite [CaMg(CO3)2]: quarry at Eastchester; Sing Sing prison quarry, Ossining; Pleasantville; marble quarry at Tuckahoe.

Dumortierite [Al7(BO3)(SiO4)3O3]: granite quarry at Valhalla.

Epidote [Ca2(Al,Fe)3(SiO4)3(OH)]: Anthony's Nose pyrrhotite mine; Bedford quarries; Todd mine, Cortlandt; West Farms; excavations on aqueduct, 2.5 miles north of Yonkers.

Epistilbite [CaAl2Si6O16 5H2O]: Bedford quarries.

Feldspar group Harrison; Larchmont; granite quarry at Valhalla.

Ferrocolumbite [Fe+2Nb2O6]: Bedford quarries.

Fluorite [CaF2]: granite quarry at Valhalla.

Pegmatites [PbS]: Sing Sing prison quarry, Ossining; old copper mine at Sparta (Agar, W. M., 1933).

Garnet group Anthony's Nose pyrrhotite mine; almandine, Bedford quarries; Crugers; Davenport's Neck; emery mines in Cortlandt Township

Goethite [Fe+3O(OH)]: Anthony's Nose pyrrhotite mine; Bedford quarries; Pleasantville.

Graphite [C]: Bedford quarries; Sing Sing prison quarry, Ossining; Peekskill; granite quarry at Valhalla.

Harmotome [(Ba,K)1-2(Si,Al)8O16.6H2O]: veins in gneiss at aqueduct excavations, Ossining; Shaft 5, New Croton aqueduct, Whitson.

Hercynite [Fe+2Al2O4]: Crugers; emery mines in Cortlandt Township (Friedman, G. M. (1952) Sapphirine occurrence of Cortlandt, New York. American Mineralogist 37:244-249).

Heulandite [(Na,Ca)2-3Al3(Al,Si)2Si13O36.12H2O]: veins in gneiss at aqueduct excavations

Hoegbomite [(Mg,Fe+2)2(Al,Ti)5O10]: emery mines in Cortlandt Township (Friedman, G. M., 1952)

ilmenite [Fe+2TiO3]: menaccanite, washingtonite, Bedford quarries.

Kaolinite [Al2Si2O5.(OH)4]: Bedford quarries.

Kyanite [Al2SiO6]: emery mines in Cortlandt Township; Golden's Bridge; Peekskill.

Langite [Cu4(SO4)(OH)6.2H2O]: Anthony's Nose pyrrhotite mine.

Magnetite [Fe+2Fe+32O4]: Anthony's Nose pyrrhotite mine; Bedford quarries, emery mines in Cortlandt Township

Melanterite [Fe+2SO4.7H2O]: Anthony's Nose pyrrhotite mine.

Microcline [KAlSi3O8]: Bedford quarries

Molybdenite [MoS2]: Anthony's Nose pyrrhotite mine; Peekskill.

Muscovite [KAl2(Si3Al)O10(OH,F)2]: Bedford quarries

Natrolite [Na2Al2Si3O10.2H2O]: Anthony's Nose.

Oligoclase [Na,Ca)Al(Al,Si)Si2O8]: Anthony's Nose pyrrhotite mine; Bedford quarries.

Olivine group emery mines in Cortlandt Township

Opal [SiO2.nH2O]: hyalite, Bedford quarries; hyalite.

Orthoclase [KAlSi3O8]: Bedford quarries.

Pectolite [NaCa2Si3O8(OH)]: veins in gneiss at aqueduct excavations

Phosphuranylite [Ca(UO2)3(PO4)2(OH)2.6H2O]: Bedford quarries.

Pyrite [FeS2]: Anthony's Nose pyrrhotite mine; Bedford quarries

Pyromorphite [Pb5(PO4)3Cl]: old copper mine at Phillips Mine.

Pyroxene group Anthony's Nose pyrrhotite mine; Bedford quarries; hypersthene, emery mines in Cortlandt Township

Pyrrhotite [Fe1-xS]: Anthony's Nose pyrrhotite mine.

Quartz [SiO2]: Anthony's Nose pyrrhotite mine; asteriated rose, citrine, milky, rock crystal, smoky, Bedford quarries; smoky, quarry at the emery mines in Cortlandt Township

Sapphirine [(Mg,Al)8(Al,Si)6O20]: emery mines in Cortlandt Township (Friedman, G. M. (1952) Sapphirine occurrence of Cortlandt, New York. American Mineralogist 37:244-249).

Sillimanite [Al2SiO5]: emery mines in Cortlandt Township; Peekskill (Chase, P. J. and Brock, P. W. G., 1976).

Staurolite [Fe+2,Mg,Zn)2Al9(Si,Al)4O22(OH)2]: Crugers; emery mines in Cortlandt Township; Peekskill.

Stilbite [NaCa2Al5Si13O36.14H2O]: Anthony's Nose

Talc [Mg3Si4O10(OH)2]: Anthony's Nose and surrounding.

Thomsonite [NaCa2Al5Si5O20.6H2O]: Peekskill.

Torbernite [Cu(UO2)2(PO4)2.8-12H2O]: Bedford quarries.

Tourmaline group schorl, elbaite, Bedford quarries; emery mines in Cortlandt Township; Harrison; Peekskill

Uranimite [UO2]: Bedford quarries (Kerr , 1935).

Uranophane-beta [(H3O)2Ca(UO2)2(SiO4)2.3H2O]: Bedford quarries.

Vanadinite [Pb5(VO4)3Cl]: old copper mine at Phillips Mine.

Vauquelinite [Pb2Cu(CrO4)(PO4)(OH)]: old copper mine at Phillips Mine.

Wulfenite [PbMoO4]: old copper mine at Phillips Mine

Zircon [ZrSiO4]: cyrtolite, Bedford quarries.

APPENDIX B: PROCESSED SAMPLES

TITLE: SAMPLE AN-142-b

NATURE: MINERAL

SAMPLE ID: AN-142-b

MINERAL TYPE: Inosilicate

MINERAL: Tremolite

GROUP: Amphibole

FORMULA: $Ca_2 Mg_5 Si_8 O_{22} (OH)_2$

COLLECTION LOCALITY: Anthony's Nose, Westchester, New York

CURRENT SAMPLE LOCATION: Author's research collection

PROCESSING CENTER: Laboratory

SAMPLE DESCRIPTION: Forms series with Actinolite and Ferroactinolite. Amphibole, variety Tremolite. Anthony's Nose, Westchester, N.Y. This sample has a fairly prominent broad band near 1μ, indicating that it contains some ferrous ion. It displays a very sharp band at 1.4μ, and less sharp bands between 2.0 and 2.5 μ due to the overtone and combination tones of the OH stretch, respectively. In particular, the bands at 2.2 and 2.3 μ are due to combination tones of the OH stretch with lattice modes. The weak band at 1.9μ is probably due to a small amount of molecular H_2O in the sample.

END SAMPLE DESCRIPTION.

XRD ANALYSIS: Tremolite + medium amount quartz + small amount of mica + large amount of others; M: ~1% magnetite, no other minerals visible (Norma Vergo)

END_XRD_ANALYSIS.

COMPOSITIONAL ANALYSIS TYPE: EM(WDS) # XRF, EM(WDS), ICP(Trace), Chem.

COMPOSITION:	SiO2	57.70	wt%	SiO_2
COMPOSITION:	TiO2	0.05	wt%	TiO_2
COMPOSITION:	Al2O3	1.00	wt%	Al_2O_3
COMPOSITION:	FeO	0.34	wt%	FeO
COMPOSITION:	MnO	0.33	wt%	MnO
COMPOSITION:	MgO	24.45	wt%	MgO
COMPOSITION:	CaO	12.26	wt%	CaO
COMPOSITION:	Na2O	0.51	wt%	Na_2O
COMPOSITION:	K2O	0.15	wt%	K_2O
COMPOSITION:	Total	97.79	wt%	

COMPOSITION_TRACE:

COMPOSITION DISCUSSION:

Average of 6 analyses.

$X_{Fe}^{+2} = 0.0083$ $X_{Fe}^{+3} = 0.0083$ $X_{Mg}^{+2} = 0.9924$ $X_{Fetot} =$ 0.0151

END COMPOSITION DISCUSSION.

MICROSCOPIC_EXAMINATION:

END MICROSCOPIC EXAMINATION.

SPECTROSCOPIC DISCUSSION:

END SPECTROSCOPIC DISCUSSION.

SPECTRAL PURITY: 1 2 3 4

LIB PECTRA HED: where Wave Range Av_Rs_Pwr Comment

LIB SPECTRA: splib04a r 5033 0.2-3.0μm 200 g.s.=

LIB SPECTRA: splib05a r 0.2-3.0μm 200 g.s.=

LIB_SPECTRA: splib06a r 1.5-25μm 250 g.s.= END ANALYSIS

TITLE: AN-143-X

NATURE: MINERAL

SAMPLE ID: AN-143-X

MINERAL TYPE: Inosilicate

MINERAL: Anthophylite

GROUP: Amphibole

FORMULA: $(Mg,Fe^{+2})_7 Si_8 O_{22} (OH)_2$

COLLECTION LOCALITY: Anthony's Nose, Westchester, NY

CURRENT SAMPLE LOCATION: Author's research collection

PROCESSING CENTER: Laboratory

SAMPLE DESCRIPTION: Forms series with Magnesio-anthophyllite and Ferro-anthophyllite. Spectra: the dominant feature in its spectrum is the very well defined band at 0.95μm due to Fe^{+2} in the octohedral site, and bands at 0.375, 0.475 and 0.65μm accompany this. The very weak 0.65μm band indicates the presence of a very little ferric iron, which enters the mineral when aluminum substitutes for silicon.

Bands at 1.4, 2.32, and 2.4μm are all due to the OH vibrations, and there is a complete absence of evidence for molecular H_2O.

SPECIAL NOTE: Some magnetite contamination, high reflectance level at 1.6 μm, trace and be very low.

END_SAMPLE_DESCRIPTION.

XRD_ANALYSIS: 40 kV - 30 mA, 6.5-9.5 keV

File: AN-102-JC (smear mount on quartz plate)

Talc, anthophyllite, minor 14 angstroms-chlorite, possible trace of mica

Comment: Talc peaks are strong and the basal reflections are very sharp; resolution of the alpha1-alpha2 reflections is good. Amphibole peaks are much less intense but sharp. Theses phases appear homogenous in composition and well crystallized. The amphibole is orthorhombic and its pattern is consistent with that of anthophyllite. (Comparison and random and smear mounts proves that talc is the dominant phase.) A minor chlorite phase displayed basal spacing consistent with chamosite 1M or clinochlore 1M. A trace of mica (reflection at 10.4 angstoms) could not be further characterized. Very weak unindexed reflections at 8.6 and 7.4 angstoms. Very fine-grained sample.

40 kV -30 mA, 6.5-9.5 keV ; subordinate orthoamphibole, minor chlorite, trace mica (?), unindexed reflections of a minor phase(s) at 7.4 angstroms (weak intensity), 4.55 (strong, broad) 3.56 (medium), 2.63 (medium, broad), 2.49 (strong, broad), 2.45 (medium, broad), 2.23 (medium weak, broad), 1.42 (weak, broad);

END_XRD_ANALYSIS.

COMPOSITIONAL_ANALYSIS_TYPE: None # XRF, EM(WDS), ICP(Trace), Wchem COMPOSITION_TRACE: None

COMPOSITION_DISCUSSION: None.

END COMPOSITION DISCUSSION.

MICROSCOPIC EXAMINATION: Asbestiform crystal habit, pale color due to Fe-staining? Length slow, straight extinction. No twinning. These characteristics are consistent with anthophyllite. Grain size is that of clumps of fibers. G. Swayze

END MICROSCOPIC EXAMINATION.

SPECTROSCOPIC DISCUSSION:

END SPECTROSCOPIC DISCUSSION.

SPECTRAL PURITY: 1 2 3 4

LIB SPECTRA HED: where Wave Range Av_Rs_Pwr Comment

LIB SPECTRA: splib04a r 490 0.2-3.0μm 200 g.s.= 150 μm

LIB SPECTRA: splib05a r 0.2-3.0μm 200 g.s.=

LIB SPECTRA: splib06a 5-25μm 250 g.s.=

END ANALYSIS

TITLE: AN-148-X

NATURE: MINERAL

SAMPLE ID: AN-148-X

MINERAL TYPE: Inosilicate

MINERAL: Rhodonite

GROUP:

FORMULA: Mn SiO_3

COLLECTION LOCALITY: Authony's Nose

CURRENT SAMPLE LOCATION: Author's research collection

PROCESSING CENTER: Laboratory

SAMPLE DESCRIPTION: This sample contains very small amounts of magnetite, pyrolusite and calcite. The visible spectrum is dominated by features typical of Mn^{2+} transitions, displaying bands at 0.35 μ, 0.37 μ, 0.42 μ, and 0.55 μ, resulting in the characteristic pink color of this mineral. The strong broad band near 1.04 μ and 1.9 μ features are typical of molecular water, probably in fluid inclusions.

END_SAMPLE_DESCRIPTION.

XRD_ANALYSIS: 40 kV - 30 mA, 7.3-9.5 keV

Comments: Peaks are symmeteric but not strong; alpha1-alpha2 are not resolved. The pattern has a high background caused by X-ray fluorescence (Mn- or Fe-rich composition is probable). HS-325 is very similar to Huebner's reference patterns for synthetic pyroxmangite of MnSiO3 composition (runs Hy-67 and run-130) and unlike that of rhodonite. Profile based search-match returns pyroxmangite. There are weak, very sharp reflections at 7.2 and 1.912 angtroms but no mineral in the PDF2 database has two strong reflections at these positions.

END XRD ANALYSIS

COMPOSITIONAL ANALYSIS TYPE: None # XRF, EM (WDS), ICP(Trace), Wchem

COMPOSITION TRACE:

COMPOSITION DISCUSSION:

END COMPOSITION DISCUSSION

MICROSCOPIC EXAMINATION

END MICROSCOPIC EXAMINATION

SPECTROSCOPIC DISCUSSION

END SPECTROSCOPIC DISCUSSION

SPECTRAL PURITY: 1 2 3 4

LIB SPECTRA HED: where Wave Range Av_Rs_Pwr Comment

LIB SPECTRA: splib04a r 4208 0.2-3.0μm 200 g.s.=

LIB SPECTRA: splib05a r 0.2-3.0μm 200 g.s.=

LIB SPECTRA: splib06a r 1.5-25μm 250 g.s.=

END ANALYSIS

TITLE: AN-155

NATURE: MINERAL

SAMPLE ID: AN-155

MINERAL TYPE: Phyllosilicate

MINERAL: Talc

GROUP:

FORMULA HTML: $Mg_3 Si_4 O_{10} (OH)_2$

COLLECTION LOCALITY: Anthony's Nose, Westchester, NY

CURRENT SAMPLE LOCATION: Author's research collection

SAMPLE DESCRIPTION: Talc is a hydrous magnesium silicate, essentially $Mg_3Si_4O_{10}(OH)_2$, of secondary origin. It may be found in altered igneous rocks, but is more typical of metamorphic varieties. It is formed by alteration of magnesian silicates such as olivine, pyroxenes and amphiboles. Talc may bear a little iron, aluminum or nickel, and ferrous ion in this talc probably accounts for the iron bands on either side of 1μ. The sample appears uncontaminated by unaltered pyroxene, which might otherwise contribute these bands. Hydroxyl bands are particularly strong and sharp in this sample, which displays them near 1.4μ and 2 to 2.6 μ. The extremely sharp, but weak feature at 0.95μ must also be due to OH.

END SAMPLE DESCRIPTION.

XRD ANALYSIS: Talc + med. amount chlorite; M: ~2% chlorite, <<2% magnetite

END XRD ANALYSIS.

COMPOSITIONAL ANALYSIS TYPE: EM # XRF, EM(WDS), ICP(Trace), WChem

COMPOSITION:	SiO2	60.47	wt%	SiO_2
COMPOSITION:	TiO2	0.04	wt%	TiO_2
COMPOSITION:	Al2O3	0.12	wt%	Al_2O_3
COMPOSITION:	Fe2O3	0.87	wt%	Fe_2O_3
COMPOSITION:	FeO	0.10	wt%	FeO
COMPOSITION:	MnO	0.01	wt%	MnO
COMPOSITION:	MgO	30.29	wt%	MgO
COMPOSITION:	ZnO	0.00	wt%	ZnO
COMPOSITION:	BaO	0.01	wt%	BaO
COMPOSITION:	CaO	0.05	wt%	CaO
COMPOSITION:	Na2O	0.04	wt%	Na_2O
COMPOSITION:	K2O	0.00	wt%	K_2O
COMPOSITION:	P2O5	0.27	wt%	P_2O_5
COMPOSITION:	Cl	0.01	wt%	Cl
COMPOSITION:	F	0.51	wt%	F
COMPOSITION:	LOI	5.31	wt%	LOI
COMPOSITION:	Total	92.31	wt%	

COMPOSITION TRACE: None

COMPOSITION DISCUSSION: Because of variability in the analyses, most Fe is probably Fe^{+2}.

NOTE: Conversion of Fe_2O_3 to FeO. This sample has too much chlorite. Therefore, Fe ratios are unusable.

END COMPOSITION DISCUSSION

MICROSCOPIC EXAMINATION:

END MICROSCOPIC EXAMINATION

SPECTROSCOPIC DISCUSSION:

END SPECTROSCOPIC DISCUSSION

SPECTRAL PURITY: 1 2 3 4

LIB SPECTRA HED: where Wave Range Av_Rs_Pwr Comment

LIB SPECTRA: splib04a r 4687 0.2-3.0μm 200 g.s.=

LIB SPECTRA: splib05a r 0.2-3.0μm 200 g.s.=

LIB SPECTRA: splib06a r 1.5-25μm 250 g.s.=

END ANALYSIS

TITLE: Sample AN-156-a

NATURE: Mineral

SAMPLE ID: AN-156-a

MINERAL TYPE: Nesosilicate

MINERAL: Titanite (Sphene)

MINERAL FORMULA: $CaTiO(SiO_4)$

COLLECTION LOCALITY: Anthony's Nose, Westchester, New York

CURRENT SAMPLE LOCATION: Author's research collection

PROCESSING CENTER: Spectroscopy Laboratory

SAMPLE_DESCRIPTION: $CaTiO(SiO_4)$: Sphene is a widespread accessory mineral in igneous and metamorphic rocks. Calcium may be replaced partially by strontium and barium, or by the rare earths and thorium, the higher valencies of the latter being balanced by the entry of trivalent iron and aluminum into the titanium position. The titanium may be partially replaced by Sn, Nb and Ta, with possible compensation of Na replacing Ca. Finally, OH or F may replace one O. This particular sample is a dark reddish brown, apparently due primarily to both the ferric iron and titanium, as described for rutile. The presence of about 5 percent opaque magnetite lowers the overall reflectivity of this sample.

Sieve interval 74 - 250μm.

END SAMPLE DESCRIPTION.

XRD ANALYSIS: 40 kV - 30 mA, 6.5-9.5 keV

Found: Titanite, minor quartz, albite, unidentified weak reflections at 7.1, 3.03, 2.90,

and 2.71 angstroms

Comment: Titanoite is the preferred name for sphene. The albite is very sodic, but the pattern is not sufficiently strong for determination of the structural state by the method of Wright (1968)

END XRD ANALYSIS.

COMPOSITIONAL ANALYSIS TYPE: None # XRF, EM(WDS), ICP(Trace), Wchem

COMPOSITION TRACE:

COMPOSITION DISCUSSION:

END COMPOSITION DISCUSSION

MICROSCOPIC

EXAMINATION:

END MICROSCOPIC EXAMINATION.

SPECTROSCOPIC DISCUSSION:

END SPECTROSCOPIC DISCUSSION

SPECTRAL PURITY: 1 2 3 4

LIB SPECTRA HED: where Wave Range Av_Rs_Pwr Comment

LIB SPECTRA: splib04a r 4593 0.2-3.0μm 200 g.s.=

LIB SPECTRA: splib05a r 0.2-3.0μm 200 g.s.=

LIB_SPECTRA: splib06a r ____ 1.5-25μm 250 g.s.=

TITLE: AN-137

NATURE: MINERAL

SAMPLE ID: AN-137

MINERAL TYPE: Phyllosilicate

MINERAL GROUP: Mg-Clinochlore (Chlorite group)

FORMULA: $(Mg,Fe^{+2})_5$ Al (Si_3Al) $O_{10}(OH)_8$

COLLECTION LOCALITY: Anthony's Nose, Westchester, New York

CURRENT SAMPLE LOCATION: Author Research Collection

SAMPLE DESCRIPTION: Forms series with Chamosite, Chlorite group.

END_SAMPLE_DESCRIPTION.

XRD_ANALYSIS: Pure magnesium clinochlore

END_XRD_ANALYSIS.

COMPOSITIONAL_ANALYSIS_TYPE: XRF # XRF, EM(WDS), ICP(Trace), WChem

COMPOSITION:	SiO2	32.0	wt%	SiO_2
COMPOSITION:	TiO2	<0.02	wt%	TiO_2
COMPOSITION:	Al2O3	16.0	wt%	Al_2O_3
COMPOSITION:	Fe2O3	3.76	wt%	Fe_2O_3
COMPOSITION:	MnO	<0.02	wt%	MnO
COMPOSITION:	MgO	33.9	wt%	MgO

COMPOSITION:	CaO	0.09	wt%	CaO
COMPOSITION:	Na2O	<0.15	wt%	Na_2O
COMPOSITION:	K2O	0.07	wt%	K_2O
COMPOSITION:	P2O5	<0.05	wt%	P_2O_5
COMPOSITION:	Total		wt%	
COMPOSITION:	O=Cl,F,S		wt%	#correction for Cl, F, S
COMPOSITION:	New Total		wt%	

COMPOSITION TRACE: None

COMPOSITION DISCUSSION:

END COMPOSITION DISCUSSION.

MICROSCOPIC EXAMINATION: Basal cleavage, pale green color, scaly aggregates, first order gray interference color, low relief, all consistent with chlorite. Trace magnetite and epidote(?); plates 35 µm thick and 500 µm in diameter.

END MICROSCOPIC EXAMINATION

SPECTROSCOPIC DISCUSSION:

END SPECTROSCOPIC DISCUSSION.

SPECTRAL PURITY: 1 2 3 4

LIB SPECTRA HED: where Wave Range Av_Rs_Pwr Comment

LIB SPECTRA: splib04a r 1064 0.2-3.0µm 200 g.s.= 500 µm

LIB SPECTRA: splib05a r 0.2-3.0μm 200 g.s.=

LIB SPECTRA: splib06a r 1.5-25μm 250 g.s.=

APPENDIX C: CALCULATION OF THE MAGNETIC SUSCEPTIBILITY

Magnetic susceptibility is defined as the magnetization of a material per unit field applied. It describes the magnetic response of a substance to an applied magnetic field. If the intensity of magnetization, a dimensionless quantity, is represented by I, and the magnetic field strength is represented by H, the magnetic susceptibility, denoted by χ, can be expressed as:

$$\chi = \frac{I}{H} \qquad (1)$$

Multiplying χ by the molar volume (M/χ), where M is the molecular weight (g/mol), and χ is the density (g/cm^3), introduces the quantity called molar magnetic susceptibility (χ_M).

$$\chi_M = \chi \times M/\chi \qquad (2)$$

For paramagnetic substances, χ_M is positive, while diamagnetic materials have negative molar susceptibilities.

When an object is placed in a homogeneous magnetic field, the field generally induces a magnetic moment (χ) in the object. An isolated electron with a tiny spinning magnetic charge creates a spin magnetic moment (χ_{spin}). Materials with no

unpaired, or isolated, electrons are considered diamagnetic, and substances with odd, unpaired electrons are called paramagnetic. Upon evaluating the constants involved, the magnetic moment of a substance can be expressed as:

$$\mu_{spin} = 2.84\sqrt{\chi_M T} \qquad (3)$$

where χ_M is the molar magnetic susceptibility, and T is the temperature in Kelvin (Spencer 278).

In the absence of an external magnetic field, the period of oscillations (T) for a simple pendulum can be approximated by:

$$T = 2\pi\sqrt{\frac{l}{g}} \qquad (4)$$

where l is the length of the string, and g is the gravitational constant (9.8 m/s^2 near the surface of the earth). When a simple pendulum containing a paramagnetic sample oscillates within a magnetic field, an additional force proportional to χH^2 pulls the pendulum into the region of highest magnetic field strength at the lowest point in its trajectory (Spencer 278). This force acts like an additional gravitational force and effectively decreases the period of the pendulum.

$$T' = 2\pi\sqrt{\frac{l}{g'}} \qquad (5)$$

The change in effective acceleration due to gravity {χg=g'-g} in relation to the period of oscillations 0can be easily received from Equations 4 and 5 as (Spencer 278):

$$\Delta g = 4\pi^2 l\left(\frac{1}{T^2} - \frac{1}{T'^2}\right) \qquad (6)$$

The value χg multiplied by the mass (m) of the sample is equivalent to an effective weight change, χW=mχg.

Substituting for χg yields the following expression for χW yields

Using a standard reference material, denoted by the subscript s, whose molar susceptibility (χ_{Ms}), molecular weight (M_s), and density (χ_s) are known, the magnetic moment of a sample can be related to a standard by modifying equation (3) (Spencer 278):

$$\mu_{spin} = 2.84\sqrt{\frac{\Delta W}{\Delta W_s}\frac{M}{M_s}\frac{\rho_s}{\rho}\chi_{Ms}T} \qquad (9)$$

where T is the temperature in Kelvin. By equating Equation 9 with Equation 3, the following equation is obtained.

$$2.84\sqrt{\chi_M T} = 2.84\sqrt{\frac{\Delta W}{\Delta W_s}\frac{M}{M_s}\frac{\rho_s}{\rho}\chi_{Ms} T} \qquad (10)$$

Solving for χ_M leads to the following relation:

$$\chi_M = \chi_{Ms}\frac{\Delta W}{\Delta W_s}\frac{M}{M_s}\frac{\rho_s}{\rho} \qquad (11)$$

Finally, substituting for ΔW and ΔW_s yields the following equation for magnetic susceptibility of a substance at a constant temperature.

$$\chi_M = \chi_{Ms}\frac{M}{M_s}\frac{\rho_s\left(\frac{1}{T^2}-\frac{1}{T'^2}\right)}{\rho\left(\frac{1}{T_s^2}-\frac{1}{T_{s'}^2}\right)}$$

Solving equation (12) for the unknown quantities $\chi_M\rho/M$ results in the following relation.

$$\frac{\chi_M\rho}{M} = \chi_{Ms}\frac{1}{M_s}\rho_s\frac{\left(\frac{1}{T^2}-\frac{1}{T'^2}\right)}{\left(\frac{1}{T_s^2}-\frac{1}{T_{s'}^2}\right)} \qquad (13)$$

By comparing molar susceptibility with this parameter for several compounds, a χ_M versus $\chi_M\chi/M$ graph can be plotted, and the magnetic susceptibility of magnetotactic bacteria can be extrapolated.

Methods

The experiment was set up as followed (see figure 7.1):

1. A coffee stirrer was cut into a 1cm length. A small hole was made in the lid of a plastic litmus paper container. The lids of six Eppendorf tubes were cut off, and a small hole was pierced in the middle of one of them.

2. Three pieces of cardboard were cut, and a hole slightly larger than the base of the variable gap magnets was cut in two of the pieces of cardboard. The three pieces were then glued together, with the uncut piece on the bottom. The magnets were placed in the depression so they would not slide out of position.

3. A table clamp was attached to a large ring stand, and a photogate was secured horizontally in the clamp.

4. A long length of string was cut, and one end was tied to the ceiling. The piece of a coffee stirrer (see Step 1) was threaded onto the string and glued in place with superglue at a point about 30cm from the floor.

5. The magnets-cardboard setup (see Step 2) was then placed under the string. The free end of the string was passed through the hole in the Eppendorf tube lid (see Step 1), and a tube was attached under it. The height of the tube was adjusted until the bottom tip of the tube extended slightly above the center of the magnets. The Eppendorf tube was then removed, and a knot was tied in the string to prevent the lid from sliding. The cardboard was taped the floor after it was in the correct location.

6. The assembly from Step 3 was positioned so that the direction of the magnetic field was perpendicular to the direction of the photogate's light path. The

height of the photogate was adjusted until the coffee stirrer on the string broke the light beam. The magnets were then removed from the setup.

7. Vernier's Precision Timer software was loaded on the computer. From the main menu, the MISCELLANEOUS option was chosen and then PENDULUM from the resulting menu. NORMAL TIME DISPLAY was selected.

8. 10g of $CuSO_42H_2O$ was dissolved into 10mL of distilled water. This solution was added to a plastic litmus paper container. The filled container was weighed on an electronic balance and attached to the lid hanging from the string.

9. $CuSO_42H_2O$ was added to an Eppendorf tube until it was almost full. The lid was secured and sticky tack was wrapped around the tube to make it heavier. It was then weighed on an electronic balance and attached to the lid hanging from the string.

The sample was pulled back and released, and the period of the resulting oscillations was timed by the computer 20 times. The first 5 The magnets were placed back in the depression in the cardboard. The sample was pulled back and released, and the period was timed by the computer until the oscillations ceased (20-80 times). This step was repeated three times.

10. Steps 3-5 were repeated with each of the paramagnetic test samples: $CoCl_26H_2O$, $CuCl_22H_2O$, $Fe(NO_3)_39H_2O$, and $Ni(NO_3)_26H_2O$

11. A NaCl solution was made and transferred to an Eppendorf tube. Steps 3B-5 were repeated for this sample.

12. Escherichia coli were cultured for 24 hours and transferred to an Eppendorf tube with NaCl. Steps 3B-5 were repeated for this sample.

13. Steps 7 and 8 were repeated with $CaCl_2$ as the solution salt.

14. Step 9 was repeated with a more concentrated E coli solution.

15. Using Microsoft Excel software, Period vs. Number of Repitions was plotted for each data set. The horizontal asymptote of the period as a function of number of pendulum oscillations under the influence of the magnetic field (see Step 5) was used for the value of T and χ in the calculations.

16. The magnetic susceptibilities for each sample were calculated using Equation 12 and compared to the actual values from literature (see Appendix A). A calibration graph comparing χ_{actual} and $\chi_{calc.}$ was plotted using Excel.

17. The fractional uncertainty was determined for the χ values using Equation 14 (see Appendix) .

18. $\chi_M\chi/M$ was determined for each test sample using both the actual and calculated values for χ_M. A calibration curve was created by plotting χ_M versus the calculated set of $\chi_M\chi/M$. The equation for the resulting line was found using the TI-85's LINR regression function. Thesusceptibility was then extrapolated for the E coli from this equation.

19. Substituting this value of χ_M into Equation 13, the ratio χ/M was determined for the E coli.

Data/Graphs

Sample	χ (sec)	χ' (sec)	$\chi_M\chi/M$ Actual	$\chi_M\chi/M$ Calc	$\chi\chi/\chi$ (%)
$CuSO_4$	3.1260	2.8911	13.36	———	———
$CoCl_2$	3.1260	2.2034	78.55	77.25	0.6210
$CuCl_2$	3.1260	2.8051	21.18	17.77	0.5944
$Fe(NO_3)$	3.1260	2.3296	63.36	60.49	0.6286
$Ni(NO_3)_26$ H_2O	3.1260	2.7718	30.31	20.07	0.5963
NaCl	3.1212	3.1942	———	-0.4488	———
E coli	3.1230	3.1311	———	54.10	———

Source: Weast, Robert C. CRC Handbook of Chemistry and Physics. Cleveland: Chemical Rubber Co., 1967.

$\chi\chi'_{measured}$ between the NaCl and NaCl/E coli samples=3.1942-3.1311=0.0631 sec

χ' for calculations for NaCl/E coli s0ample=3.1230-0.0631=3.0599 sec

Equation for the $\chi_M\chi/M$ graph: y=117.2x+1.055

Discussion

In Step 3A of the procedure, the hypothesis was tested with the paramagnetic compounds in water solutions. No effect of the magnetic field could be observed or measured for these solutions. Magnetic properties are largely determined by the valence shell electron configuration. When dissolved in water, dissociation of the ions changed the valence shell electrons' configuration (which determined magnetic moment). Since the period of oscillations for the pendulum with and without the magnetic field should be different in order to obtain any measurement of susceptibility, this method was dismissed in favor of using the samples in their crystalline form.

As Table 1 and the test sample graphs illustrate, the period for the pendulum was lowered when the sample was oscillating through the magnetic field. Following a downward curve, the value for the period was decreased until the magnetic moments of the molecules became oriented to the magnetic field, thus stabilizing the period at some value. Substances with lower susceptibilities were stabilized over a longer period of time with more accurate stabilization than ones with higher susceptibilities. This difference was caused by the varying magnitudes of magnetic susceptibility in the samples.

In the graphs for the four test samples, the value of the horizontal line (with no magnetic field) was recorded as T. To find T', the last few values for each magnetic field trial which seemed to lie along some horizontal asymptote were averaged and recorded as T'. From these numbers and the other parameters in Equation 12, the

magnetic susceptibilities were calculated for these compounds. The linear nature of the $\square_{M\ actual}$ versus $\square_{M\ calc}$ graph confirmed that the results were valid. The differences in the actual and calculated susceptibilities can be attributed to several factors:

1) some mass being lost through transferal during the procedure

2) slight temperature variations during experimentation

3) not enough trials to determine T' precisely enough

To determine T'for the NaCl solution with E coli, some careful analysis of Graph 8 had to be applied. Since the trend for T' for the NaCl solution was greater than T (no magnetic field), it was reasoned that it was diamagnetic because it's trend was the inverse of the graphs' trends for test samples A-D. Because this value was lowered almost to the neutral point (no magnetic field) by the E coli, it was deduced that the E coli were paramagnetic because they counteracted the diamagnetism of the NaCl. The change in this period was subtracted from the neutral value for the E coli sample and used as T' for the calculations.

Using Equation 13, the relationship $\chi_M\chi/M$ was determined with both the actual and calculated values for χ_M for each of the four test samples A-D. This value was also calculated for samples E and F, which were comprised of a NaCl solution and NaCl solution with E coli respectively. An increase in $\chi_M\chi/M$ parallel to χ_M was the general trend for the graph of this data. The paramagnetic nature of the four test samples was evidenced by the positive $\chi_M\chi/M$ value while the diamagnetic character of the NaCl solution was shown by the negative value for $\chi_M\chi/M$. (A value of zero

for $\chi_M\chi/M$ would indicate that the sample had no magnetic properties) When the E coli were added to the NaCl solution, this value was increased to 54.10 cgs, due to the cancelling of the NaCl's diamagnetism by the E coli's paramagnetism. If the density were known, the molar mass of the E coli could readily be determined.

As stated previously, a virtually linear representation for both $\chi_{M\ actual}$ and $\chi_{M\ calc}$ was obtained. To check the validity of these values for χ, the fractional uncertainty was derived using the rules of error propagation (see Appendix 3). The accuracy of this method and precision of the results were confirmed by these small derivations in $\chi_{\ calc}$. The measurements in the experiment were performed as accurately as possible to reduce erroroneous data.

Implications and Future Questions

Many implications could result from the outcomes of this project. Since the set up and procedure were found to be viable as a technique of determining magnetic susceptibility, the more costly and complicated methods currently used could be substituted by this appproach. Since the magnetic susceptibility of the *Escherichia coli* was determined, the movement and physical parameters of *Escherichia coli* magnetic cells could be predicted and possibly controlled by taking advantage of their magnetic properties. This was the primary reason of the author to determine this parameter. Most significant would be the prospect of magnetically separating or "purifying" water (or other liquids) of unwanted bacteria. Applications could also be extended into laboratory work in the medical field.

In a postdoctorate research there are new questions to be explored:

- Do other magnetotactic bacteria have magnetic susceptibilties which can be found using this method?
- Is the magnetic susceptibility of the bacteria affected by using different concentrations of media, such as saline solutions, for example in marine environment?
- How does the magnetic susceptibility of magnetotactic bacteria relate to the processes of deposition of biogenic minerals?
- Are the biogenic minerals grain size and distribution noticeably affected by this method of determining magnetic susceptibility?

Table of Compounds Used*

Name	Formula	Molar Mass	Density (g/cm^3)	Susceptibility ($1\chi10^{-6}$cgs)
Copper Sulfate	$CuSO_45H_2O$	249.675	2.284	1460.0
Iron Nitrate	$Fe(NO_3)_3\chi9$ H_2O	403.994	1.684	15200.0

*Source: Weast, Robert C. CRC Handbook of Chemistry and Physics. Cleveland: Chemical Rubber Co., 1967.

Types of Magnetotactic Bacteria

Aquaspirrillum (Magnetospirillum) magnetotacticum

Magnetospirillum gryphiswaldense

Magnetic vibrio MV1

Magnetic coccus MC1, CS310, C103, CS308

APPENDIX D : BACTERIA'S MAGNETIC MOMENT

For the average magnetotactic bacteria, the magnetic moment is 1.6 x 10-13 [emu], which works out to be 1.6 x 10-15 [Am2]. The average magnetic field of the earth is 50,000 [nT]. Let us assume that the magnetotactic bacteria are stirred up from the sediments and oriented at a 90 ° angle to the field. We want to find the torque that the magnetic field of the earth applies to the magnetotactic bacteria to align it along the field.

$$\tau = m \times B$$

$$\tau = 1.6 \times 10^{-15} i \times 50{,}000 \times 10^{-9} - z$$

$$\tau = \begin{vmatrix} i & k & z \\ 0 & 1.6 \times 10^{-15} & 0 \\ 0 & 0 & -50{,}000 \times 10^{-9} \end{vmatrix}$$

$$\tau = (1.6 \times 10^{-15}(-50000 \times 10^{-9}) - 0)i - (0 - 0)y + (0 - 0)k$$

$$\tau = -8 \times 10^{-20}\ Nm\ k$$

This is the torque the geomagnetic field applies to the magnetotactic bacteria. It will align the bacteria so that the north pole of the bacteria will be in front, in the direction of the field. Now let's see if we could find the force that is applied to each pole of the magnetite dipole within the bacteria. Assume that the length (l) is 50 [nm].

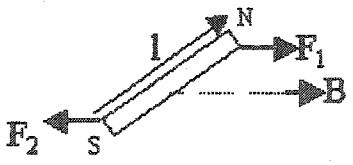

$m = |q_m|$

$1.6x10^{-15} = q_m(50x10^{-9})$

$q_m = 3.2x10^{-8}\ Am$

$F = q_m B$

$F = 3.2x10^{-8}(50{,}000x10^{-9})$

$F = 1.6x10^{-12}\ N$

These are the forces that are applied at each end of the bacteria to get the resultant torque that rotates the bacteria. In this proposed experimental design, any force greater than this torque will reorient the bacteria in another direction. The new force's magnitude is controlled by the intensity of magnetic field produced by the electric current-carying wires coil setting.

APPENDIX E: MATERIALS AND METHOD OF MTB COLLECTION

In this project, there are a few pointers that might be useful for obtaining good enrichments of magnetotactic bacteria. The first collection of bacterial culture is from the north side of the pond. In a closed basin, like a pond, Magnetotactic Bacteria do wind up in greater numbers there. Magnetotactic bacteria need the aerobic/anaerobic interface. The aerobic/anaerobic interface in ponds is typically within the first few centimeters or so of sediment, unless there is an unusually heavy load of organics, like agricultural run off or a large population of water fowl, in which it would be closer to the surface. This was not the case at this pond, but excavated materials can be noticed nearby water. We carefully use the correct end of the magnet marked North and South at its ends. The bacteria are be attracted to the end of a our stir bar that attracts the north-pointing needle of the compass. To observe the bacteria, we take a drop of the surface sediment and place it on a microscope slide. We place a drop of clear pond water next to the drop of sediment, then place the magnet to the side of the water drop so that the bacteria swim out of the sediment into the clear water. We keep looking for bacteria to collect at the edge of the water drop closest to the magnet. We use a dissecting scope (and a low powered microscope at the Ferris HSNJ Lab) with dark field illumination to observe them. To observe them at higher magnification, we make a modified hanging drop slide. Then, we place two pieces of labeling tape on the glass slide to raise the cover glass. We carefully place the cover glass over the drops of water and sediment so that they are suspended between the slide and cover glass (see figure below). Look at the edge of the drop under oil imersion (100X). We lastly find few of them and save the container of sediment

collected in and check on it periodically for a month until they bloom. The jar (mayonaise or peanut butter sized) itself is filled 1/3 with sediment, 1/3 water, and loosely capped (see figure below).

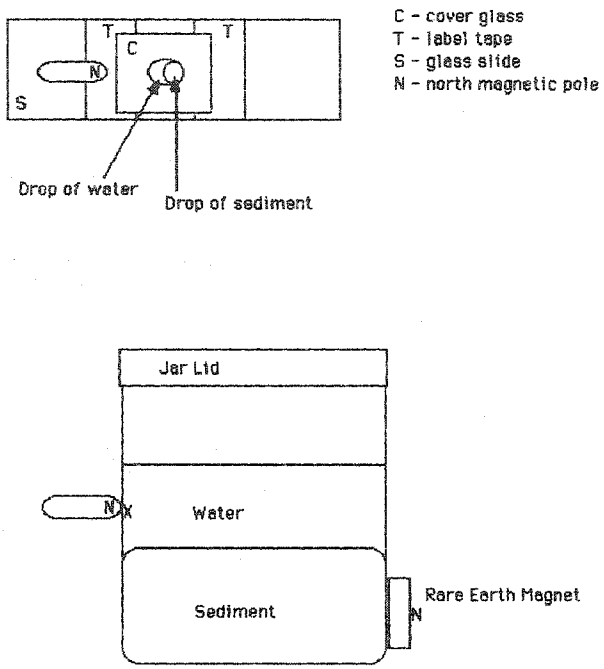

Figure: Bacteria collection materials used during field trip at Anthony's Nose, Westchester New York.

APPENDIX F: Statistical Analysis, Derivation of the Fractional Uncertainty

1. For the standard $CuSO_4 5H_2O$ sample, the standard deviation of the mean for T_s' was found. (T=SD of T_s')

2 . In Equation 12,

$$A=\chi\frac{M}{M_s}\frac{\rho_s}{\rho} \qquad B=\left(\frac{1}{T_s^2}\frac{1}{T_s'^2}\right) \qquad C=\left(\frac{1}{T^2}\frac{1}{T'^2}\right)$$

Since Term A was a constant, it was disregarded, and the following expression remained.

$$\chi=\frac{\frac{1}{T^2}\frac{1}{T'^2}}{\frac{1}{T_s^2}\frac{1}{T_s'^2}}$$

3. Using the rule: If C=A/B, then $\Delta C/C=(\Delta A/A)+(\Delta B/B)$ [taking the derivative]

$$\frac{\Delta\chi}{\chi}=\frac{\Delta\left(\frac{1}{T^2}-\frac{1}{T'^2}\right)}{\frac{1}{T^2}-\frac{1}{T'^2}}+\frac{\Delta\left(\frac{1}{T_s^2}-\frac{1}{T_s'^2}\right)}{\frac{1}{T_s^2}-\frac{1}{T_s'^2}}$$

Since the second term of this was identical to the first except for the subscript s, the derivation continued with only the first term, and the result was later applied to the second term.

4. Taking the numerator of the first term and using the rule: If C=A-B, then $\Delta C=\Delta A+\Delta B$

$$\Delta\left(\frac{1}{T^2}-\frac{1}{T'^2}\right)=\Delta\left(\frac{1}{T^2}\right)+\Delta\left(\frac{1}{T'^2}\right)$$

5. The first term from this was taken, and the rule from Step 3 was applied.

$$\frac{\Delta C}{C} = \frac{\Delta I}{I} + \frac{\Delta T^2}{T^2}$$

6. This result was substituted into the second term of the previous equation, where $C=1/T^2$ from Step 4.

$$\frac{\Delta(\frac{I}{T^2})}{\frac{I}{T^2}} = \frac{2\Delta T}{T}$$

Solving for $\Delta(1/T^2)$,

$$\Delta(\frac{I}{T^2}) = \frac{2\Delta T}{T_3}$$

7. Substituting $2\Delta T/T^3$ back into the equation in Step 4, yields:

$$\Delta(\frac{I}{T^2} - \frac{I}{T'^2}) = \frac{2\Delta T}{T^3} + \frac{2\Delta T}{T'^3} = 2\Delta T(\frac{I}{T^3} + \frac{I}{T'_3})$$

8. Because this applied to Terms B and C, this was substituted into both terms of the equation. The result was the expression for fractional uncertainty of the calculated magnetic sucsceptibility.

$$\frac{\Delta\chi}{\chi} = \frac{2\Delta T(\frac{I}{T^3} - \frac{I}{T'^3})}{\frac{I}{T^2} - \frac{I}{T'^2}} + \frac{2\Delta T(\frac{I}{T_s^3} - \frac{I}{T_{s'}^3})}{\frac{I}{T_s^2} - \frac{I}{T_{s'}^2}} \qquad (14)$$

References:

Agar, W. M. (1933) The pegmatites of Bedford, New York. 16th International Geological Congress, v. 9, p. 123-128.

Balkwill, D., Maratea, D., and Blakemore, R.P. (1980) Ultrastructure of a magnetotactic spirillum. J. Bacteriol. v. 141, p. 1399-1408.

Balzer, Philippe & Jurg Hulliger (1984) Comment on the Measurement and Interpretation of Susceptibility Data. Inorganic Chemistry v. 23, p. 4772-4773.

Bazylinski, Dennis A., Richard B. Frankel, & Holger W. Jannasch (1988) Anaerobic Magnetite Production by a Marine, Magnetotactic Bacterium. Nature v. 344, p. 518-519.

Bazylinski, Dennis A., Brigid R. Heywood, Stephen Mann, & Richard B. Frankel (1993) Fe_3O_4 and Fe_3S_4 in a Bacterium. Nature v. 366, p. 218.

Bazylinski, D. A. (1990) Anaerobic production of single-domain magnetite by the marine, magnetotactic bacterium, strain MV-1, Iron Biominerals, edited by R. B. Frankel and R. P. Blakemore, Plenum, New York, p. 69- 77.

Bazylinski, D.A., 1992, Bacterial production of iron sulfides, in Materials synthesis based on biological processes, edited by M Alpert, P. Calvert, R.B. Bazylinski, D.A., and R.B. Frankel, Production of iron sulfide minerals by magnetotactic bacteria in sulfidic environments, Biomineralization Processes of Iron and Manganese---Modern and Ancient Environments, edited by H.C.W. Skinner and R.W. Fitzpatrick, Catena, Cremlingen-Destedt, p. 147-159.

Bazylinski, D. A., B.R. Heywood, S. Mann, and R.B. Frankel, 1993, FeO and FeS in a bacterium, Nature v. 334, p. 218-366.

Bazylinski, D. A., A. J. Garratt-Reed, A. Abedi, and R.B. Frankel, 1993, Copper association with iron sulfide magnetosomes in a magnetotactic bacterium, Arch. Microbiol. v. 160, p. 35-42.

Bazylinski, D. A., A. J. Garratt-Reed, and R.B. Frankel, 1994, Electron microscopic studies of magnetosomes in magnetotactic bacteria, Microscopy Res. Techn. v. 27, p. 389-401.

Bazylinski, D. A. & Moskowitz, B. M., 1997, Geomicrobiology: Interactions between Microbes and Minerals, editions Banfield, J. F. & Nealson, K. H., Mineralogical Society of America, Washington, DC, p. 181–223.

Beck, Lewis C., 1842, Mineralogy of New York. Albany, New York Third Annual Report of the New York State Cabinet of Natural History, Albany, N.Y., p. 445-447.

Beck, L. C., 1842, The Mineralogy of New York, White & Visscher, New York Third Annual Report of the New York State Cabinet of Natural History Albany, p. 536.

Berkey, Charles P., 1911, Geology of the New York City (Catskill) Aqueduct. New York State Museum Bulletin 146, Albany, New York City and Vicinity, p. 321-323.

Berkey, C. P., and Rice, M., 1919, Geology of the West Point quadrangle. New York State Museum Bulletin, p. 225-226.

Black, D., 1948, Some minerals of Bedford, New York. Rocks and Minerals v. 23, p. 710-712.

Blakemore, Richard P., 1975, Magnetotactic Bacteria. Science v. 190, p. 377-379.

Blakemore, Richard P. & Nancy A., 1989, Magnetic Bacteria: Lessons in Physics and Biology. Science Education v. 77, p. 213-217.

Blakemore, Richard P., 1979, Magnetotactic Field Effects on Biological Systems. New York: Plenum Press, , p. 13-15.

Blakemore, Richard P., Richard B. Frankel, & Ad. J. Kalmijn, 1993, South-seeking Magnetotactic Bacteria in the Southern Hemisphere. Nature v. 259, p. 384-385.

Blakemore, R., 1975, Magnetotactic bacteria. Science v. 190, p. 377-379.

Blakemore, R.P., 1982, Magnetotactic bacteria. Annual Review of Microbiology v. 36, p. 217-238.

Blakemore, R.P., Frankel, R.B., and Kalmijn, Ad. J., 1980, South-seeking magnetotactic bacteria in the southern hemisphere. Nature, v. 286, p. 384-385.

Braun, V., Hantke, K. & Koster, W., 1998, Metal Ions. Biological Systems, v. 35, p. 67–145.

Broughton, J. G., Fisher, D. W., Isachsen,Y. W., & Rickard L. V., 1966, The Geology of New York State. A Brief Account, New York State Museum and Science Service Educational Leaflet #20, Albany, p. 50.

Borg, L. E., Connelly, J. N., Nyquist, L. E., Shih, C.-Y., Wisemann, H. & Reese, Y., 1999, Biomineralization Perpective. Science v. 286, p. 90–94.

Butler, R.F., and Banerjee, S.K., 1975, Theoretical single-domain grain size range in magnetite and titanomagnetite. Journal of Geophysical Research, v. 80, p. 4049-4058.

Cadwell, Donald H., 1989, Surficial Geologic Map of New York. Lower Hudson Sheet, Map and Chart Series Number 40 of the New York State Museum and Science Service, Albany.

Carr, M. H., 1996, Water on Mars. Oxford Univ. Press, New York, p. 56-67.

Chang, S.R., and Kirschvink, J.L., 1985, Possible biogenic magnetite fossils from the Miocene marine clay of Crete, in Kirschvink, J.L., Jones, D.S., and McFadden, B.J., eds., Magnetite biomineralization and magnetoreception in organisms: A new biomagnetism. New York, Plenum Press., p. 647-669.

Chang, S.-B. R. & Kirschvink, J. L., 1989, Annu. Rev.pp. Earth Planet. Sci. v. 17, p. 169–195.

Chase, P. J., and Brock, P. W. G., 1976, Sillimanite and sillimanite-orthoclase isograds in the Croton Falls quadrangle, Southeast New York. Geological Society of America, Northeast section, Abstracts 11th Annual Meeting 8.

Clemett, S. J., Dulay, M. T., Gilette, J. S., Chillier, X. D. F., Mahajan, T. B. & Zare, R. N., 1998, Faraday Discussion v. 109, p. 417–436.

Clement, B.M., and Kent, D.V., 1983, The upper Olduvai polarity transition as recorded in southern hemisphere deep-sea core. EOS (American Geophysical Union Transactions), v. 63, p. 219.

Connerney, J. E. P., Acuna, M. H., Wasilewski, P. J., Ness, N. F., Re`me, H., Mazelle, C., Vignes, D., Lin, R. P., Mitchell, D. L. K. & Cloutier, P. A., 1999, Science v. 284, p. 794–798.

Dana, J. D., 1892, A System of Mineralogy. Sixth edition, John Wiley & Sons, New York, p. 270.

Davis, R.S., 1992, Using Small, Rare-earth Magnets to Study the Susceptibility of Feebly Magnertic Metals. American Journal of Physics v. 60, p. 365-370.

Delong, Edward F., Richard B. Frankel, Dennis A. Bazylinski, 1993, Multiple Evolutionary Origins of Magnetotaxis Bacteria. Science v. 259, p. 803-806.

Devouard, B., M. Posfai, X. Hua, D.A. Bazylinski, R.B. Frankel, and P.R. Buseck, 1998, Magnetite from magnetotactic bacteria: size distributions and twinning. Am. Mineral. v. 83, p. 1387-1399.

Doyle, J.F. ,Wachtel H. and P. Todd, 1999, Magnetotactic bacteria and Gravity, NASA's grant, Colorado University, Boulder, NASA Bulletin 453 Reports.

Dunlop, D.J., 1990, Developments in rock magnetism, Rep. Prog. Phys v. 53, p. 707-792,

Eaton, S.S. & G.R., 1979, An Inexpensive, Convient Demonstration of Magnetic Susceptibility. Journal of Chemical Education, v. 56, p. 170-171.

Egleston, T., 1892, A Catalogue of Minerals and Pseudonyms. John Wiley & Sons, New York, p. 56-58.

Evans, M.E., and F. Heller, 1994, Magnetic enhancement and paleoclimate: study of a loess/paleosol couplet across the loess plateau of China, Geophys. J. int. v. 117, p. 257-264,

Erice Roden and Johnm Zachara, 1996, Extraction methodology. Department of Biological Sciences; The University of Alabama, Environmental Science Technology, v. 30, p. 1618-1628.

Farina, Marcos, Darci Motta S. Esquivel, & Henrique G.P. Lins de Barros, 1990, Magnetic Iron-sulfur Crystals from a Magnetotactic Microorganism. Nature v. 343, p. 256-258.

Farina, M., D. Motta, S. Esquivel, H.G.P. Lins de Barros, 1990, Magnetic iron-sulphur crystals from a magnetotactic microorganism, Nature, v. 343, p. 256-258,.

Farina M., B. Kachar, U. Lins, R. Broderick, and H. L. De Barros, 1994, The observation of large magnetite crystals from magnetotactic bacteria by electron and atomic force microscopy, J. Micros. v. 173, p. 1-8.

Fassbinder, Jörg W.E., Helge Stanjek, & Hojatollah Vali, 1990, Occurrence of Magnetic Bacteria in Soil. Nature v. 343, p. 161-163.

Fassbinder, J.W.E., H. Stanjek and H. Vali, 1990, Occurrence of magnetic bacteria in soil, Nature v. 343, p. 161-163.

F.D. Stacey, 1992, Arrangement of magnetic moments, Ferrimagnets ferromagnets and anti-ferromagnets, Environmental Science Technology, v. 30, p. 1673-1680.

Fleischer, M., 1987, Glossary of Mineral Species 5th edition, the Mineralogical Record, Inc., Tucson, p. 227.

Flint, Richard Foster, 1971, Glacial and Quaternary Geology. Editions John Wiley & Sons, p. 692.

Frankel, Richard B., 1987, Anaerobes Pumping Iron. Nature v. 330, p. 208.

Frankel, R.B., and D.A. Bazylinski, 1994, Structure and function of magnetosomes in magnetotactic bacteria, in Design and Processing of Materials by Biomimicking, edited by I. Aksay and M. Sarikaya, American Institute of Physics, New York, p. 87-90.

Frankel, R.B., and R. P. Blakemore, 1990, Iron Biominerals, Plenum Press, New York, p. 435.

Frankel, R.B., and S. Mann, 1994, Biomineralization, in Encyclopedia of inorganic chemistry, edited by R. Scott, Wiley and Sons, New York, p. 456-460.

Frankel, R. B., Blakemore, R. P. & Wolfe, R. S., 1979, Science 203, p. 1355–1356.

Frankel, Richard B., 1986, Magnetic Skeletons in Davy Jone's Locker. Nature v. 320, p. 575.

Frankel, R.B., Blakemore, R.P., Torres de Aranjo, F.F., Esquivel, D.M.S., and Danon, J., 1981, Magnetotactic bacteria at the geomagnetic equator. Science v. 212, p. 1269-1270.

Frankel, R. B., Bazylinski, D. A., Johnson, M. S. & Taylor, B. L., 1997, Biominerals and Biomaterials. Biophys. J. v. 73, p. 994–1000.

Friedman, G. M., 1952a, Sapphirine occurrence of Cortlandt, New York. American Mineralogist, p. 244-249.

Friedman, G. M., 1952b, Study of hoegbomite. American Mineralogist v. 37, p. 600-608.

Friedman, G. M., 1956, The origin of spinel-emery deposits with particular reference to those of the Cortlandt Complex, New York. New York State Museum Bulletin v. 351, p. 68.

Gooding, J. L., Wentworth, S. J. & Zolensky, M. E., 1991, Bacterial Mineral Magnetic Records. Meteoritics v. 26,
p. 135–143.

Gould, Stephen Jay, 1980, The Panda's Thumb. More Reflections in Natural History, New York, W.W. Norton & Co., p. 306-313.

Gorby, Y. A., Beveridge, T. J. & Blakemore, R. P., 1988, Magnetic Bacteria: Lessons in Physics and Biology. J. Bacteriol. v. 170, p. 834–841.

Guerinot, M. L., 1994, Magnetotactic Bacteria. Annu. Rev. Microbiol. v. 48, p. 743–772.

Hall, Leo M., 1968, Field Trip in the vicinity of White Plains, New York, New York State Geological Association Guidebook of the annual meeting of 1968 at Queens College, p. 454-467.

Hall, Leo M., 1968, Times of The Origin and Deformation of Bedrock in the Manhattan Prong, in Studies of Appalachian Geology: Northern and Maritime, Edited by E-An Zen et al, p. 676-683.

Hawthorne, T.B., and J.A. McKenzie, 1993, Biogenic magnetite: Authi-genesis and diagenesis with changing redox conditions in Lake Greifen, Switzerland, in Applications of Paleomagnetism to Sedimentary Geology, edited by D.M. Assaoui, N.F. Hurley, and B.H. Lidz, Soc. Sed. Geol. special publication v. 49, p. 3-15.

Hess, P.P., 1994, Evidence for bacterial paleoecological origin of mineral magnetic cycles in oxic and sub-oxic Tasman Sea sediments, Marine Geology v. 117, p. 1-17.

Howell, William T., 1934, The Hudson Highlands, Volume II. Reprinted 1982,Walking News, New York, N.Y, p. 45-49.

H. C. W. Skinner and R.W. Fitzpatrick, 1992, Biomineralization. Editions Catena-Cremlingen-Destedt, 1992, p. 133-145.

Jensen, David E., 1978, Minerals of New York State. Editions Ward Press, p. 219.

Kemp, J. F., 1894, Pyrrhotite Deposits at Anthony's Nose on the Hudson, N.Y. American Institute, Min. Eng. Transactions, p. 620.

Kerr, P. F., 1935, U-Galena and uraninite in Bedford, New York, cyrtolite. American Mineralogist v. 20, p. 443-450.

Kirschvink, J. L., 1982, Biomimetics Materials from Fe-sulfide Bacteria. Earth Planet. Sci. Lett. v. 59, p. 388–392.

Kirschvink, J.L., A. Kobayashi-Kirschvink, and B.J. Woodford, 1992, Magnetite biomineralization in the human brain, Proc. Natl. Acad. Sci, USA, v. 89, p. 7683-7687.

Klemic, H., Eric, J. H., McNitt, J. R., and McKeown, F.A., 1959, Uranium in Phillips Mine-Camp Smith Area, Putnam and Westchester Counties, New York. U.S.G.S. Bulletin 1074-E, Washington, D.C.

Leshin, L. A., 2000, Observations of magnetosome organization, surface structure, and iron biomineralization of undescribed magnetic bacteria: evolutionary speculations. Geophys. Res. Lett. v. 27, p. 2017–2020.

Long, L. E., 1969, Whole Rock Rb-Sr Age of the Yonkers Gneiss, Geological Society of America Bulletin, v. 80, p. 1232-1235

Loveman, Michael Heilprin, 1911, Geology of the Phillips Pyrites Mine Near Peekskill, New York. Economic Geology, Vol. VI, No. 3, p. 235.

Lovley, D. R.; Phillips, E. J. P., 1986, Magnetotactic Bacteria, Method of Cells Quatification, Appl. Environ. Microbiol. v. 51, p. 683-689.

Lowenstam, H.A., 1981, Minerals formed by organism, Science v. 211, p. 1126-1131.

Lowenstam, H.A., and S. Weiner, 1989, On Biomineralization, Oxford University Press, New York, p. 12-54.

Luquer, L. M., 1896, The minerals of the pegmatite veins at Bedford, N.Y. American Geologist v. 18, p. 259-261.

Maher, B., and R. Thompson, 1992, Paleoclimatic significance of the mineral magnetic record of the Chinese loess and paleosols, Quater. Res. v. 37, p. 155-170.

Manchester, James G., 1931, The Minerals of New York City and Its Environs. New York Mineralogical Club, Bulletin v. 3, No. 1, New York, NY.

Manchester, James G., 1931, The Minerals of New York City and Its Environs. New York Mineralogical Club, Bulletin Volume 3, No. 1, New York, NY, p. 567-569.

Mann, Stephen. Nicholas H.C. Sparks, Richard B. Frankel, Dennis A. Bazylinski, Holger W. Jannasch, 1990, Biomineralization of Ferromagnetic Greigite and Iron Pyrite in a Magnetotactic Bacterium. Nature v. 343., p. 258-261.

Mann, S., 1993, Molecular tectonics in biomineralization and biomimetic materials chemistry, Nature v. 365, p. 499-505.

Mann S., N. H.C. Sparks, R.B. Frankel, D.A. Bazylinski, and H.W. Jannasch, 1990a, Biomineralization of ferrimagnetic greigite (FeS) and iron pyrite (FeS) in a magnetotactic bacterium, Nature 343, p. 258-261.

Mann, S., Sparks, N. H. C. & Wade, V. J., 1991, Iron Biominerals. Editions Frankel, R. B. & Blakemore, R. P., Plenum, New York, p. 21–49.

Matsuda, T., Endo, J., Osakabe, N., and Tonomura, A., 1983, Morphology and structure of biogenic magnetite particles. Nature v. 302, p. 411-412.

Matsunaga, Tadashi, Chikashi Nakamura, J. Grant Burgess, & Koji Sode, 1992, Gene Transfer in Magnetic Bacteria: Transposon Mutagenesis and Cloning of Genomic DNA Fragments Required for Magnetosome Synthesis. Journal of Bacteriology v. 174, p. 2748-2753.

McCabe, C., Van tier Voo, R., Peacor, D.R., Scotese, C.R., and Freeman, R., 1983, Diagenetic magnetite carries ancient yet secondary remanence in some Paleozoic sedimentary carbonates: Geology, v. 11, p. 221-223.

Meyer, C., 1998, Mars Meteorite Compendium. JSC. # 27672, Website address: htt://www.curator.jsc.nasa.gov/curator/antmet/mmc/mmc.htm.

Merguerian, Charles, 1987, The Geology of Cameron's Line, West Torrington, Connecticut, Geological Society of America, Northeastern Section Field Guide of 1987, p. 91-112.

Merguerian, Charles, 1987, Geology of Manhattan Island and the Bronx, New York City, New York, Geological Society of America, Northeastern Section Field Guide, p. 1123-1144.

Merguerian, Charles, & Mose, D.G., 1985, Rb-Sr Whole-Rock Age Determination on parts of the Manhattan Schist and Its Bearing on Allochthony in the Manhattan Prong, Northeastern Geology, v. 7, no. 1, p. 543-587.

Mose, D.G., 1982, 1300 Million Year Old Rocks in the Appalachians, Geological Society of America Bulletin, v. 93, p. 78.

Mullen, M.D. et al., 1985, Bacterial Sorption of Heavy Metals. Applied and Environmental Microbiology. v. 55, p. 3143-3149.

Nakamura, Noriyuki, Kohji Hashimoto, & Tadashi Matsunaga, 1991, Immunoassay Method for the Determination of Immunoglobulin G Using Bacterial Magnetic Particles. Analytical Chemistry v. 63, p. 268-272.

Nelson, Jane Bray & Jim, 1992, Magnetic Bacteria. The Science Teacher 1992, p. 48-53.

Newman, W. S., et al, 1969, Late Quaternary Geology of the Hudson River Estuary, Transactions of the New York Academy of Science v. 31, p. 160.

Oldfield, F., 1992, The source of fine-grained magnetite in sediments, Holocene, Geoph. Res. v. 2, p. 180-182.

Oldfield, F., 1994, Toward the discrimination of fine grained ferrimagnets by magnetic measurements in lake and near-shore marine sediments, J. Geophys. Res., v. 99, p. 9045-9050.

Owen, T., 1992, Mars. Editions Kieffer, H. H., Jakosky, B. M., Snyder, C. W. & Matthews, M. S., Univ. of Arizona Press, Tucson, AZ, p. 818–834.

Peterson, Ivars, 1984, A Magnetic Way to Wiggle and Grow. Science News v. 126, p. 87.

Peterson, Ivars, 1991, Digging for Bacterial Magnetism. Science News. v. 139, p. 367.

Peterson, Nikolai, Tilo von Dobeneck, & Hojatollah Vali, 1986, Fossil Bacterial Magnetite in Deep-sea Sediments from the South Atlantic Ocean. Nature v. 320, p. 611-615.

Popper, K.R., M.J. Russel, & A.J. Hall, 1990, Pyrite and the Origin of Life. Nature v. 344, p. 387.

Pough, F. H., 1936, Bertrandite and epistilbite from Bedford, New York. American Mineralogist v. 21, p. 264-265.

Pough, F. H., 1976, A Field Guide to Rocks and Minerals: 4th Edition, Houghton Mifflin Company, Boston, p. 317.

Prucha, John J, 1956, Geology of the Brewster Magnetite District of Southeastern New York, Circular #43 of the New York State Museum and Science Service, Albany, p. 48.

Prucha, John J., Scotford, David M., & Sneider, Robert M., 1968, Bedrock Geology of Parts Of Putnam and Westchester Counties, New York and Fairfield County, Connecticut, Map and Chart Series #11, New York State Museum and Science Series. p. 26.

Robinson, S., 1825, A Catalogue of American Minerals, with their Localities. Cummings, Hilliard, & Co., Boston, p.115.

Ricci, Juan C. Diaz, Barbara J. Woodford, Joseph L. Kirschvink, & Michael R. Hoffmann, 1991, Alteration of the Magnetic Properties of Aquaspirillum magnetotacticum by a Pulse Magnetization Technique. Applied & Environmental Microbiology v. 57, p. 3248-3254.

Roberts, W. L., Campbell, T. J., Rapp, G. R., Jr., and Wilson, W. E., 1990, Encyclopedia of Minerals 2nd edition, Van Nostrand Reinhold, New York, p. 979.

Robinson, S., 1825, A Catalogue of American Minerals, with their Localities. Editions Cummings, Hilliard, & Co., Boston, p.115.

Sakaguchi, T., J.G. Burgess, and T. Matsunaga, 1993, Magnetite formation by a sulphate-reducing bacterium, Nature v. 365, p. 47-49.

Schuberth, Christopher J., 1968, Geology of New York City and Environs. Natural History Press, p. 121

Snowball, I.F., 1994, Bacterial magnetite and the magnetic properties of sediments in a Swedish lake, Earth Planet. Sci. Lett. v. 26, p. 129-142.

Spring, S., Amann, R., Ludwig, W., Schleifer, K.H., Gemerden, H.v., and Petersen, N. (1993) Dominating role of an unusual magnetotactic bacterium in the microaerobic zone of a freshwater sediment. Appl. Environ. Microbiol. v. 59, p. 2397-2403.

Sparks, N. H. C., Mann, S., Bazylinski, D. A., Lovley, D. R., Janasch, H. W. & Frankel, R. B., 1990, Biomineralization of ferrimagnetic greigite ($Fe^{II}S^{IV}$) and iron pyrite (FeS^{II}) in a magnetotactic bacterium. Earth Planet. Sci. Lett. v. 98, p. 14–22.

Stolz, J. F., 1992, Magnetotactic bacteria: biomineralization, ecology, sediment magnetism, environmental indicator. Biomineralization Processes of Iron and Manganese---Modern and Ancient Environments, edited by H.C.W. Skinner and R.W. Fitzpatrick, Catena, Cremlingen-Destedt, p. 133-145.

Stolz, J. F., 1992, Magnetotactic bacteria: biomineralization, ecology, sediment magnetism, environmental indicato. Biomineralization Processes of Iron and Manganese - Modern and Ancient Environments, edited by H.C.W. Skinner and R.W. Fitzpatrick, Catena, Cremlingen-Destedt, p. 133-145.

Stolz, John F., 1970, Magnetosomes. Journal of General Microbiology v. 139, p. 1663-1670.

Spencer, Bert & Richard N. Zare, 1988, Magnetic Susceptibility Measurements Using a Laser-Pendulum Apparatus. Journal of Chemical Education, p. 277-279.

Tauxe, L., Tucker, P., Petersen, N.P., and Labrecque, T. L., 1983, The magnetostratigraphy of Leg 73 sediments: Palaeogeography, Palaeoclimatology, Palaeoecology, v. 42, p. 65-90.

Thompson, and Oldfield, 1984, Magnetic hysteresis loop with initial magnetization curve, Earth Planet. Sci. Lett. v. 26, p. 129-142.

Thomas-Keprta, K. L., Bazylinski, D. A., Kirschvink, J. L., Clemett, S. J., McKay, D. S., Wentworth, S. J., Vali, H., Gibson, E. K., Jr., & Romanek, C. S., 2000, Geochim. Cosmochimica Acta v. 64, p. 4049–4081.

Thomsen, Dietrick E., 1985, Swinging Magnetic Bacteria. Science News v. 128, p. 171.

Tracy, R, Ratcliffe, N and Bender J, 1987, Igneous and Contact Metamorphic Rocks of the Cortlandt Complex, Westchester County, New York, Geological Society Of America, Centennial Field Guide, Northeastern Section, 1987, p. 67-108.

Vali, H. and J. L. Kirschvink, 1990, Observations of magnetosome organization, surface structure, and iron biomineralization of undescribed magnetic bacteria: evolutionary speculations. Iron Biominerals, edited by R. B. Frankel and R. P. Blakemore, Plenum Press, New York, p. 97-115.

Verosub, K.L., 1977, Depositional and postdepositional processes in the magnetization of sediments: Reviews of Geophysics and Space Physics, v. 15, p. 129.

Vali, H. & Kirschvink, J. L., 1991, Iron Biominerals. Editions Frankel, R. B. & Blakemore, R. P, Plenum, New York, p. 97–115.

Weisburd, Stefi, 1991, Marine Magnetite Made by Bacteria. Science News v. 43, p. 396.

Williams, R. J. P., 1990, Iron and the Origin of Life. Nature, v. 343, p. 213-214.

Walker, A. L., 1983, The effects of magnetite on oxalite and dithionite extractable iron. Soil Science Society of America Journal, v. 47, p. 1022-1026.

Walker, M.M., Kirschvink, J.L., Chang, S.R., and Dizon, A.E., 1984, A candidate magnetic sense organ in the yellow fin tuna, Thunuus albacarex Science, v. 224, p. 2232-2254.

Waite, E., 1940, New localities in Westchester County, N.Y. Rocks and Minerals v. 15, p. 327-329.

Wissig, George C., 1979, Bedrock Geology of the Ossining Quadrangle, New York, New York State Museum Map and Chart Series Number 30, p. 54.

Wycoff, Jerome, 1971, Rock Scenery of the Hudson Highlands and Palisades, Adirondack Mountain Club, p. 96.